Influence of the Interphase on the Mechanical Properties of Nylon 66 Composites

by

Richard L. Clark, Jr.

Dissertation submitted to the Faculty of the

Virginia Polytechnic Institute and State University

in partial fulfilment of the requirements for the degree of

Doctor of Philosophy

in

Materials Engineering Science

APPROVED:

Ronald G. Kander, Chairman

Brian J. Love

Bryan B. Sauer

Thomas C. Ward

James P. Wightman

August, 1996
Blacksburg, Virginia

Influence of the Interphase on the Mechanical Properties of Nylon 66 Composites

by

Richard L. Clark, Jr.

Committee Chairman: Ronald G. Kander

Materials Engineering Science

(Abstract)

The mechanical properties of glass fiber and carbon fiber reinforced nylon 66 were investigated using both microscopic and macroscopic testing techniques. The objective was to determine how different interphase morphologies affect the adhesion and properties such as damping, ultimate stress and strain, and modulus of the composite. This was accomplished using a modified fiber debond test on single filament composites, and dynamic mechanical analysis, vibrational adhesion testing, and uni-axial tension testing on bulk composite samples. Additional techniques such as scanning electron microscopy, profilometry, thermogravimetric analysis, differential scanning calorimetry, and water absorption measurements were performed to assist in data interpretation.

The specific interphase that forms in both glass reinforced and high modulus carbon fiber reinforced nylon 66 is termed transcrystallinity. Previous work has shown that this region can be altered by the addition of a specific diluent, poly(vinyl pyrrolidone), as either a blend to the matrix or as a fiber sizing. The diluent serves to dampen nucleation on the fiber surface thus causing the interphase to change from transcrystalline in nature to spherulitic. The changes in composite properties that the different interphases produce were examined.

Results from the modified fiber debond test showed that the interfacial shear strength decreases as the interphase becomes more spherulitic. Scanning electron microscopy revealed a more cohesive fracture surface of the samples having a transcrystalline interphase. Dynamic mechanical analysis showed that the damping behavior of E-glass/nylon 66 composites does not change with PVP sizing, while carbon fiber/nylon 66 composites showed a decrease in damping with the addition of sizing. Vibrational adhesion testing showed similar effects in the loss tangent of both composites versus fiber sizing. In addition, uni-axial tensile testing revealed an increase in the ultimate strength and toughness of both composites. On the other hand, neither the ultimate strain or modulus was a strong function of fiber sizing.

Acknowledgments

I would like to thank the following individuals and organizations for their contributions to this research:

Dr. Ron Kander, my advisor, for his continuing support and excellent mentorship. His approach to teaching, research, and advising has prepared me well for the future.

Dr. B. J. Love, B. B. Sauer, T. C. Ward, and J. P. Wightman, for serving on my committee. I want to particularly thank Bryan Sauer for his willingness to take time out of his busy schedule at DuPont and serve as both a mentor and committee member.

Center for Adhesive and Sealant Science and the Adhesive and Sealant Council Education Foundation for funding.

Acadia, Inc. and James Jacks for partial funding and helping me keep an industrial perspective of both academics and research.

Mr. Mike Craven who, with his excellent work ethic and valued friendship, helped complete some critical testing and data evaluation during the summer of ‘96.

My group colleagues, Mr. Joel Lee, Dr. Shannon Namboordi, Mr. Mike Farrell, Dr. Linda Vick, Mrs. Jennifer Howard, Mr. Shannon Arnold, Ms. Julie Martin, Dr. Watson Srinivas, Dr. Ravi Verma, Dr. Helene Cornelis, Ms. Liz Meyers, and Dr. Joannie Chin for their friendship, experiences, and encouragement.

Dr. Ron Gordon, the MSE department head, for having faith and accepting me as a graduate student here at Virginia Tech.

Finally, my family, who has supported me from day one. Especially, my wife Julie Clark, all my love to you through our Lord.

TABLE OF CONTENTS

LIST OF FIGURES

1. Introduction

1.1 Problem statement

Today's ever increasing demand for newer, lighter materials with higher strength, greater stiffness, and better reliability has led to extensive research on and development of composite materials. These materials offer a combination of strength and modulus that are either comparable to or better than many traditional materials such as metals. Because of their low specific gravities, the strength-to-weight ratios as well as modulus-to-weight ratios make these materials markedly superior to those of metallic materials. In addition, fatigue strength-to-weight ratios as well as fatigue damage tolerances of many composites are excellent and make them viable candidates for many applications.

Until recently, the use of composites has primarily been limited to high performance aerospace and sporting applications. However, with the explosion of the information age and higher demand for materials with superior properties from the private sector, composites are now making their way into more common applications. Along with this demand comes the necessity to understand the static and dynamic mechanical behavior, long term durability, and environmental stability of these materials.

Most composites are reinforced with long continuous or short chopped fibers and are primarily carbon or glass based. On the other hand, the matrix can either be a thermoset or thermoplastic. Furthermore, the interface between these materials must have the proper level of adhesion so that the properties of both materials can be used fully. This must lead to a composite which has a balance of strength, environmental protection, and damage tolerance.

Until recently, thermosets have accounted for most composite matrices. This is largely due to the low viscosity of thermosetting resins which makes composite fabrication a relatively simple process. Epoxies account for most of these thermosetting matrices because they are easy to process, have a low shrinkage upon cure, have good electrical properties, have high chemical resistance, and adhere well to many reinforcing materials. But epoxies have upper use temperature and environmental limitations. This drastically limits their use in many common durability applications. Furthermore, the high demand for recycleability makes thermosets unappealing. This has spawned new studies investigating the replacement of thermosets with high temperature thermoplastics.

In contrast to thermosets, thermoplastics do not have a crosslinked structure and therefore can be recycled. Furthermore, thermoplastics have the potential for high volume processing, low cost, and parts with superior impact resistance as compared to their thermosetting counterparts. Thermoplastics also have an infinite shelf life, shorter fabrication time, and meet many other requirements such as abrasion resistance and UV resistance. But thermoplastics also have their disadvantages: creep, limited temperature capability, and limited processing techniques.

Although the use of thermoplastics poses several limitations, efforts are currently being made to synthesize thermoplastics that can be used in a wider range of applications. Initial efforts have looked at using semicrystalline thermoplastic matrices to enhance thermoplastic composite properties, however, these composites are more complex than amorphous materials, and their microstructures are not well understood. For example, in many semicrystalline polymer matrix composites, an interphase morphology between the fiber and matrix termed transcrystallinity is formed due to the presence of the reinforcement. This region forms due to the high nucleation density on the fiber surface, and its effect on the mechanical properties of the composite is not well understood. There has been much debate in the literature as to whether this region is important in composites, how it is formed, and what effects it has on the composite properties.

1.2 Research objectives

The objective of this work is to examine what effect transcrystallinity has on the mechanical properties of a specific composite system: a polyamide, nylon 66, reinforced with high modulus carbon fibers and glass fibers. Previous work has shown that this region can be removed from the composite by using a sizing which is known to alter the nucleation density of the matrix. Therefore, the mechanical properties of samples were examined as a function of fiber sizing on a high energy surface using several techniques. A modified fiber debond test was used to measure interfacial shear strengths which gives information on composite adhesion. The macroscopic damping characteristics of both composites were analyzed using dynamic mechanical analysis and a new vibrational testing technique. Furthermore, the ultimate static properties and moisture up-take of the composites were measured using uniaxial tension and a simple weighing technique, respectively. Additional tests such as profilometry, scanning electron microscopy, thermogravimetric analysis, and differential scanning calorimetry aided in the understanding of the mechanical property results.

This work showed that the mechanical properties of semicrystalline thermoplastic composites change as the interphase is changed from a transcrystalline morphology to a spherulitic morphology. The interfacial shear strength decreases, while ultimate strength and toughness increases. Ultimate strains and moduli are only marginally affected, and the damping properties of the composites were found to decrease.

2. Background

This work involves the study of the mechanical performance of a composite system in terms of adhesion, ultimate mechanical, and dynamic mechanical responses. More specifically , how the interphase structure influences these properties is investigated. Therefore, an extensive review of these concepts and how they can be determined was performed.

2.1 Adhesion

The concept of adhesion can be described theoretically using principles of thermodynamics or in terms of adhesion performance [1-5]. Both are discussed in the subsequent pages, along with several theories used to describe the performance of a bond.

2.1.1 Thermodynamic

Thermodynamic adhesion is the atomic or molecular attractive force across an interface [1-5]. Because attractive interfacial forces of a solid are difficult to directly measure, the thermodynamic definition of adhesion is a qualitative, not quantitative, description explaining why materials that are bonded resist separation from one another [3].

The equilibrium condition for a surface in terms of the Gibbs' free energy (G) is defined as follows:

$$dG = \sum \quad {}_i dn_i + VdP - SdT + \; dA = 0 \qquad [2.1]$$

where $_i$ is the chemical potential of species i, n_i is the number of moles of species i, P is the pressure, V is the volume, T is the absolute temperature, S is the entropy, is the surface tension, and A is the surface area [6, 7]. Therefore, surface tension can be defined as the change in free energy with change in surface area as follows: [6, 7]

$$= \left(G/\ A \right)_{T,P,n} \qquad [2.2]$$

In common usage, the terms 'surface tension, 'surface free energy,' and 'surface energy' can be used interchangeably [4, 7] and will be done so in this document.

In order to determine the work of adhesion between two solids, which is the reversible work per unit area required to separate two phases in intimate contact to give two clean surfaces, theories have been borrowed from surface chemistry of liquids on solids. The Dupré equation states that the work of adhesion (W_a) must be equal to the free energy change of the system as follows:

$$W_a = {}_1 + {}_2 - {}_{12} \qquad [2.3]$$

where $_1$ and $_2$ are the respective surface tensions of the two phases and $_{12}$ is the interfacial surface tension between phase one and phase two [4-8].

The work of adhesion between a liquid and a solid is determined from equilibrium or quasi-equilibrium measurement of contact angles [3]. Figure 2.1 shows the balance of surface tensions from the contact angle experiment [7]. When θ = 0°, the liquid spreads over the surface of the solid and is said to completely wet the solid. Complete wetting occurs when the molecular attraction between the liquid and solid molecules is

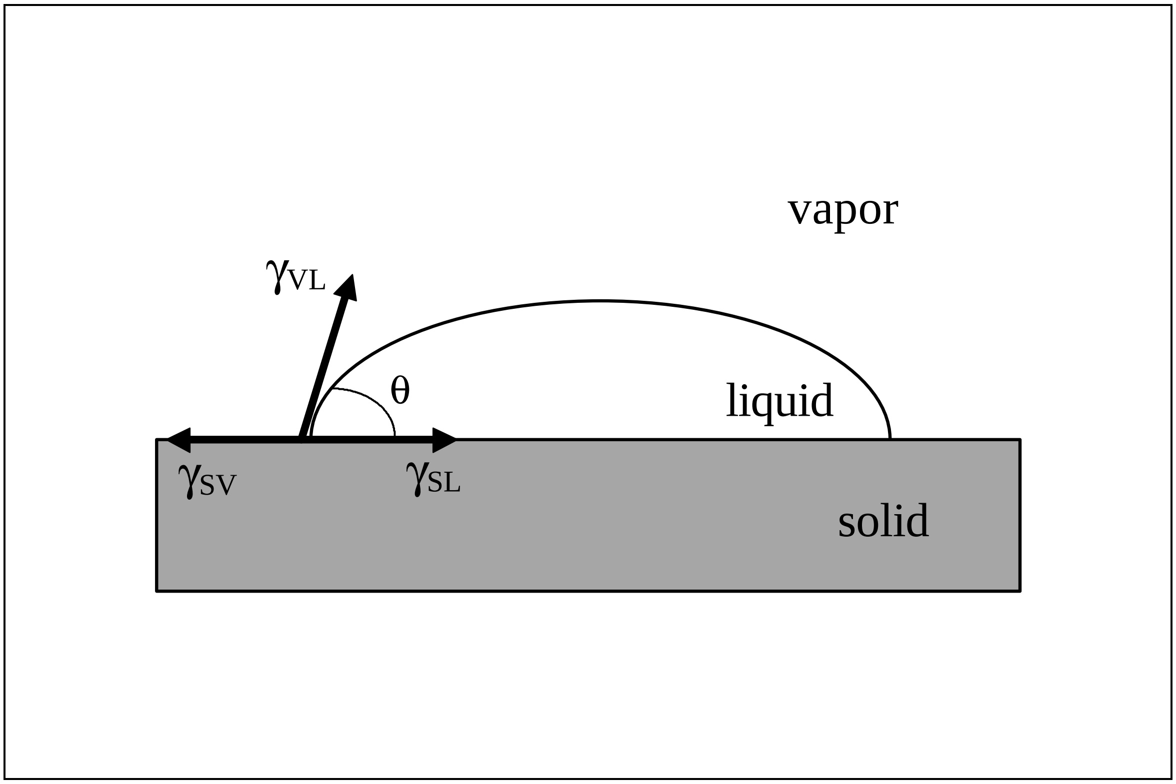

Figure 2.1 Balance of surface tensions in the contact angle experiment [5].

greater than that between similar liquid molecules [8]. Any angle above θ = 0° would indicate some degree of nonwetting, and a liquid with θ > 90° is said to not wet the solid at all.

The equilibrium contact angle is such that the total surface free energy of the system (i.e., $\gamma_S A_S + \gamma_L A_L + \gamma_{SL} A_{SL}$) is at a minimum. If the liquid making an equilibrium contact angle (θ) spreads an infinitesimal amount further to cover an extra area (*dA*) of the solid surface, the increase in the liquid-vapor interfacial area is *dA*cosθ and the change in the free energy of the system (*dG*) is given as follows:

$$dG = \gamma_{SL} + \gamma_L dA\cos\theta - \gamma_S dA \qquad [2.4]$$

where γ_S is the surface tension of the solid surface in equilibrium with the vapor of the wetting liquid, γ_L is the surface tension of the liquid, and γ_{SL} is the interfacial surface tension between the solid and the liquid [5]. If the system is at equilibrium, then the change in Gibbs' free energy is equal to zero (i.e., *dG* = 0), and the balance of surface free energies is expressed as follows:

$$\gamma_{SV} = \gamma_{SL} + \gamma_{LV}\cos\theta \qquad [2.5]$$

This equation is commonly known as the Young equation [4, 6].

When equations 2.3 and 2.5 are combined with one another, the work of adhesion can be expressed as follows:

$$W_a = \gamma_{LV}(1+\cos\theta) \qquad [2.6]$$

This equation is commonly known as the Young-Dupré equation [4]. More recently, there have been many other theories formulated to determine the work of adhesion, but only small improvements have been made. Therefore, those theories will not be discussed here.

2.1.2 Performance-based

Due to the inability to directly determine solid surface tensions and having to estimate them with thermodynamic theories, the adhesion between materials is commonly studied using adhesive performance. Adhesive performance is a measure of the mechanical resistance to separate a system of joined materials and is influenced by the follows parameters: surface chemistry of the materials, interface topography, the mechanical and viscoelastic responses of the materials, testing environment, testing rate, sample geometry, and such unknowns as the thermodynamic state of the system [2, 3]. Adhesive performance is a quantitative measure of the energy required to break an adhesive bond [3].

2.2 Adhesion Theories

All of theories that have been proposed to explain adhesion between solids can be grouped into five separate categories: 1) mechanical interlocking, 2) interdiffusion, 3) adsorption, 4) electrostatic attraction, and a 5) rheological phenomenon [3, 8, 9, 10]. To date, there is really no one single theory which can explain all adhesion-related phenomena. This is most likely due to the wide range of materials used as adhesives and substrates, and also because of the complex nature of adhesion itself.

2.2.1 Mechanical Interlocking - Hooking

The mechanical interlocking theory proposes that adhesion is due to irregularities on the substrates into which a polymeric adhesive may flow or around which the adhesive may solidify or cure. [8]. Hooking is further enhanced by increasing the substrate surface roughness or by promoting penetration of the adhesive into surface pores. To separate the adhesive from the substrate, energy must be expended and work done to deform and draw the material of lower compliance, provided that the surface features of the more rigid material are strong enough to withstand the separating force and do not fracture [9].

Although mechanical interlocking or hooking arises solely from the topography of the substrate surface, it seems to have a substantial effect on specific systems. For example, the adhesion in rubber bonded to anodized metals [11, 12] and textiles [13] seems to be dominated by this phenomenon. However, it must be noted that the means for altering surface topography (i.e., sand blasting, etching techniques, etc.) may induce additional adhesive mechanisms such as reactive surface groups, adsorption interactions, etc. [3].

2.2.2 Interdiffusion

The interdiffusion or diffusion theory, which was first introduced by Voyutskii, attributes adhesion to intermolecular entanglements across an adhesive/adherend interface [14]. This theory proposes that a liquid adhesive may dissolve and diffuse into the substrate or that polymer chains in a polymer/polymer bond may become entangled with one another across the solid interface. This would occur when the system is heated above the glass transition temperature of the two constituents. The extent of interdiffusion depends upon both the affinity for the different types of molecules for one another and also the mobility of diffusivity of the polymer chains within the other material.

2.2.3 Adsorption

The theory of adsorption assumes that adhesion is caused by physical and/or chemical adsorption interactions between molecules of the adhesive/adherend system [3, 9]. The interactions which may occur across an interface include the following: London dispersion forces, dipole/dipole interactions, dipole/induced dipole forces, hydrogen bonding, acid/base interactions, and covalent bonds [9, 15]. Since these forces are effective over distances in the range of several angstroms, the two surfaces must be in extremely close contact with one another if these types of interactions are to occur.

2.2.4 Electrostatic Attraction

Deryaguin proposed that electrostatic forces can develop at an interface between an adhesive and a substrate with different electronic band structures [16]. Electrons are transferred across and interface, inducing positive and negative charges that can attract one another. Again, in order for this type of bonding to occur, the surfaces must be in extremely close contact.

2.2.5 Rheological

To take a more engineering approach, Bikerman has stated that the performance of an adhesive joint is due to the mechanical properties of the materials used and the local stresses which arise in the adhesive/adherend bond [17]. This theory emphasizes the bulk properties of materials due to rare occurrences of a purely adhesive bond failure.

2.3 Interface v. Interphase

Although not inherently stated, what many of the above theories assume is that the interface in the adhesive/adherend joint is similar in response to the bulk material. In many cases, the chemical and physical nature and the morphology of the surface is assumed to be identical to that of the bulk, but almost always, this is an invalid assumption. First, the surface is an inherent ‘flaw’ of a material because the surface atoms are missing nearest neighbor atoms which alters the bonding with its remaining adjacent atoms. This idea clearly indicates that the chemical nature, and thus, surface energy will be different from that of the bulk material. Looking a few atomic distances into the material from the surface would show that the atomic positions are slightly different from that of the bulk material; this due to the altered bonding forces of the surface.

Not only do surfaces themselves contribute to variations from bulk properties, but processing and handling may also drastically change surface properties. [3, 10, 18]. Furthermore, in many materials, various chemical species may migrate to this surface region, and the migration of these chemical species or the substrate to which the material is bonded may have a profound effect on the microstructure or morphology of the near surface region, or what has been termed the ‘interphase.’

The term ‘interphase’ has been adopted to distinguish between an interface, or a defined plane where material and property changes are evident, and a region that has gradual transition of properties from one material to another. Also, the concept of interphase has been used to describe systems that have an intermediate morphology between that of the two materials being bonded together. Sharpe defined this region or the interphase “as a region intermediate to two phases in contact, the composition and/or structure and/or properties of which may be variable across the region and which also may differ from the composition and/or structure and/or properties of either of the two contacting phases” [3, 10]. Herrera-Franco and Drzal illustrated the complexity of the interphase found in fiber reinforced polymer composites using the schematic illustration in Figure 2.2 [19]. The interphase region here is characterized by the fiber morphology, fiber topography, fiber surface chemistry, and adsorbed material or coatings on the fiber, and by the properties of the matrix in close proximity to the fiber surface.

2.3.1 Transcrystallinity

2.3.1.1 General

As mentioned, an interphase may have a completely different morphology from that of either of the two materials being bonded together. In particular, in many reinforced thermoplastic polymer composites, an interphase which has been termed the

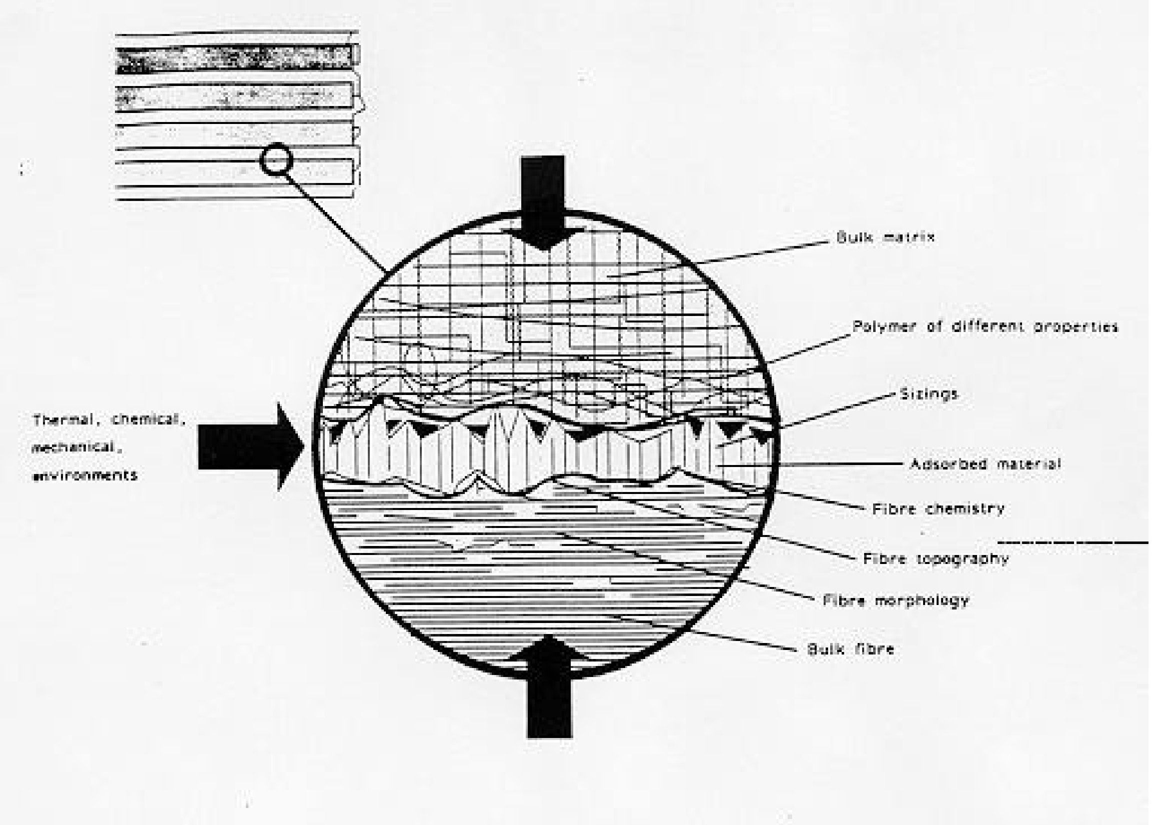

Figure 2.2 The complexity of characteristics of the fiber/matrix interphase in a composite system [19].

transcrystalline region can be found. The formation of this region is very system and thermal history specific, and it has a morphology completely different from that of the bulk matrix material. A micrograph of this region is shown in Figure 2.3.

Although transcrystallinity is of importance today in many fiber reinforced thermoplastics, it was first found in the early 1950's in other systems. [20-24] Barriault and Gronholz [21] reported that extruded nylon 66 transcrystallizes under nearly all conditions except severe quenching. This, they believed, indicated that a nucleating agent is not required and proposed that a temperature gradient is sufficient to induce a high nucleation density on the surface. Furthermore, Eby [22] reported that a transcrystalline surface layer developed in polyethylene when the polymer was crystallized under a temperature gradient. It was also stated that the thickness of this layer could be increased by increasing the temperature gradient between the surface and the interior of the melt.

Studies in the late 1960's and early 1970's expanded upon these findings. Fitchmun and Newman [25] studied samples of polypropylene produced by compression molding, and the major variables in this process were mold surface, melt temperature, cooling rate, and crystallization temperature. The focus of the study was how these variables influence the surface structure. Initially, they studied the influence of melt history and found that it did not induce transcrystallinity but the melt temperature must be sufficient enough to remove the thermal history of the polypropylene which influences the spherulitic growth of the polymer. They also

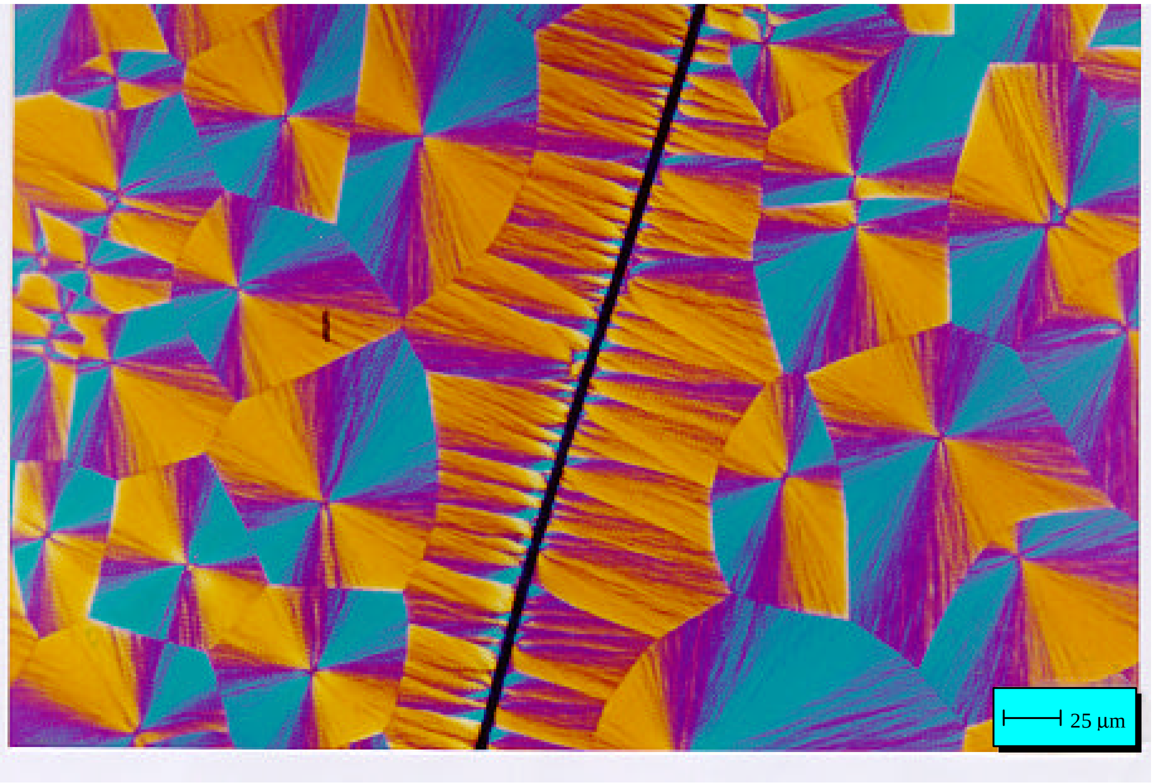

Figure 2.3 The transcrystalline interphase in a high modulus carbon fiber reinforced nylon 66 composite [51].

found that a temperature gradient itself was not an effective procedure for the development of transcrystallinity in polypropylene when molded against oxidized aluminum. However, when polypropylene was molded against Mylar, they found that with moderate cooling rates, the surface morphology changed from spherulitic to transcrystalline. Furthermore, the thickness of the zone was controlled by the cooling rate. Finally, they found that the crystallization temperature has a profound influence on surface morphology. For instance, when polypropylene is crystallized in contact with Teflon at 125°C, transcrystallinity forms, but with a crystallization temperature of 118°C, small spherulites formed uniformly throughout the sample. Furthermore, at elevated crystallization temperatures, the transcrystalline region formed when polypropylene was in contact with the oxidized aluminum surface.

Huson and McGill [26] also studied transcrystallinity in polypropylene which was in contact with a poly(ethylene terephthalate) substrate. They concluded that the transcrystalline growth in this system cannot be ascribed to the surface energy, chemical composition, crystal morphology, or moisture content of the substrate. Rather it was shown that the topography of the sample plays a major role. When the substrate was very active (ideal topography) it would cause transcrystallinity regardless of the rate of cooling. For less active substrates, rapid cooling may be essential for transcrystalline growth to occur. Furthermore, they observed channels or cracks that occurred as a result of the spherulitic growth of the polypropylene, and they suggested that when these flaws present in the surface of crystalline polymers are of a suitable size, they allow a degree of prealignment of polymer chains leading to preferential nucleation at the surface.

Transcrystallinity was not only found in polypropylene but also in several other systems. For instance, Lovering [27] showed that transcrystallinity had a pronounced effect on x-ray spectra obtained by the reflection technique, but little or no effect on transmission spectra of *trans* 1, 4 polyisoprene. This was due to the fact that the reflected x-rays are affected only by the surface layers of the reflecting material. Luongo [28] studied the orientation effects in transcrystalline films of polyethylene using polarized infrared spectroscopy with varying angles of incidence. It was found that the average orientation of the unit cells in the transcrystalline structure to be such that the a-axes were predominantly parallel to the surface of the films, and the b-axes were predominantly perpendicular to the surface. Similar results were established by Weinhold et al. [29] who studied the transcrystallization of poly(vinylidene fluoride) (PVDF).

2.3.1.2 Fiber-reinforced composites

Although transcrystallinity can be found in many different systems, fiber reinforced composites are of special interest for this study. The early 1980's was the beginning of study for such systems. For instance, Burton and Folkes [30] studied the spherulitic growth at the interface between fibers and matrix in reinforced nylon 66. The fibers that were used were carbon, Kevlar, and glass, with the carbon fibers having a series of surface treatments and coatings. They found that the production of transcrystallinity is strongly dependent on the type of fiber (Type I versus Type II or Type A carbon fibers, glass fibers, and Kevlar). The surface treatment of carbon fibers and the application of coatings and coupling agents had little or no effect. Furthermore, the results showed that transcrystallinity does not occur easily in injection moldings other than by remelting them. Ishida and Bussi [31] added polyethylene fibers to a poly(e-caprolactone) melt and found that transcrystallinity is formed on the fiber surface due to the high degree of epitaxial matching between the fiber and the matrix.

Avella et al. [32] primarily reevaluated the study performed by Fitchmun and Newman, but they studied the effects of Kevlar fiber on polypropylene instead of molding surfaces such as Teflon. They investigated the nucleating ability of the fibers, and the presence of the transcrystalline region was related to crystallization parameters such as crystallization temperature, melt precrystallization temperature, and residence time at precrystallization temperature. The crystallization temperature influenced the occurrence of transcrystallinity, and changed the surface morphology from transcrystalline to spherulitic, with increasing crystallization temperature. When the annealing temperature in the melt and the residence time in the melt was increased, the number of nuclei on the fiber surface was drastically lowered. In contrast, the growth rate and the melting temperature of the transcrystalline phase was found to equal those of bulk-nucleated spherulites. The transcrystallinity phenomenon observed was related to the fact that some polypropylene crystalline residues can survive after melting in the numerous imperfections present on the surface of the Kevlar fibers and act as self-seeded nucleation sites.

He' and Porter [33] studied the melt transcrystallization of polyethylene on high modulus polyethylene fibers. They found that the structural similarity of the matrix and the fiber lead to transcrystallization of the HDPE matrix on the PE fiber surface, even in the absence of fiber coatings (nucleating agents). The transcrystalline growth consisted of an inner and an outer zone. Huson and McGill [34] studied the effect of transcrystallinity in a polypropylene matrix reinforced with copper fibers. It was shown that the transcrystalline zone allows thinning of the fiber in the matrix up to the point at which compressive forces created by the shrinkage of the polymer around the fiber on cooling are removed and fiber pullout occurs.

Devaux and Chabert [35] studied the non-isothermal crystallization of glass fiber reinforced polypropylene. In this system, it was shown that a transcrystallization region never occurred when the glass fibers were in a quiescent state. Rather, a shear stress applied to the glass fibers below the melting temperature of the polymer caused a particular crystalline superstructure (transcrystallinity) adjacent to the fiber to appear. They also added organic fibers to polypropylene, and the presence of a transcrystalline phase was always observed adjacent to these fibers. They indicated that the origin of the transcrystalline region in the presence of the organic fibers was not the same as the crystallization observed when a shear stress was applied to the glass fibers. In the case of the organic fibers, transcrystallinity was directly linked to the topography of the fibers. This was verified by the fact that when silicon oil was deposited on the organic fibers, transcrystallinity did not appear. Devaux and Chabert suggested that the transcrystalline superstructure is probably due to the multiplication of macromolecular entanglements adjacent to the fibers. These entanglements help play the role of nucleation sites constrained to develop in one direction, because of their high density. This was confirmed by the fact that when a single glass fiber is pulled out during crystallization, the transcrystallized superstructure also appears in the region out of which the fiber was pulled. From this premise, they distinguished between this superstructure and a transcrystallization for which the nucleation occurs actually on the fiber. Later, Devaux et al. [36] constructed a simulation of crystalline growth fronts in the polypropylene composites.

Xavier and Misra [37] also studied the influence of glass fiber content on the morphology of polypropylene composites, but these were injection molded. They concluded that the fiber concentration exerts an enormous influence on the morphology of the composites. It was found that with the rise of fiber concentration, the skin-core structure of the composite gradually disappeared. Furthermore, the spherulitic size decreased while transcrystallinity increased with increasing fiber content.

In more recent studies of composite systems, fibers have been added to high performance polymers, and the results are very similar to those mentioned thus far. For example, Lee and Porter [38] studied the crystallization of poly(etheretherketone)

(PEEK) in carbon fiber composites. They found that the carbon fibers serve as a nucleating agent for PEEK, and the number of ordered regions or nuclei in PEEK decreased as the total melt-annealing time is increased. Reducing the number of nuclei in the matrix favored PEEK transcrystallization on the carbon fibers, which made a stronger interfacial bond. Furthermore, Tung and Dynes [39] investigated the effect of processing conditions on the morphology of PEEK/carbon fiber composites. A two-stage crystallization process was found in samples quenched at low rates (i.e., <5°C/min.). Crystallinity, spherulite size, and orientation were also affected by the quenched rates, with high crystallinity, large spherulites, and transcrystallinity being observed in very slow quenched samples. Reinsch and Rebenfeld [40] analyzed the crystallization processes in poly(ethylene terephthalate) (PET) as modified by fiber reinforcement. It was found that the crystallization rate and glass transition temperature of PET was strongly affected by the fibers. Furthermore, the degree of crystallinity of PET was independent of crystallization temperature and the presence of fibers.

In addition, systems composed of poly(phenylene sulfide) (PPS) reinforced with carbon fibers was also scrutinized. Lopez and Wilkes [41] studied the effects of crystallization temperature, molecular weight of the polymer, and type of carbon fiber and its surface treatment on the nucleation behavior of PPS. They reported that lowering the crystallization temperature of PPS induced transcrystallinity because of two possible reasons: differences in heat transfer coefficients and the different thermal expansion coefficients of the fiber and the polymer. Again, the idea of cooling rate is addressed, and in this study it was found that as the cooling rate decreased, the nucleation density at the fiber surface increased; a contradiction to the work mentioned earlier from Fitchmun and Newman. Different fibers showed a change in the nucleation efficiency of the transcrystalline region, and they attributed this phenomenon to either the chemical composition of the fiber surface, the topography or the fiber surface, the surface energy of the fiber surface, or a combination of all these factors. Also the surface treatment of the fibers was changed, and as the value of the polar component of the surface energy of the surface treatment was increased, the nucleation efficiency of the fiber was lowered. Desio and Rebenfeld [42] had similar findings. They concluded that the transcrystalline region in PPS composites is not only fiber-specific but also strongly dependent on the surface treatment. Finally, Lopez and Wilkes showed that transcrystallinity is not favored in higher molecular weight systems due to the fact that the higher molecular weight polymer has a high nucleation density. These results paralleled those found by Folkes and Hardwick [43] who studied the molecular weight dependence of transcrystallinity in fiber reinforced polypropylene.

2.3.1.3 Nylon 66 reinforced with glass & carbon fiber

As can be seen, the transcrystalline region is found in many systems and occurs due to a number of different reasons that seem to be system specific. Therefore, a study of previous work on nylon 66 reinforced with glass fiber and carbon fiber will be conducted due to its applicability of the work presented in this document. There have been many studies of nylon 66 reinforced with glass [44-50] and carbon fibers [47, 49, 51-55], but only a few directly investigate the interphase morphology and its influence on the mechanical performance of the composite. In addition, there have been several studies involving Kevlar reinforced nylon 66 [51, 54], but again, this particular composite is not under investigation in this work.

Shiao et al. [44] investigated the effects of glass fibers and annealing on the microstructure of glass fiber reinforced nylon 66. Among their conclusions, they observed no transcrystallinity at the glass-fiber interfaces in the injection molded nylon 66 composites. The effects of transcrystallinity on the mechanical properties of glass-filled nylon 66 would therefore be negligible. However, transcrystallinity was observed to grow along the glass fibers in melt-crystallized nylon 66 thin composite films. Shaio et al. [44] stated that the absence of the transcrystalline region in the injection molded composites was most likely a result of the significant reduction of matrix spherulite size which was also found by Bessell and Shortfall [56]. This reduction in spherulitic size was due to sample thickness and the presence of the glass fibers. In addition, they also mention that a slower cooling rate, which Thomason and Van Rooyen [57] showed to affect transcrystalline formation, in the injection molded composites may have inhibited transcrystallinity. In an additional paper, Shaio et al. studied the fracture toughness of the glass filled nylon 66 composite as a function of fiber volume fraction and annealing time. However, in this paper they used injection molded composites, and due to absence of transcrystallinity in these composites found in the earlier paper, they assumed that the transcrystalline region had no effect on the composite’s mechanical properties.

Sato et al. [46] investigated the microfailure behavior of glass reinforced nylon 66 composites. Scanning electron microscopy was carried out on the surface of the composites under load to directly observe fracture behavior. They found interfacial microfailure at the fiber tips and along the fiber sides. The interfacial failure was caused by the cohesive failure of the matrix very near the interface and not by adhesive failure at the interface. Unfortunately, the morphology in this region was not directly investigated, however, three methods to suppress this strong nylon/glass bond in order to increase composite toughness were mentioned.

As mentioned, there have been many works studying the mechanical properties of the carbon fiber reinforced nylon 66 composite, but very few focus upon the interphase, its formation, and its role in composite mechanical performance. Previous work conducted by Clark [51] focused extensively upon the interphase in carbon fiber/nylon 66 composites. Clark observed that under a specific thermal history transcrystallinity formed in the carbon fiber/nylon 66 composite. Furthermore, the study showed that this interphase could be removed from composite by adding an additional polymer to the composite either as a matrix diluent or fiber sizing. The additional polymer, poly(vinyl pyrrolidone) [PVP], removed the transcrystalline region by affecting the surface energy of the fiber, thus reducing the number of nucleating sites caused by the fiber surface. If added as a diluent, at high enough concentrations the diluent seemed to migrate to the fiber surface and dampen nucleation, whereas if the PVP was used as a fiber sizing, the dampening effect was enhanced. Therefore, the interphase could be ‘tailored’ depending upon how much and where the PVP was added. Ultimately, adding the PVP both as a diluent and a fiber sizing at high enough concentrations removed the transcrystalline region completely from the composite. In addition, Clark altered the PVP molecular weight and studied its effect on transcrystallinity, however only slight shifts in critical concentrations for maximum nucleation dampening were found.

Moving to the forefront in trancrystalline investigation, Klein and Marom [52] have conducted several studies on many systems, including the nylon 66/carbon fiber composite. They investigated the crystallization behavior of nylon 66 in the presence of carbon and aramid fibers under isothermal and non-isothermal conditions. Hot-stage optical microscopy revealed that a high nucleation density along the reinforcements produced transcrystallinity. Being a nucleation-controlled process, the transcrystallization depended heavily on the thermodynamic conditions such as crystallization temperature and cooling rate. With the use of differential scanning calorimetry, the crystallization process was studied and the influence of two main parameters - the presence of fiber and cooling rate - was analyzed. The fibers were found to behave like a giant nucleating site and to enhance the rate of crystallization of nylon 66. Hot-stage microscopy confirmed this by indicating that the system favored transcrystalline formation over bulk spherulitic formation. Finally, they concluded that the presence of such an interphase affected the thermal expansion of the composite.

2.4 Fiber/matrix adhesion & tests

There is general agreement that the degree of adhesion between the fiber and the matrix and the nature of this interphase, whether is be of a different chemical structure or morphology, has a major influence on the mechanical properties of a composite. [19, 58]. Therefore, depending upon what composite property is needed, the fiber/matrix adhesion will need to be altered accordingly. For strength, “good” adhesion is required, whereas, for toughness, intermediate adhesion is necessary.

A number of mechanical tests have been formulated which determine the effective adhesion and stress transfer from the matrix to the fiber in a composite. Tests which measure fiber/matrix interface strength include tests on single-fiber composites, and those conducted on real composites [59]. The most commonly used tests on single fiber composites are the fiber fragmentation test, the microdebond test, and the fiber debond test. The short beam shear test, iosipescu shear test, off-axis tensile test, and indentation tests are typical experiments used to test adhesion in real composite samples. The geometries of all of these tests are shown in Figures 2.4, 2.5, and 2.6 [19, 59-61].

In the single-fiber fragmentation test, a single fiber is embedded in a dogbone shaped tensile sample, and the sample is strained in the fiber axial direction to near its

a) Fiber debond

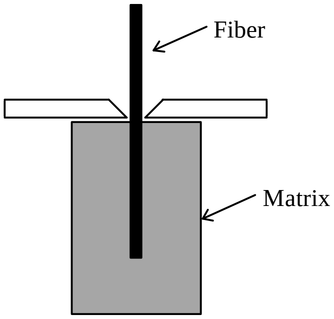

b) Fiber Fragmentation

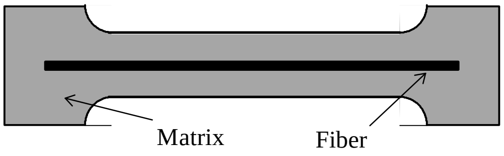

c) Microbond

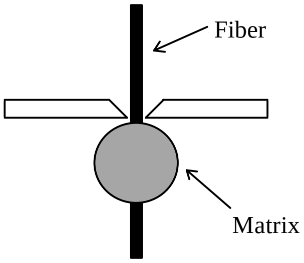

Figure 2.4 Mechanical tests used to determine τ_{avg} using single fiber composites: a) Fiber debond, b) Fiber fragmentation, and c) Microbond [19, 59].

a) Iosipescu

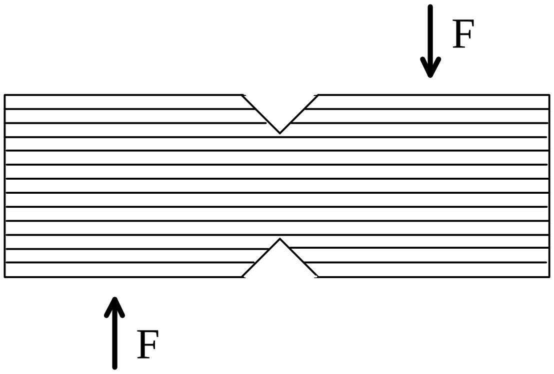

b) Short beam shear

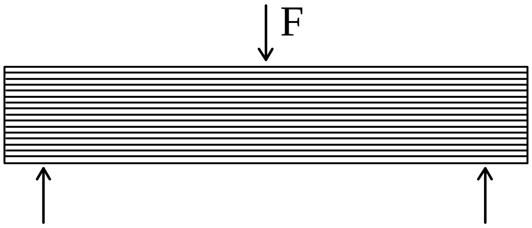

c) Off-axis

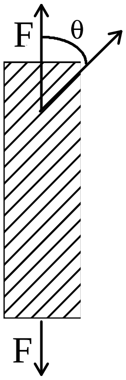

Figure 2.5 Mechanical tests used to determine interface strength of real composite samples: a) Iosipescu, b) Short beam shear, and c) Off-axis tensile [19, 59].

a) Micro-indentation (single filament or real composite)

b) Meso-indentation

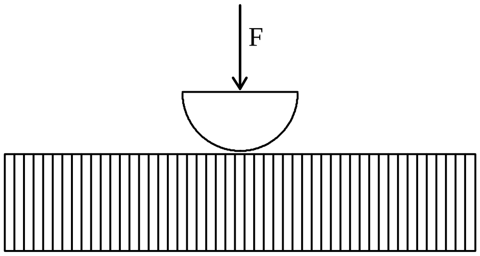

Figure 2.6 Other mechanical tests used to determine interface strength of composite samples: a) Micro-indentation and b) Meso-indentation [19, 60, 61].

point of rupture. Then the fiber fragment lengths that remain inside the specimen are measured. This imposes several limitations on what systems this technique can be used because the matrix must be translucent, and it must have a relatively high yield strength. Upon measuring the fiber lengths, the fiber/matrix shear strength is calculated by applying Weibull statistics to the distribution of fragment lengths [19, 59]. In a fiber debond test, the end of a single fiber is embedded in a resin matrix with the fiber axis perpendicular to the surface of the matrix. When the resin is an axi-symmetric resin drop, the debond test becomes the microbond test. Therefore, similarities between test methods and analyses can be drawn between these two methods. The average interfacial shear strength is measured in both of these tests by measuring the force required to pull the fiber from the matrix or bead [19, 59].

In the iosipescu shear test, a state of uniform pure shear is achieved when the test section of the specimen is loaded as shown in Figure 2.5 (b) [62]. The fibers can be aligned either in the direction or perpendicular to the direction of the applied force. In off-axis tensile tests, unidirectional composites are subjected to an off-axis tensile stress by varying the angle (θ) between the direction of the applied load and the fibers, i.e., 0° and 90°. A unidirectional composite specimen with a small span-to-depth ratio is loaded in such a way that failure occurs in a shear mode parallel to the fibers. The fibers are oriented in the direction perpendicular to the axes of the support [63]. The short beam shear test is used to estimate the interlaminar shear strength in a composite [64].

Indentation tests may also be performed using either a microscopic indenter or a macroscopic indenter. A composite specimen is sectioned perpendicular to the fiber axis, and the surface is polished flat. In the micro-indentation experiment, the end of a single fiber is compression-loaded with a very fine diamond tip, and the fiber is debonded from the matrix [60]. Micro-indentation tests can be performed on real composite sections [19, 65] or on single filament composites [66]. The meso-indentation test is more of a macroscopic test in that the spherical indenter loads several fibers at a time [61].

Each of these test methods have inherent problems that limit its applicability as a universal test for characterization of interfacial shear strength [67]. For example, Herraro-Franco and Drzal performed iosipescu, short beam shear, ± 45° tensile, micro-indentation, single filament, and microbond tests on an epoxy reinforced with AU-4 and AS-4 carbon fibers [19]. Furthermore, Lesko performed the meso-indentation test on the identical system. From all the tests combined, there was quite a bit of scatter in the data, but all tests revealed that the AS-4/epoxy system has a higher interfacial shear strength.

Although there is extensive literature covering each of the testing procedures mentioned, only the fiber debond test will be discussed in detail since it is the primary testing procedure used in this work. Reasons for choosing this particular test method will be made evident in the experimental chapter.

2.4.1 Fiber Debond

In the fiber debond test, a single fiber is partially embedded in a matrix of a given geometry. An increasing force is applied to the exposed end of the fiber until the fiber is pulled completely from the matrix. Assuming that the shear stress is uniformly distributed along the embedded length, L, of the fiber, the average of the interfacial shear strength, , can be calculated as follows:

$$= \frac{F_d}{dL} \qquad [2.7]$$

where F_d is the force required for fiber debonding and d is the fiber diameter [59].

Although a fairly simple test to describe mathematically, the fiber debond test has disadvantages. In a system where small diameter fibers are used, i.e., < 100 μm, and where the adhesion is quite high, very small embedded lengths (i.e., < 150 μm) must be used to ensure fiber debond instead of fiber breakage. This leads many researchers to using the microdebond technique, but this technique also has its limitations such as inability to control sample thermal history, of which do not allow it to be used in this study. Furthermore, the microdebond technique produces data with large scatter.

2.4.1.1 Theoretical analysis

Désarmot and Favre [68] state that in spite of the unrealistic character of the single fiber debond test when compared to the complexity of a realistic composite, much information can be derived that has to do with the most fundamental aspects of the fiber/matrix mechanical interaction [68]. The shear stress in the debond test has been analyzed using a shear lag approach and a fracture energy approach. The analyses presented can be applied to either data from the fiber debond test or the microdebond test.

2.4.1.2 Shear lag approach

The shear lag analysis proposed by Greszczuk shows that the elastic interfacial shear strength ($_x$) varies as a function of the depth (x) as described in Figure 2.7 [59, 68, 69]. (Note: This is also a function of how the the sample is held. For example, if the end of the matrix was 'grabbed' instead of using a vice at the fiber end, the $_x$ would be highest at the 'grabbed' matrix end.) Assuming that debonding occurs catastrophically, the shear stress at any point x is given by:

$$_x = \quad L\left[\coth(\ L)\cosh(\ x) - \sinh(\ x)\right] \qquad [2.8]$$

where t is the average interfacial shear strength found in equation 2.7, and is an elastic coefficient defined as:

$$= \frac{2G_i}{b_i r_f E_f} = \frac{2G_m}{r_f^2 E_f \ln\left(R/2r_f\right)} \qquad [2.9]$$

where b_i is the thickness of the interfacial layer, G_i is the shear modulus of the interface, G_m is the shear modulus of the matrix, E_f is Young's modulus of the fiber, and R is the radius of the matrix involved by the shear stress. Therefore, at $x = 0$, the shear stress reaches its maximum value which mathematically is

$$_{\max} = \quad L\coth(\ L) = \frac{F_d}{d}\coth(\ L) \qquad [2.10]$$

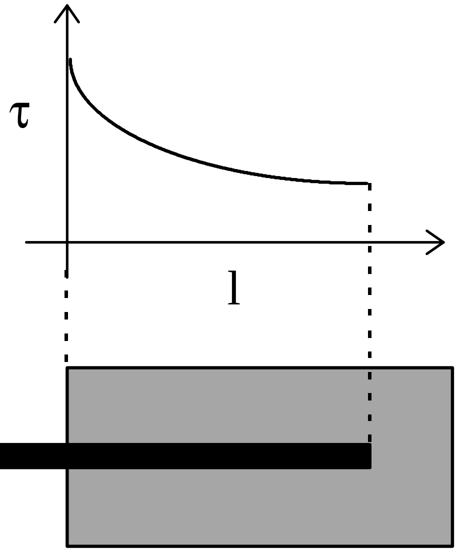

Figure 2.7 Schematic illustrating the change in interfacial shear strength versus embedded length [59].

However, normally when performing a fiber debond test, the force required to pull the fiber from the matrix is measured, and this is used to calculate the average interfacial shear strength. If the above equation is rearranged, the measured force can be found in terms of , which gives:

$$F_d = 2\ r_f \tanh(\ L)\frac{{}_d}{n} \qquad [2.11]$$

where the term n is described as:

$$n^2 = \frac{E_m}{E_f(1+\ {}_m)\ln(R/r_f)}. \qquad [2.12]$$

Here, $_m$ is the Poisson's ratio of the matrix. Reviews of analyses based on this shear lag model have been written by Herrera-Franco and Drzal [19] and Désarmot and Favre [68].

2.4.1.3 *Fracture energy approach*

Another approach to describing the fiber debond model mathematically is the fracture energy approach. This model is based on the fact that the fiber debond test is sudden and catastrophic. In this case, the total interfacial fracture energy (U_t) is equal to the sum of the energy stored in the fiber (U_f) and in the matrix (U_m):

$$U_t = U_f + U_m = 2\ r_f L G_a \qquad [2.13]$$

where G_a is the interfacial fracture energy per unit area [70-73]. Using this concept, the debonding force, F_d can be found as follows:

$$F_d^2 = 4\ {}^2 r_f^3\ L E_f G_a \tanh(\ L) \qquad [2.14]$$

where is described as:

$$ = \frac{2G_m}{r_f^2 E_f \ln\left(R/r_f\right)}. \qquad [2.15]$$

However, at long embedded lengths, tanh (L) ≈ 1, and the debonding force is found to be proportional to the square root of the fiber embedded length, L. Therefore, equation 2.14 can be rewritten as:

$$F_d = 2 \ r_f \sqrt{\ r_f L E_f G_a} \propto \sqrt{L} \qquad [2.16]$$

where all the other variables are material properties of the materials being used in the composite. On the other hand, at short embedded lengths, tanh (L) ≈ L, and the debonding force is then proportional to L as follows:

$$F_d = 2 \ r_f \ \ L\sqrt{r_f E_f G_a} \propto L \, . \qquad [2.17]$$

Penn and Lee expounded upon this fracture energy approach by introducing the concept of an initial crack length [74]. Furthermore, Jiang and Penn expanded this analysis further by dividing the fiber debond sample into three regions as shown in Figure 2.8, and they added a matrix compression term and a work of friction term which originates between the debonded fiber and matrix [75]. An energy balance was applied to the interfacial crack propagation process. Some of the strain energy (U) stored in the system upon loading and released during debonding propagates a crack through the bonded interface and some is dissipated by friction. This is defined as:

$$\frac{1}{2 \ r} \frac{U}{a} \geq G_c + \frac{1}{2 \ r} \frac{W_f}{a} \qquad [2.18]$$

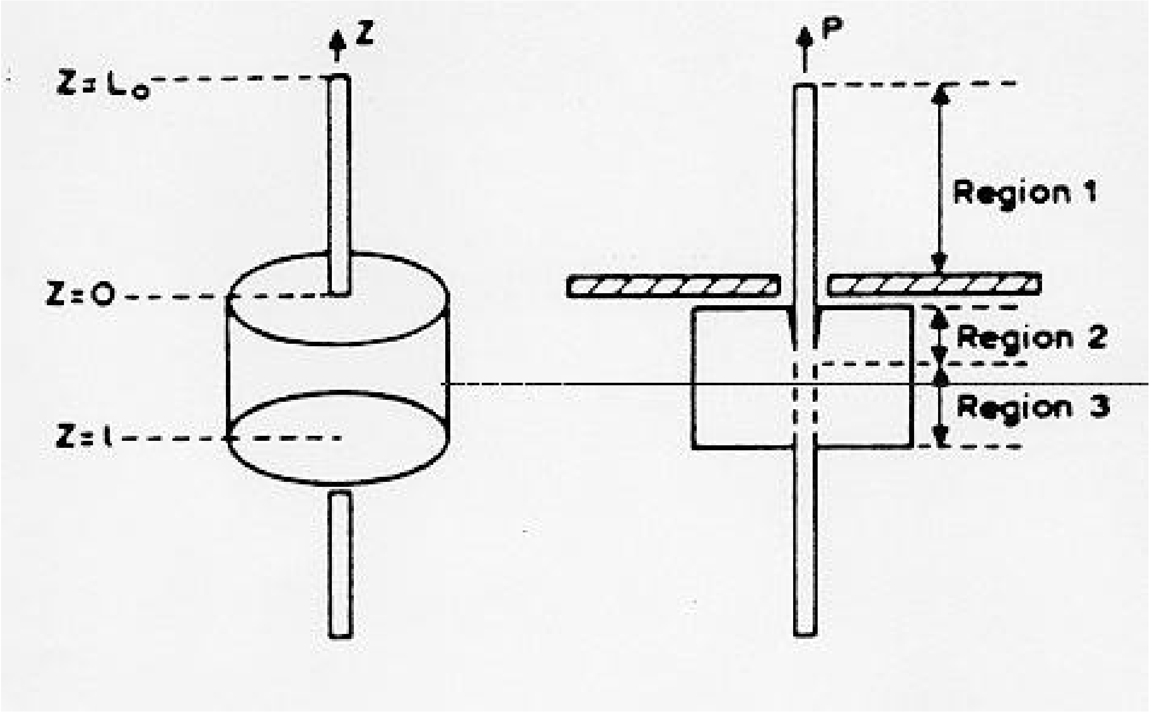

Figure 2.8 Schematic of the single fiber debond test specimen [75].

where U is the total elastic strain energy stored in the system, W_f is the work of friction, G_c is the interfacial fracture energy per unit area, and a is the initial crack length. The analysis is very mathematically rigorous and will not be shown here, but can be found in appendix A. Studies by DiFrancia et al. [96, 97] also investigated this work of friction.

After completing the analysis, Jiang and Penn used their mathematical model to generate debonding versus embedded length curves, however the model did not accurately predict all experimental data. At long embedded lengths, the model fit quite well, but for small embedded lengths, the model overestimated the interfacial shear strength.

2.5 Composite mechanical properties

The particular composite that is studied in this work is a nylon 66 and nylon 66/PVP blend matrix reinforced with both E-glass fibers and carbon fibers. Therefore, it is of particular interest to review works that have investigated these materials specifically.

2.5.1 Matrix - Nylon 66 & PVP

There have been numerous studies scrutinizing the crystallization behavior and mechanical properties of neat nylon 66. However, the focus of this document is on the mechanical properties of nylon 66 composites, therefore, it would be inappropriate to discuss papers involving these aspects of pure nylon. A detailed investigation of such findings can be found in the literature [51].

On the other hand, it is of importance to investigate the morphology of nylon 66 and that of the nylon 66/PVP blend. Two documents focus specifically upon this topic; the master's thesis of Srinivas and the master's thesis of Clark. Srinivas [76] was interested in the thermodynamics of the nylon 66/PVP blend and studied the crystallization behavior of nylon 66 and the nylon 66/PVP blend. In addition, glass transition and melting phenomenon shifts were analyzed. Furthermore, wide angle and small angle x-ray studies were conducted in order to characterize the crystal structure and spherulitic growth of nylon 66 and its alteration due to the presence of the PVP in the blend.

It was found that nylon 66 had a glass transition temperature around 50°C and a triple melting behavior. The addition of PVP showed an increase in the glass transition of the blend (only one T_g was found indicating the miscibility of nylon 66 and PVP at the molecular level), and subtlety effected the triple melting behavior of nylon 66; it changed the intensities of the three peaks. The x-ray data did not show any changes in the crystalline structure of nylon 66 due to the presence of PVP, nor was there any change in the long spacing. This indicated that the PVP was excluded to the amorphous phase of nylon 66. Similar projections were made by Keith et al. [77] in a paper where they studied the blending of poly(ε-caprolactam) with compatible polar diluents. At the end of this work, Keith et al. concluded that the PVP migrates to the crystal growth fronts of the nylon, thus causing banding in the spherulites, and is expelled to the amorphous phase.

Clark in his work studied the morphology of nylon 66, given a specific crystallization history, and that of nylon 66/PVP blends. He blended the polymers at very low diluent concentrations (i.e., < 7% by weight) and found drastic morphology changes due to the diluent. Figure 2.9(a) shows an optical micrograph of pure nylon 66 melt-crystallized at 235°C, and 2.9(b) shows that of a nylon 66/3% PVP blend. Note the dramatic increase in spherulitic size, resulting from the nucleation suppression of the PVP, and also the banding introduced. Clark continues in his study to show the effects of varying the molecular weight and concentration of the PVP. It was found that at concentrations of less than 3% PVP (by weight), spherulitic size increased up to ten-fold.

2.5.2 Fiber

In this study two different types of materials are used as reinforcements: high modulus carbon fibers and E-glass fibers. A typical stress-strain curve of these fibers and others used in composite reinforcement is shown in Figure 2.10.

2.6 Thermoplastic composites & adhesion studies

In all of the literature available in reference to adhesion studies, very few investigate composites consisting of thermoplastic matrices. Most studies analyze thermosetting composite systems because of the large number of commercially available adhesives and composites. However, there has been some research in comparing the use of different matrices, i.e., thermosetting versus thermoplastic, reinforced with carbon fibers, and it was found that where the thermosetting matrix

a) Nylon 66

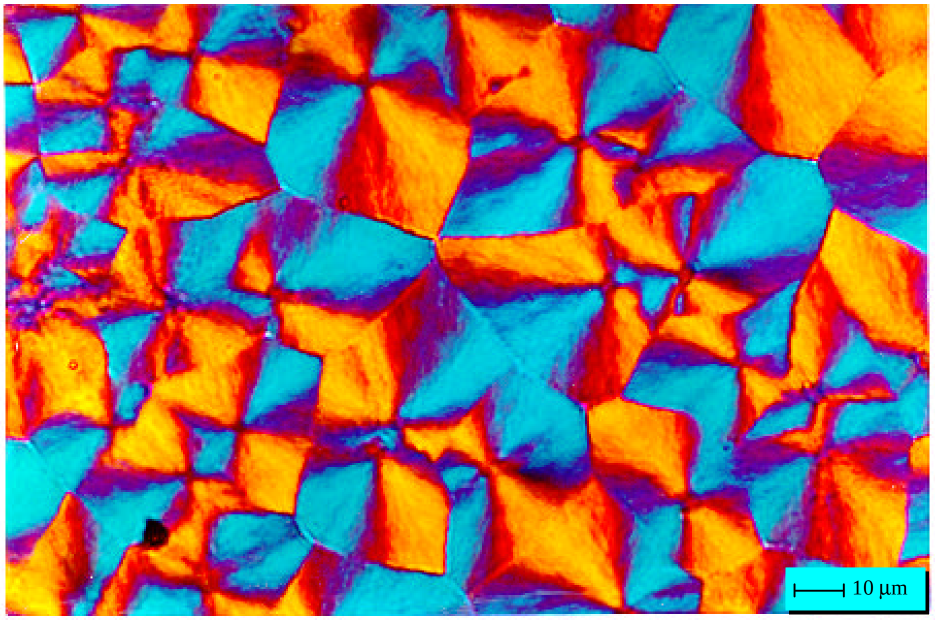

b) Nylon 66/3% PVP

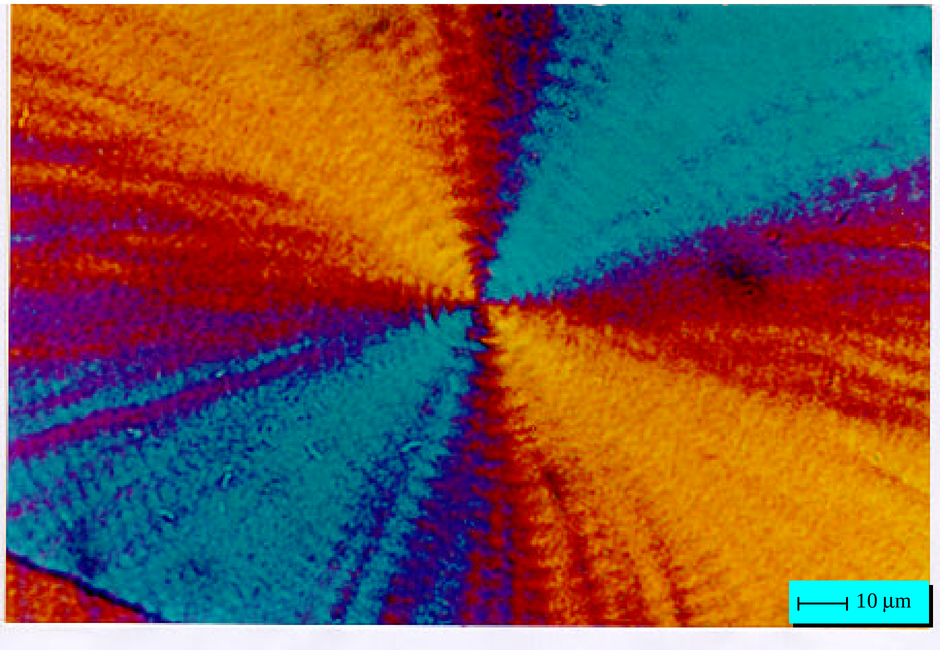

Figure 2.9 a) Nylon 66 cyrstallized at 235°C and b) Nylon 66/3% PVP blend crystallized at 235°C [51].

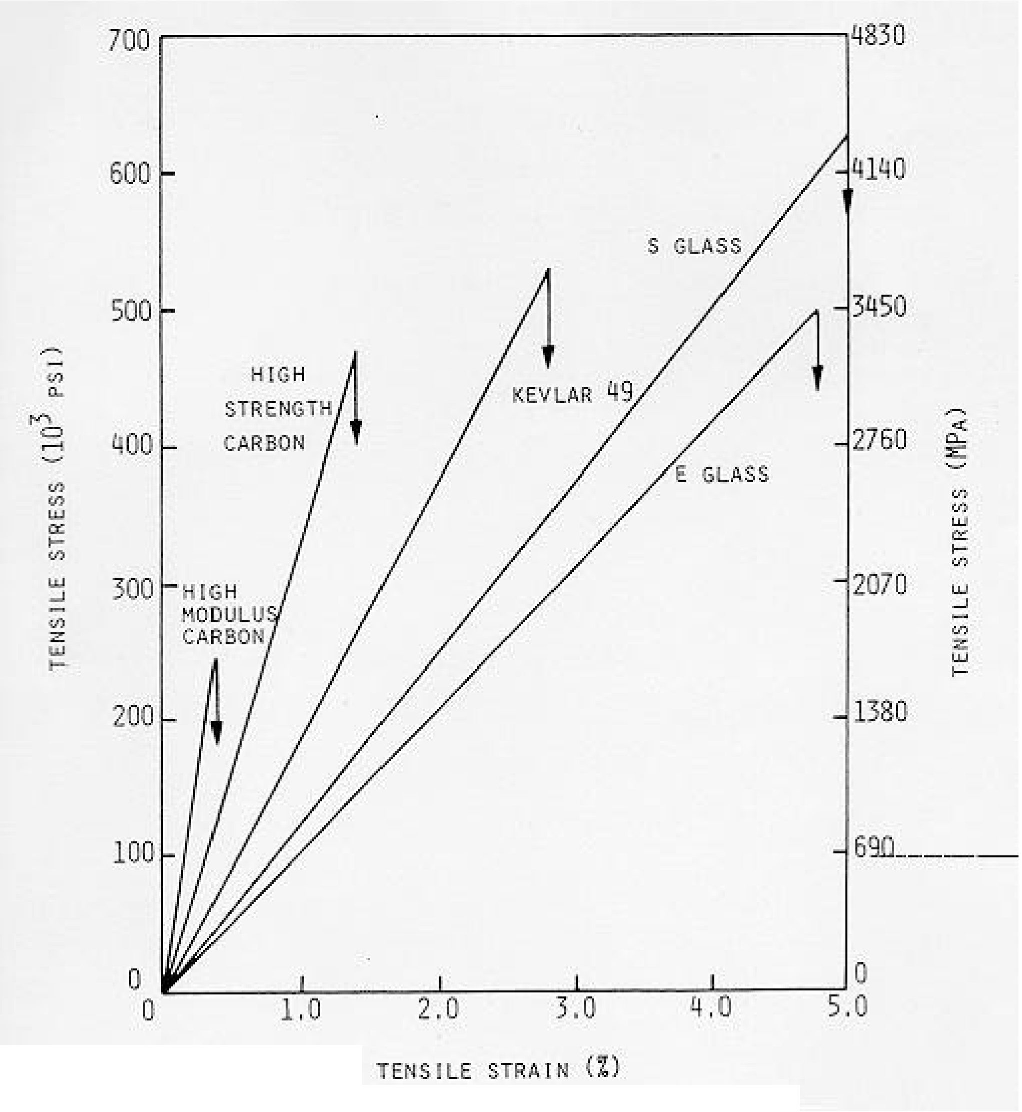

Figure 2.10 Tensile stress-strain diagrams for various reinforcing fibers [79].

showed good adhesion to the fibers, the thermoplastic matrix did not. This is not completely understood, but the difference in adhesion has been attributed to the fact that thermoplastic do not have functional groups that can covalently bond to groups on the fiber surface. In general, adhesion in thermoplastic composites is a function of the polymer chemistry, polymer morphology, and conditions under which the samples were prepared and tested.

Although not great in number, a few specific studies have investigated the adhesion in thermoplastic composites. Bascom et al. [78] found that conventional fiber surface treatments and various organic sizings had no influence on the adhesion in carbon fiber reinforced polycarbonate, but oxygen plasma treating improved the adhesion [78, 80].

Gaur et al. showed that acid plasma treating carbon fibers increased the adhesion in a carbon fiber/poly(phenylene sulfide) composite [81]. In addition, Bolvari and Ward [82] used a modified fiber fragmentation test to study the importance of acid-base interactions in carbon fiber reinforced thermoplastics and concluded that they attributed only to a portion of the fiber/matrix interfacial shear strength. Commercon and Wightman [83] found that the adhesion of poly(ethersulfone) to IM-7 carbon fibers was improved with an ammonia plasma treatment of the fibers and an annealing above the glass transition of the polymer.

2.7 Dynamic mechanical analysis of thermoplastic composites

2.7.1 General

Dynamic mechanical analysis (DMA) of polymeric and composite materials is one of the most powerful techniques for studying structure-property relationships in that the damping behavior of these materials is directly related to molecular structure. Therefore, before looking at specific studies, an overview of the theory behind DMA will be examined to thoroughly understand dynamic mechanical behavior.

DMA is a mechanical test that measures the response of a polymer to a sinusoidal or other periodic stress. The stress and resulting strain are generally not in phase, and from this, two quantities can be determined: a modulus and a phase angle or a damping term. Furthermore, these tests can be conducted over a wide temperature and frequency range to give information about a material's glass transitions, secondary transitions, and morphology.

Linear viscoelastic behavior of materials can be explored theoretically using several models. The earliest models used are the Maxwell element and Voight element. Each element is characterized by a relaxation or retardation time, and when subjected to a constant stress, the elements respond accordingly. More elaborate models include combinations of these two basic elements, and more recently, more advanced theories such as the Havriliak and Negami [HN] and KWW models have been devised to explain a polymer's response to DMA.

Dynamic results are given in terms of a complex modulus or compliance. The stress and strain are defined as:

$$= {}_{o}\sin(\ t+\ ) \qquad [2.19] \qquad \text{and} \qquad = {}_{o}\sin(\ t) \qquad [2.20]$$

where is the angular frequency, and is the phase angle. Then

$$= {}_{o}\sin(\ t)\cos\ + {}_{o}\cos(\ t)\sin\ . \qquad [2.21]$$

The stress can be considered to consist of two components: one in phase with the strain ($_{o}$ cos), and the other 90° out of phase ($_{o}$ sin). When these are divided by the strain, we can separate the modulus into an in-phase (or real) and out-of-phase (or imaginary) component. These relationships are:

$$= {}_{o}E'\sin(\ t)+{}_{o}E''\cos(\ t) \qquad [2.22]$$

where $E'=\frac{{}_{o}}{{}_{o}}\cos$ [2.23] and $E''=\frac{{}_{o}}{{}_{o}}\sin$, [2.24]

Using the expressions for the stress and strain in equations [2.19] and [2.20], the complex modulus can be expressed as:

$$E^{*}=\frac{}{}=\frac{{}_{o}}{{}_{o}}(\cos\ +i\sin\ )=E'+iE'' \qquad [2.25]$$

where *E'* is the storage (or real) portion of the modulus, and *E"* is the loss (or imaginary) portion of the modulus. This second term is a damping or energy dissipation term. Again, the angle that reflects the time lag between the applied stress and strain is , and it is defined by a ratio called the loss tangent or dissipation factor as follows:

$$\tan \quad = \frac{E''}{E'} . \qquad [2.26]$$

Tan , a damping term, is a measure of the ratio of energy dissipated as heat to the maximum energy stored in the material during one cycle of oscillation.

Much research has been done on the relationships between molecular parameters and the dynamic behavior of polymers. For instance, McCrum, Read, and Williams [84] have published a book which gives a comprehensive review of dynamic mechanical spectroscopy in relation to the molecular structure of polymers. A number of useful generalizations and interpretations on this subject can also be found in texts by Nielsen and Ferry [85, 86]. Takayangi has proposed other interpretations on the relaxation [87, 88], and more recently Boyer has reviewed molecular motions in amorphous and semicrystalline polymers with respect to the anelastic spectra [89, 90].

2.7.2 Specific systems

2.7.2.1 Nylon 66

Numerous polyamide materials have been studied using DMA [85, 86, 91, 93]. The classical work of Takayanagi [87] revealed the dynamic mechanical spectrum of nylon 66; however, this study is investigating the nylon 66 polyamide. One of the studies involving the DMA of nylon 66 was conducted by Bell and Murayama [92]. Figure 2.11 shows the dynamic mechanical spectrum of nylon 66 where three peaks can be discerned. The peak at approximately -150°C, -70°C, and 80°C are known as the γ, β, and α peaks, respectively. The γ peak is associated with very localized

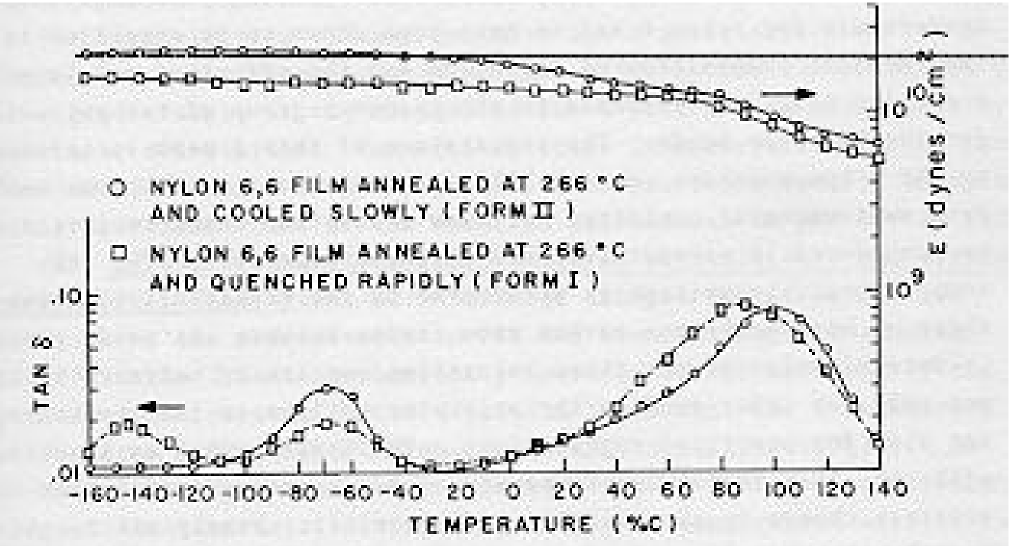

Figure 2.11 Temperature versus tan δ for nylon 66 [93].

"crankshaft" rotation of three or more methylene carbon atoms between the amide groups. The β peak is attributed to the amide groups in the amorphous region, and the α peak is believed to result from the rupture of the hydrogen bonds between polymer chains, giving rise to long-chain segmental motions in the amorphous region, i.e., the glass transition temperature of the nylon. In addition, the height of this peak is found to be a function of the percent crystallinity of the nylon 66, reinforcing the idea that this is the T_g of the material [92]. Marom et al. [52] have also studied nylon 66 using DMA, but they added a unique angle to the study: they compared samples of neat nylon with spherulitic morphology and spherulitic/transcrystalline morphology, and a sample of aramid reinforced nylon 66. They found the typical spectrum for spherulitic nylon 66, but in the sample containing transcrystallinity a loss of energy damping was found. This was attributed to presence of the trancrystalline region adding stiffness and reduced chain mobility. Furthermore, energy damping of the microcomposite was given by a rule of mixtures which sums the proportional contributions of the spherulitic matrix and transcrystalline region. Finally, there are several studies in the literature investigating the DMA behavior of nylon 66 in fiber form and the effect of moisture on nylon 66.

2.7.2.2 Reinforced nylon 66

Although the dynamic nature of nylon 66 is quite well known, only a few studies have researched that of a reinforced nylon. As mentioned above, Marom et al. [52] examined aramid reinforced nylon 66, but this current study is interested in glass fiber and carbon fiber reinforced nylon 66. Cinquin et al. [50] scrutinized the viscoelastic effect of glass reinforced nylon 66, and they found that a specific fiber sizing reduced the damping effect of the composite. This was attributed to a chemical bonding apparition caused by the sizing, therefore, increasing the interface stiffness which resulted in increasing the composite stiffness. Ishak and Berry [53] added short carbon fibers to nylon 66, and they observed the three peaks in the dynamic mechanical spectrum with a suspected amplitude decrease due to presence of the fibers. There have been previous studies of carbon fiber and glass fiber reinforced nylon 66, but these focused on other properties of the composite.

3. Experimental

3.1 Materials description

3.1.1 Polymers & solvents

A laboratory grade Nylon 66 powder (Zytel 101) and Zytel composite panels were obtained from E.I. DuPont, and two molecular weights of poly(vinyl pyrrolidone), PVP, were purchased from Aldrich Chemical Company (CAS #9003-39-8). The low molecular weight species had a molecular weight of ≈10,000 (denoted as PVP_{10}) and the other had a molecular weight of ≈ 360,000 (denoted as PVP_{360}).

Nylon 66 or poly(hexamethylene adipamide) is prepared from the condensation polymerization of hexamethylenediamine and adipic acid and has the following chemical structure

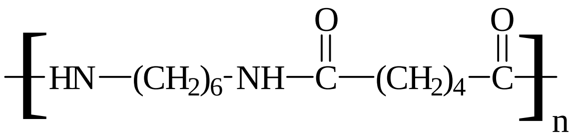

$$\left[\mathrm{HN{-}(CH_2)_6{-}NH{-}\overset{O}{\overset{\|}{C}}{-}(CH_2)_4{-}\overset{O}{\overset{\|}{C}}} \right]_n$$

Poly(vinyl pyrrolidone) is a vinyl polymer having a pendent amide group and has the following structure

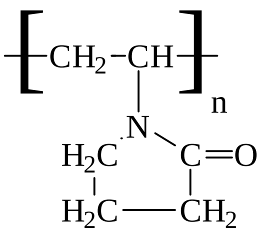

Isopropanol was used as a solvent for PVP which had a purity of 99% and was purchased from the chemistry department's stockroom. Furthermore, benzene with a 99% purity and also purchased from the chemical stockroom, was used as a wash for carbon fibers.

3.1.2 Fibers & fabric

Glass fibers were made from E-glass fiber precursor, while large diameter carbon fibers (LDC) were obtained from a source at E. I. DuPont. The LDC fibers were composed of a carbon center with a coating of SiC, which was then coated with a final carbon layer. The diameter of these fibers was ≈ 120μm, and a schematic of the fiber diameter is shown in Figure 3.1. Although the composition of the LDC fibers was not completely carbon, only the surface composition was important for this study, which again was entirely carbon. In addition, the tensile strength of these fibers was sufficient so as not to cause any failure within the fiber during debond tests. These particular fibers were also chosen as candidates due to their stiffness which results from their larger diameters (i.e., ~100μm). This stiffness is necessary when fabricating fiber debond samples where a fiber is inserted into a molten matrix. Typical carbon fibers from a tow are ~ 10μm in diameter and cannot easily be immersed in a matrix to make debond samples.

Fabric weave of both E-glass and high modulus AS-4 carbon fibers were obtained from the Department of Engineering Science and Mechanics. Spools were donated for research by a third party who received the fabrics from Mutual Industries, Inc. Both

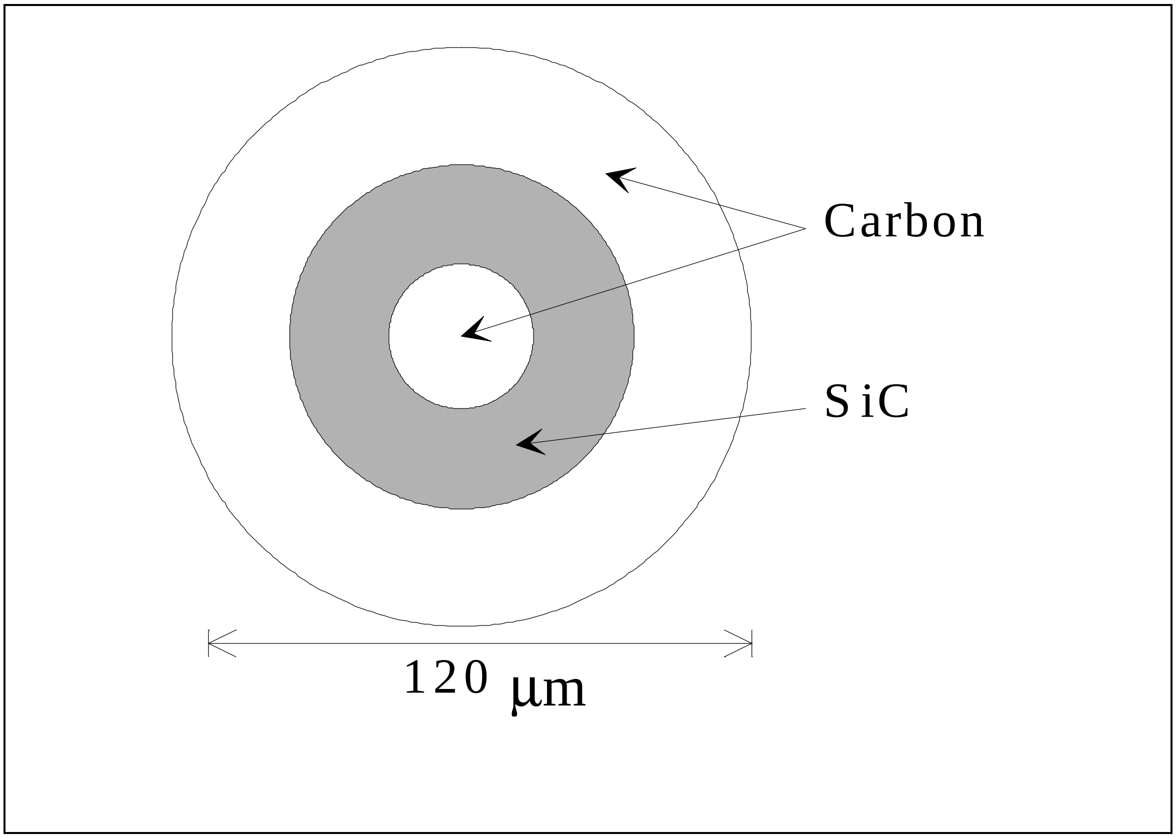

Figure 3.1 Schematic of the large diameter carbon fibers supplied by E. I. DuPont.

fabrics were comprised of 0°-90° plain weave tow. The E-glass fabric was unsized, and the carbon fiber fabric was initially thought to be unsized. However, further investigation indicated that the carbon fabric contained a compatiblizer used to aid in prepreg processing. Information regarding the specifics of the sizing were unavailable due to the proprietary nature of the material.

3.2 Sample preparation

3.2.1 Glass fiber formulation

Fibers of E-glass were formulated by softening pieces of the glass in the flame of a propane torch. They were then quickly removed from the flame and pulled apart rapidly. This method produced E-glass fibers with diameters ranging from 50μm to 150μm, which depended on the pull rate once the glass was removed from the flame. This method of fiber production was chosen because the surface chemistry and topography of the fibers could be easily determined and controlled.

3.2.2 Laboratory sizing of fibers & fabric

E-glass and LDC single fibers were sized with the diluent, PVP, by exposing several fibers of either kind to solutions of isopropanol and PVP. The following solutions were made: 1% PVP_{10}, 10% PVP_{10}, and 1% PVP_{360}. Additional fibers exposed only to isopropanol were used as a reference. After an exposure time of one hour, the fibers were removed and dried at 50°C for 24 hours. Prior to exposing fibers to solutions, fiber ends were cut with ceramic scissors to insure a clean perpendicular cross section. Optical microscopy was used for verification.

E-glass and carbon fiber fabrics were sized in a similar fashion. Fabrics of each fiber approximately 4” X 4” in size were stirred in a PVP solution for one hour. However, the solution concentration of PVP in isopropanol was 20% for the fabrics. This concentration was used to insure complete coating of the fabric with the PVP. After removal from the solution, the fabrics were dried at 25°C for 4 hours. Prior to molding, these fabrics were placed in an oven at 100°C for more than 24 hours to assure the removal of solvent and moisture. An overall sizing concentration of each fabric was approximately 2% PVP.

3.2.3 Unsizing carbon fiber fabric

The AS-4 carbon fibers were exposed to a bath of benzene for 24 or 48 hours. This process was used to remove the commercial sizing and any other residue from the surface of the fiber. Upon removal from the benzene, the fibers were dried in an oven at 120°C for times of 4 hours, 24 hours, or 72 hours to remove any residual solvent or sizing. These fibers were then used as 'unsized' fibers in all of the following experiments.

3.2.4 Fiber debond test samples

After removing the fibers from the oven, each was mounted to an aluminum tab for testing using an epoxy resin. The fibers were aligned with the center of a hole in the tab to insure a uni-axial loading condition when tested.

Next, films of either nylon or a nylon/1% PVP_{10} blend were made on very small laboratory quantities. Approximately 50mg of powder of either matrix was heated on a hot plate to 300°C between to Kapton sheets for 5 to 10 seconds. The film was then removed from the Kapton, folded, and remelted. This was performed 3 to 5 times to assure good mixing of the powders. On the final melt, the film was pressed between Kapton sheets with shimstock introduced to achieve a film thickness of approximately 100μm.

The matrix films were created using this technique for three reasons. First, the solution film-making process was abandoned because samples with adequate thickness could not be formulated. Second, this method removes the environmentally unsafe solvent, formic acid, from the process. Third, melt blending is a common practice in industry and could be easily upscaled if necessary.

These films were then placed on a Linkam THMS 600 hot stage and heated to 300°C under a nitrogen purge. Immediately after melting, a fiber was inserted into the matrix. An apparatus was constructed to hold the fiber so that during insertion, the fiber would be perpendicular to the matrix. Once the fiber was embedded, the sample was then cooled to 235°C at approximately 90°C/min. The sample was held at this temperature for 15 minutes to allow for complete crystallization to occur. After the given time, the sample was removed and was ready for testing. Over 300 of these test specimens were made. A schematic of the completed test sample is shown in Figure 3.2.

3.2.5 Compression molding

Bulk composite samples of nylon 66 reinforced with either E-glass fabric or carbon

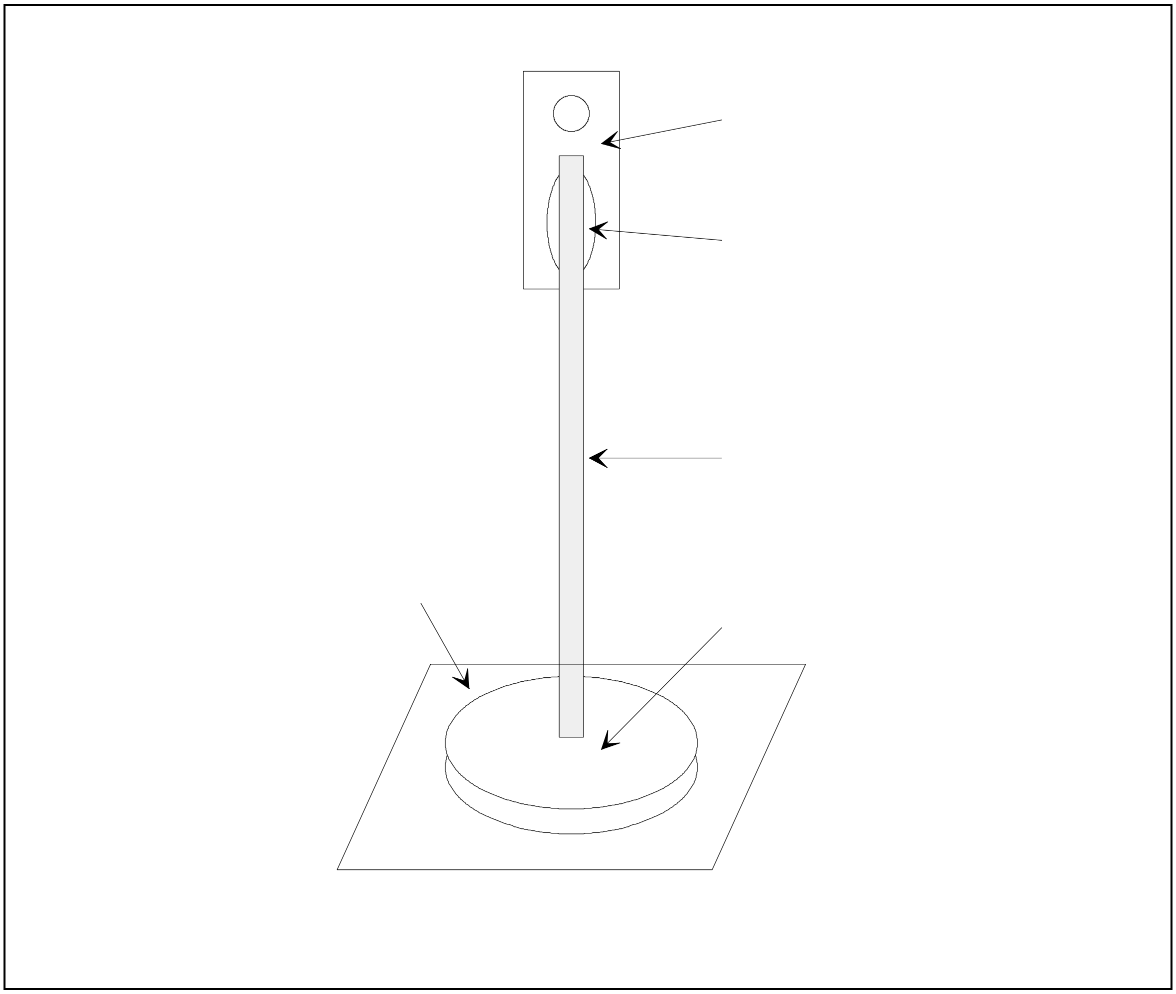

Figure 3.2 Schematic of fiber debond test sample.

fiber fabric used for macroscopic testing were fabricated using compression molding. Samples of varying thicknesses were made depending on the characterization test used. 1-ply samples were made for moisture up-take studies, while 2-ply samples were used for DMA, vibrational, and tensile testing. Furthermore, 4-ply samples were manufactured for impact testing. All samples were compression molded by exposing alternating layers of nylon 66 film and fiber fabric, depending upon the number plys needed. For example, the 1-ply sample consisted of a fabric between two nylon 66 films. The nylon films weremade by placing approximately 5 grams of sample between Kapton sheets and pressing it at 290°C for 1 minute. The film was removed and cooled in an adjacent hot press. The temperature of the additional press was approximately 235°C for early studies and was reduced to room temperature for additional studies. Once the nylon films were made, the alternating layered samples were placed in the hot press for 3 minutes at 290°C. These were also cooled in the second hot press at the above mentioned temperatures.

3.3 Characterization

3.3.1 Modified fiber debond test

The fiber debond samples were tested in tension using an apparatus constructed by Commercon [98] and Heisey [99] in the laboratory of Dr. Wightman, located in the chemistry department to evaluate fiber/matrix adhesion. The aluminum tab of each sample was fastened to a microbalance, and a micro-vise was positioned over the matrix against the fiber. An Oriel motorized stage was lowered at a rate of 0.5

mm/min. in order to pull the fiber from the matrix. The microbalance is connected to a computer which recorded the maximum load output for debonding. This value, along with the fiber diameter and embedded length, was used to determine interfacial shear strengths of the samples using a simple shear lag model. This test procedure and sample preparation technique were chosen because the crystallization history of the sample could be controlled, whereas other interfacial testing techniques (i.e., fragmentation) did not allow the thermal history to be precisely controlled.

3.3.2 Optical microscopy and scanning electron microscopy (SEM)

Both optical microscopy and SEM were used to image fibers before embedding to get an indication of fiber surface, sizing uniformity, and sizing thickness. In addition, both techniques were used to examine the debonded interface of the fibers and matrix in order to observe the embedded length and possible interphase morphology. The optical microscope was an Olympus BHSM with crossed polarizers and a light frequency compensator of 540nm. All optical micrographs are taken using a 35mm camera. The SEM was an ISI-SX-40 machine and was operated at an acceleration voltage of 10kV and used to take photomicrographs at magnification less than 10,000X. All samples were sputtered with gold so that the materials would not ‘charge’ during examination.

3.3.3 Profilometry

Optical profilometry was performed on selected fibers at E. I. DuPont to determine fiber surface and sizing uniformity and thickness. To determine the sizing thickness, a portion of the fiber was exposed to water. This removed a portion of the water-soluble PVP sizing so both the fiber and sizing could be scanned. In addition, mechanical profilometry was conducted at Virginia Tech in the laboratories of Dr. Desu and Dr. Eiss. Samples were also coated with a thin film of gold to remove the possibility of probe ‘scraping’ off the soft polymer sizing.

3.3.4 Dynamic mechanical analysis

Dynamic mechanical analysis, in single cantilever mode, was performed on 2-ply samples of both composites using a DuPont 983 DMA to determine a specific composite’s damping characteristics. An amplitude of 0.2mm and a frequency of 1Hz was used over two ranges of temperatures. All tests originated at 30°C (due to cryogenic inability) and were heated at a rate of 2°C/min. to either 150°C or 220°C. Two scans were performed on each sample, and at least 3 samples were tested for each condition.

All sample dimensions were approximately 4cm X 1cm X 0.75cm, and a cantilever length of 25mm was used. In addition, samples were mounted using a torque of ~1.13 N-m (10 lb.-in.).

3.3.5 Vibrational adhesion testing

A fellow graduate student in the Materials Engineering Science program, Weiqun Gu, has devised a nondestructive technique to evaluate fiber/matrix adhesion. A schematic of the test is shown in Figure 3.3. The theory of the analysis is based on the damping characteristics of the materials and interface present.

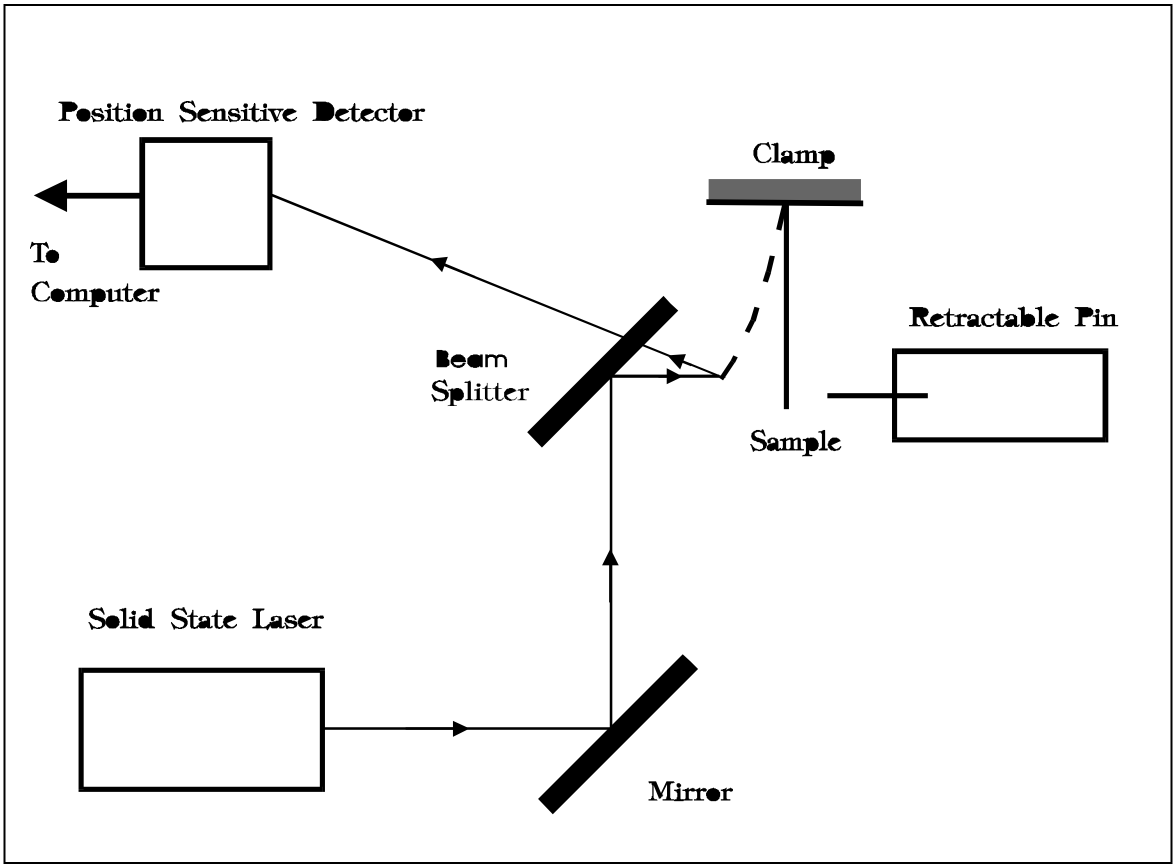

Figure 3.3 Schematic of vibrational adhesion testing procedure.

Samples for this testing technique were 40mm X 3mm X 0.75mm. After mounting, an end of the sample is freely vibrated and its damping ability is detected using a laser. From this information, a tan δ is obtained, from which insight into the level of adhesion in a composite can be determined.

3.3.6 Minimat tensile testing

Tensile testing was used to determine composite ultimate break loads as a function of reinforcement and fiber sizing. Samples were taken from compression molded plaques at 45° to the fiber fabric orientation, and test specimens were made using a dogbone punch with a gauge length of approximately 7.5mm and a width and thickness of approximately 2.75mm and 0.72mm, respectively. All tests were conducted using a Polymer Laboratories Minimat Materials Tester equipped with a 200N load cell at a crossshead rate of 1mm/min. Four samples from each condition of interest were tested.

3.3.7 Thermogravimetric Analysis (TGA)

Dynamic thermogravimetric analysis was performed using a DuPont Model 951 TGA. All composite samples were tested to determine fiber and matrix volume fractions and water up-take amounts, while nylon 66 and PVP were tested to determine thermal stability and water up-take. The samples were heated in an open aluminum pan in an atmosphere of compressed air with a flow rate of 80ml/min. They were heated from 30°C to 500°C at a rate of 10°C/min. The percent weight loss of each sample was measured as a function of temperature.

3.3.8 Differential scanning calorimetry (DSC)

Differential scanning calorimetry was performed on all materials and composites to determine if complete crystallization was obtained in samples and also to observed the thermal transitions of the materials. Initial tests were run on a Polymer Laboratories DSC (PL-DSC), and more recent tests were performed on a DuPont 910 DSC. Tests conducted using the PL-DSC ran from 0°C to 300°C at a heating rate of 10°C/min under ambient conditions. The additional tests performed on the DuPont instrument were run from 30°C to 300°C at a heating rate of 10°C/min under ambient conditions.

3.3.9 Water absorption study

When working with polyamides, it is important to examine the amount of water the material absorbs. Therefore, water absorption profiles for all composites and neat nylon 66 were measured by exposing 1-ply samples to a distilled water bath which as held constant at 50°C. Initial weights and periodic weighings were taken using a Mettler AE 50 microbalance.

4. Results and Discussion

4.1 Modified fiber debond

The modified fiber debond test was used to determine the average interfacial shear strength of a single filament model composite. An SEM micrograph showing an actual modified fiber debond sample is shown in Figure 4.1. Both E-glass and large diameter carbon fibers (LDC) were used as reinforcements. The matrix used was primarily nylon 66, however, one series of tests was performed using a nylon 66/1% PVP blend matrix. The details are discussed below.

4.1.1 E-glass fibers embedded in nylon 66

Over twenty samples at each fiber surface condition, i.e. , fibers that had been exposed to isopropanol, a 1% solution of PVP_{10}, a 10% solution of PVP_{10}, and a 1% solution of $PVP_{360,}$ were embedded in nylon 66 and tested. The load required to debond the fiber from the matrix was recorded, and along with fiber diameter and embedded length taken from optical microscopy, the average interfacial shear strength was determined using a simplified shear lag analysis:

$$ {}_{avg} = \frac{F}{dl} = \frac{mg}{A} \qquad [4.1] $$

where ${}_{\text{avg}}$ is the average interfacial shear strength, *F* is the debond force, *d* is the fiber diameter, *l* is the embedded length, *m* is the debond mass, *g* is the gravitational constant, and *A* is the contact area.

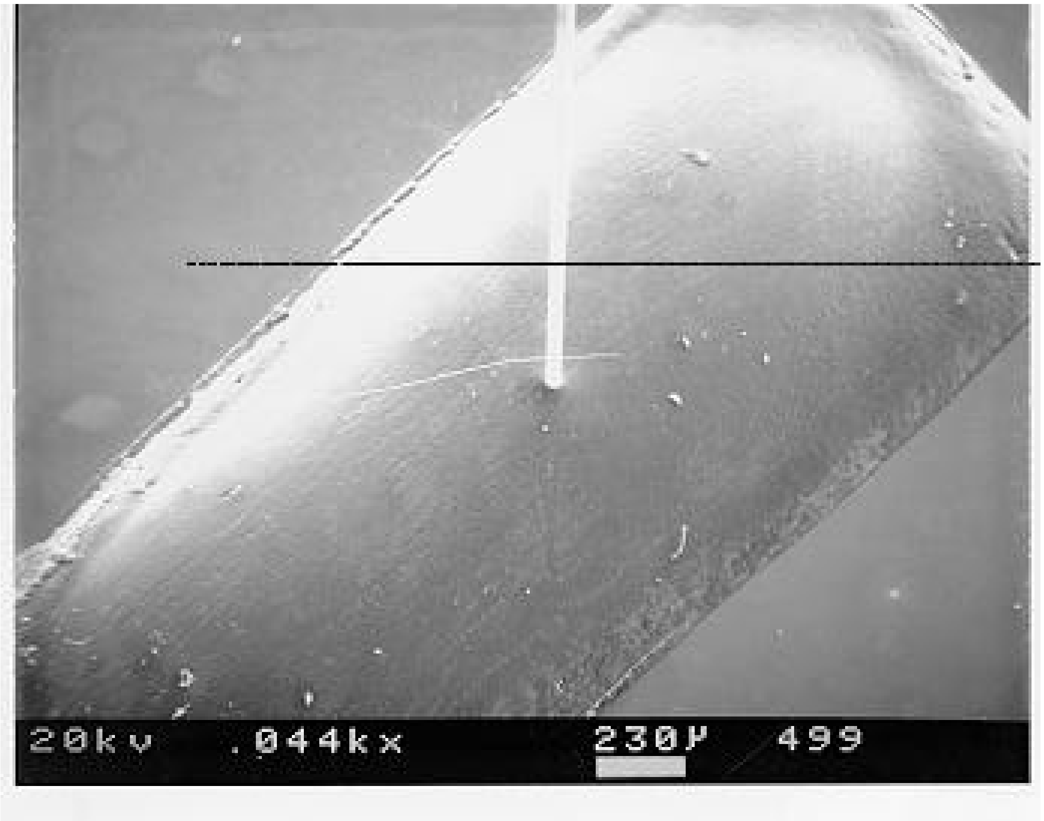

Figure 4.1 SEM photograph of a modified fiber debond test sample.

Figure 4.2 shows the $_{avg}$ plotted as a function of fiber sizing. The data indicates that $_{avg}$ is ≈ 51 MPa when unsized E-glass fibers are embedded in nylon 66. This value is within the same order of magnitude as the ultimate strength of neat nylon 66, which is reported between 55MPa and 80MPa [94, 44], depending upon processing and environmental exposure. This agreement is expected due to the high level of adhesion in the E-glass/nylon 66 system which causes the mode of failure to be cohesive. In addition, the high level of adhesion is attributed to the polarity of both the glass and nylon that produces hydrogen bonding across the interface, which is the strongest secondary bonding force.

In addition, the plot indicates that the $_{avg}$ is slightly decreased when the low molecular weight PVP is used as a sizing from a 1% solution. The 10% solution has the same effect, but more enhanced. Finally, fibers sized with the high molecular weight diluent decreases $_{avg}$ when compared to the unsized fibers. The effect of the high molecular weight diluent at a low concentration seems to have the same effect on $_{avg}$ as the low molecular weight diluent does at a high concentration.

These reductions in average interfacial shear strength are postulated to be a consequence of the morphology alterations in the interphase. In the unsized E-glass/nylon 66 sample an interphase morphology, better known as, transcrystallinity, is produced. This type of formation was found by both Clark [51] and Shiao et a. [45] when samples were made under similar conditions. Figure 4.3 contains a micrograph illustrating this specific interphase [51]. With the introduction of the PVP sizing, this

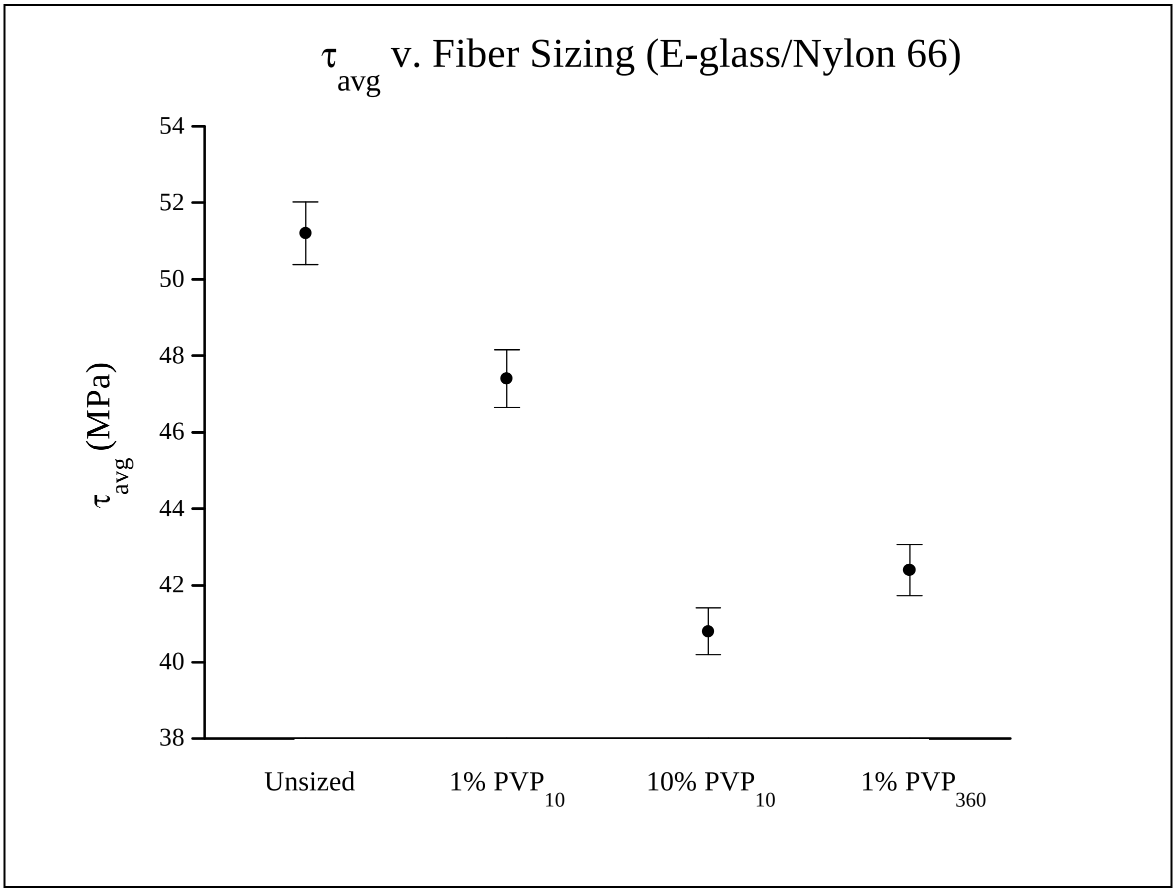

Figure 4.2 Average interfacial shear strengths of E-glass fibers with various surface compositions embedded in nylon 66.

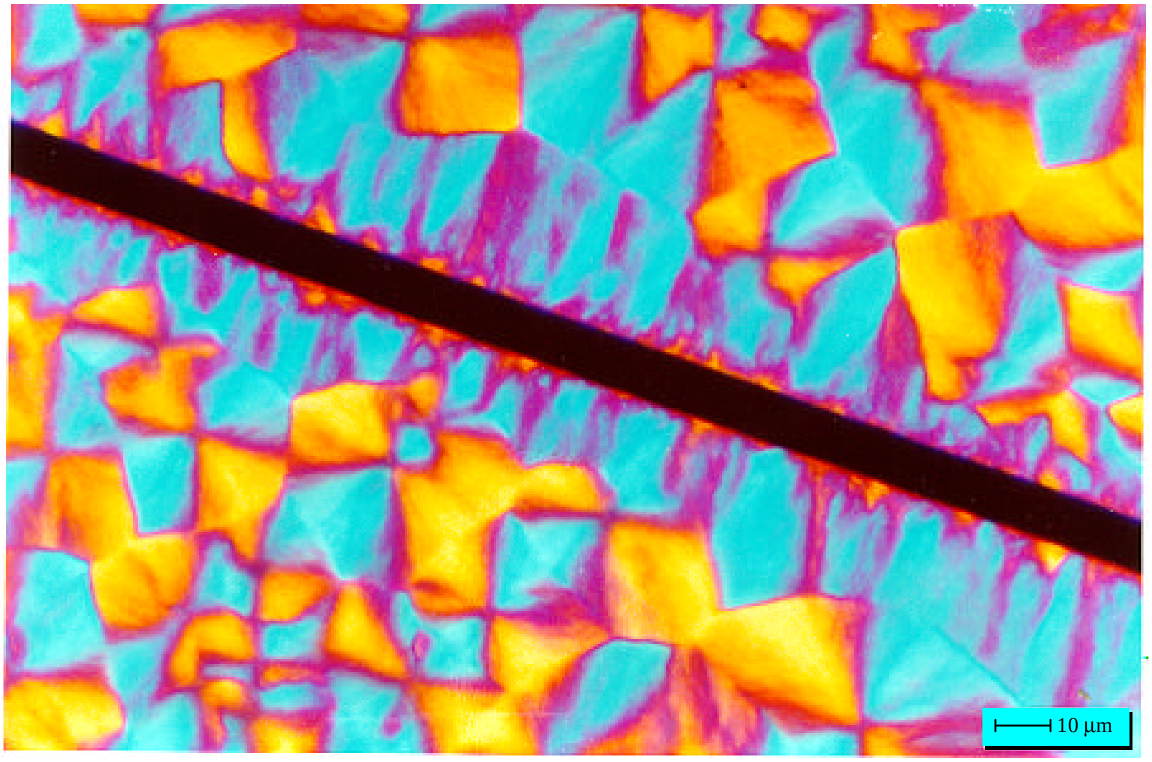

Figure 4.3 An unsized carbon fiber embedded in a nylon 66 matrix melt crystallized at 235°C.

interphase will change from a transcrystalline morphology to a more spherulitic morphology. Previous work has indicated this phenomenon [51], and results from the crystallization kinetics of nylon 66 being influenced by the nucleation density reduction. Furthermore, it was shown that a higher concentration or higher molecular weight sizing will produce an even more spherulitic interphase. This is due to the fact that more of the diluent remains at the carbon fiber surface. Since nylon and PVP are miscible, the PVP will diffuse into the nylon and a higher concentration of the low molecular weight diluent increases the probability of the PVP remaining at the fiber surface. In addition, the high molecular weight PVP has a much lower diffusion rate in the nylon, therefore smaller amounts will have dramatic nucleation damping effects . This is illustrated in Figure 4.4 which contains a micrograph of a carbon fiber sized from a 10% solution of PVP_{10} embedded in nylon 66. Here the transcrystalline region is essentially removed from the composite. Similar morphologies resulted when fibers from the 1% PVP_{360} solution were used [51]. (Note: The micrographs in Figures 4.3 and 4.4 are showing carbon fibers embedded in nylon 66. This is purely for visual purposes, and identical morphologies and morphological changes were found when E-glass fibers were embedded in nylon 66.) Therefore, the data in Figure 4.2 indicates that as interphase morphology is changed from transcrystalline to spherulitic, the average interfacial shear strength decreases.

Efforts were made to determine the actual interphase morphology of the tested samples in Figure 4.2. Both optical microscopy and SEM were used. Cross-sections

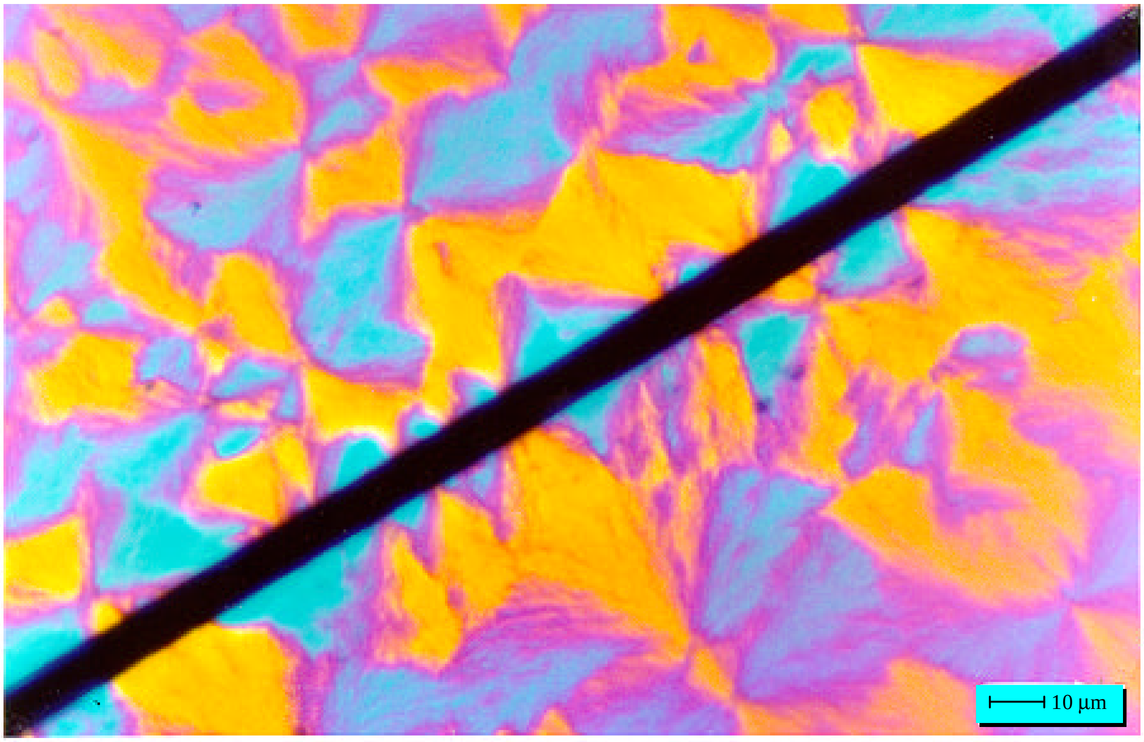

Figure 4.4 A carbon fiber sized from 10% concentration solution of PVP$_{10}$ embedded in a nylon 66 matrix melt crystallized at 235°C.

of the debonded area of the matrix and that of the fibers were examined, but neither technique could be used to determine the actual interphasial structure. This problem has been attributed to several causes. First, the debond area was extremely small (i.e., ≈ 100μm X 100μm), limiting the size of the interphase region. Second, the curvature of the samples did not permit the optical microscope, which has a poor depth of field, to be focused clearly enough to indicate interphase morphology. Third, there was no contrast in the different morphologies of the samples to be viewed using SEM. Basic staining techniques were used but did not enhance the region. Therefore, it can only be assumed that the interphase in these samples parallels those in Figures 4.3 and 4.4.

An additional study was performed using this system to substantiate the decrease found in $_{\text{avg}}$. The results are shown in Figure 4.5 which are plotted along with the first series of tests. It can be seen in both instances that a reduction in $_{\text{avg}}$ is found with the addition of fiber sizing. There is a larger standard deviation in this data, however, it is still well within experimental error for this type of test. In addition, this second data set shows a decrease in $_{\text{avg}}$ with all three different sizing solutions. This is most likely due to a change in the amount of sizing at each concentration which is dependent not only on solution concentration, but also fiber removal rate from the solution and drying conditions. This will be discussed further when analyzing profilometry.

4.1.2 E-glass fibers embedded in nylon 66/1% PVP

After embedding the various E-glass fibers in neat nylon 66, efforts were made to then add them to the other blends of nylon and PVP. However, melt blending the

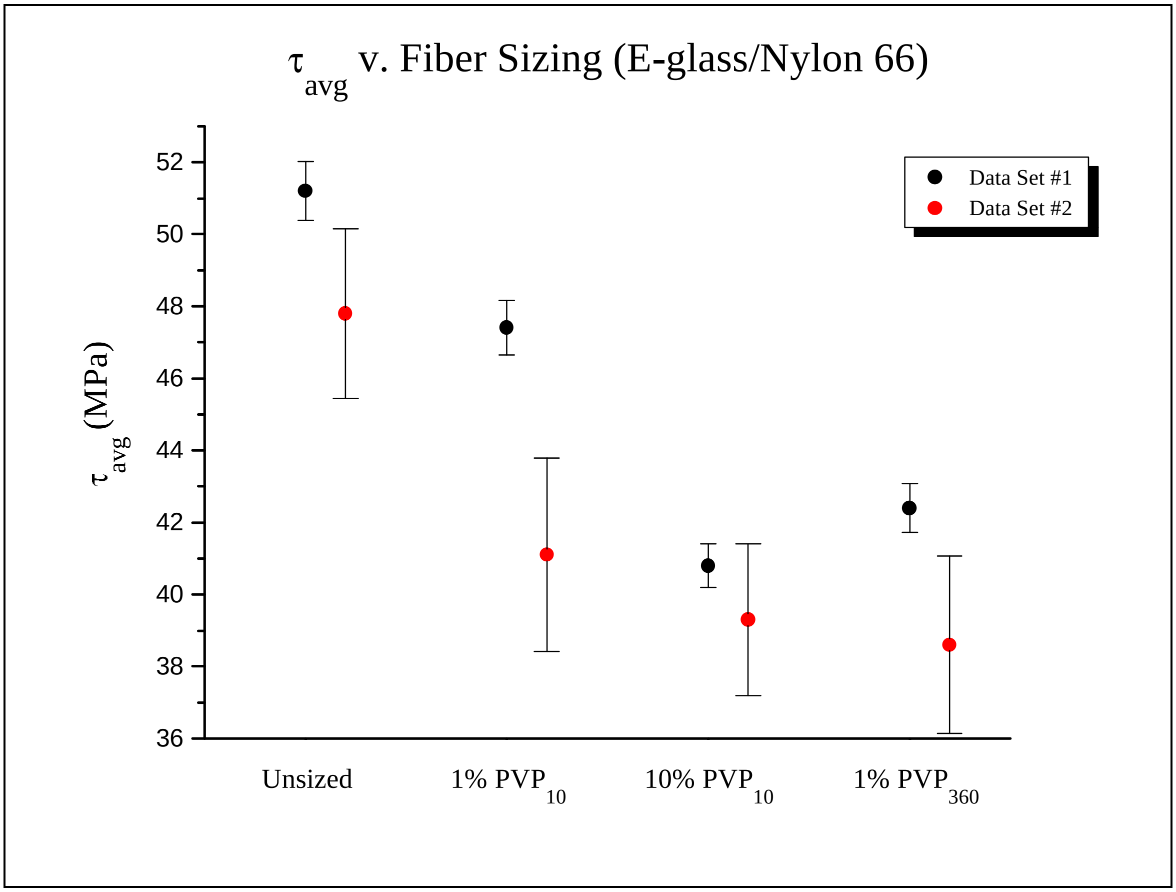

Figure 4.5 Average interfacial shear strengths of E-glass fibers with various surface compositions embedded in a nylon 66: Both data sets.

nylon and PVP did not produce complete blend miscibility. In all cases, phase separation was noticed using optical microscopy, except for the nylon 66/1% PVP blend. Although it is still unclear as to whether the PVP and nylon are miscible in the melt (this issue will be addressed in future work), E-glass fibers were embedded in the 1% PVP/nylon blend.

Again, over twenty samples from each of the fiber sizing solutions were embedded in a film of nylon 66/1% PVP. These were tested, and the debond force was measured. Using equation [4.1], the average interfacial shear strengths were calculated and are plotted versus fiber sizing in Figure 4.6, along with the results from Figure 4.2.

It can be seen that the interfacial shear strength of the unsized fibers in the nylon/1% PVP blend is similar to that of the nylon matrix. This is expected since the morphologies of the two systems were found to be similar in previous studies [51]. Furthermore, from Figure 4.6, the addition of the sizing seems to have no effect on the interfacial shear strength. Previous work showed that the interphase morphology does not change significantly which would suggest that the average interfacial shear strength should not change either, as shown. Figure 4.7 shows the interphase of a fiber sized with the high molecular weight diluent embedded in a nylon/1% PVP matrix.

As with the previous samples, optical microscopy and SEM did not lead to any conclusive answers as to interphase morphology in these samples either. Again, it was assumed that morphologies in the fiber debond samples were similar to those found in

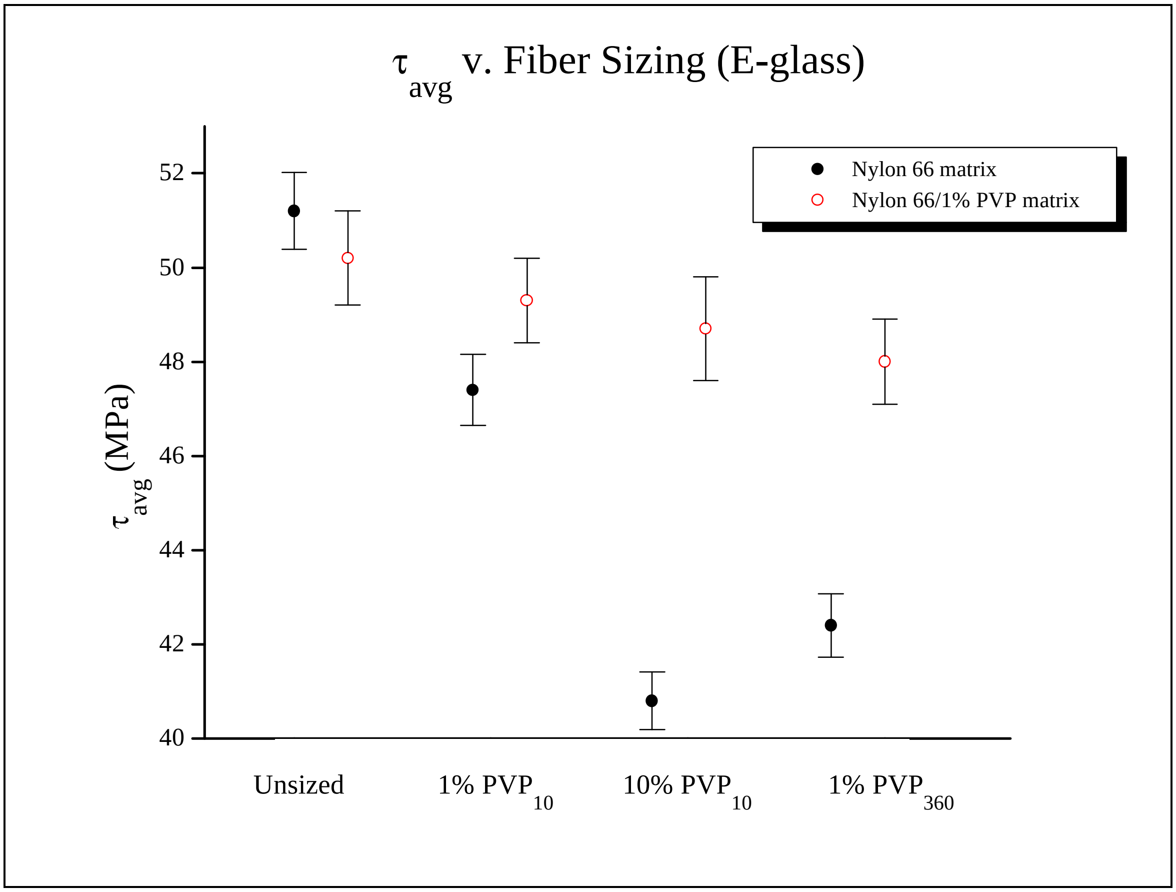

Figure 4.6 Average interfacial shear strengths of E-glass fibers with various surface compositions embedded in a nylon 66 and nylon 66/1% PVP matrix.

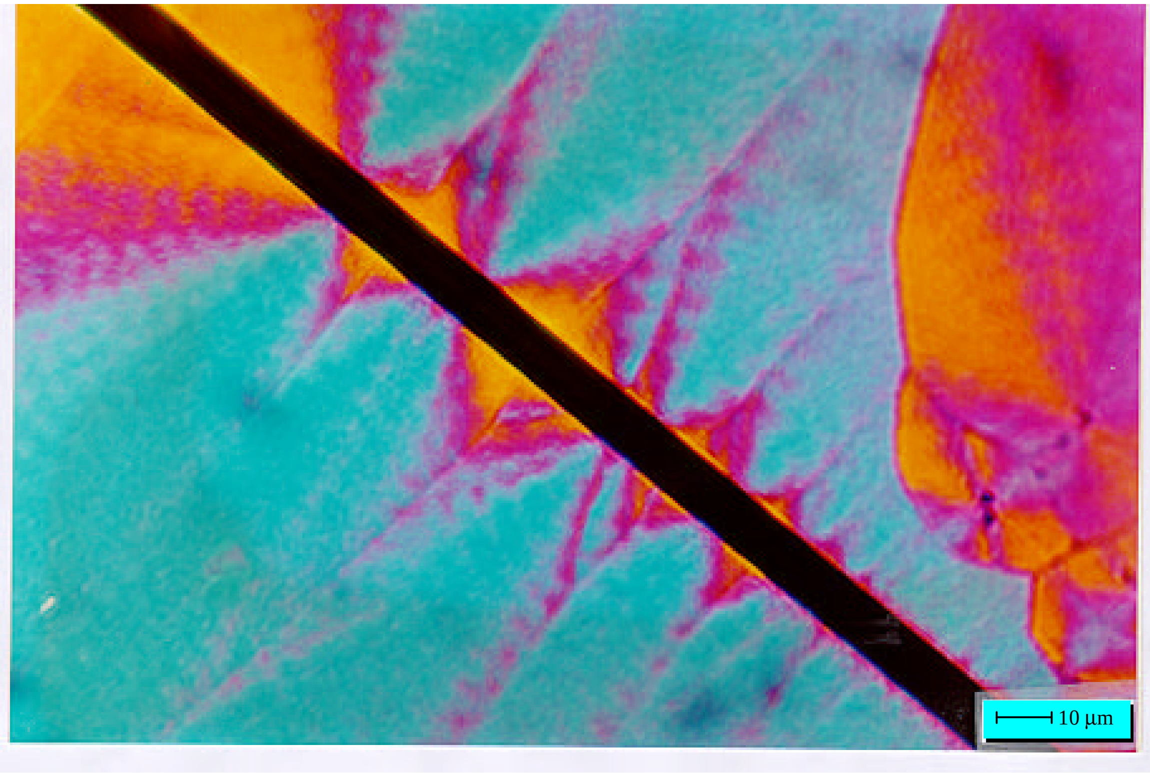

Figure 4.7 A carbon fiber sized from 1% concentration solution of PVP_{360} embedded in a nylon/1% PVP_{10} blend matrix melt crystallized at 235°C.

the films cast from solution.

4.1.3 LDC fibers embedded in nylon 66

Although glass fibers are a major reinforcement for semicrystalline polymers, carbon fibers are also widely used, and since previous work focused on carbon fibers as a reinforcement [51] in nylon as well as glass fibers, average interfacial shear strengths for a carbon fiber/nylon composite was investigated. In these systems, only 10 samples were formulated from each solution due to the limited amount of LDC fiber. The final results are plotted in Figure 4.8 along with the results for the E-glass fibers shown in Figure 4.2. From this figure, it can be seen that the average interfacial shear strength for the LDC fiber composites are less than that of the E-glass composites in all cases. Furthermore, a strong reduction in the interfacial shear strength due to the fiber sizing is not prevalent. In addition, the scatter in the data is much larger for this composite system.

The difference in $_{avg}$ between the two composites is due to the different mechanisms of adhesion in the two systems. Nylon has a much stronger bond with the glass than the carbon surface, as mentioned, due to the polar nature of the glass fiber and nylon 66. Therefore, a higher $_{avg}$ will result. The fact that the sizing had no effect on $_{avg}$ in this system was peculiar. Therefore, an investigation of the interphase formed by exposing these LDC fibers to films of nylon cast from solution was made. It was found that there was no transcrystallinity in these composites, and the interphase was comprised of spherulitic growth. This leads to an inquiry into the structure of the

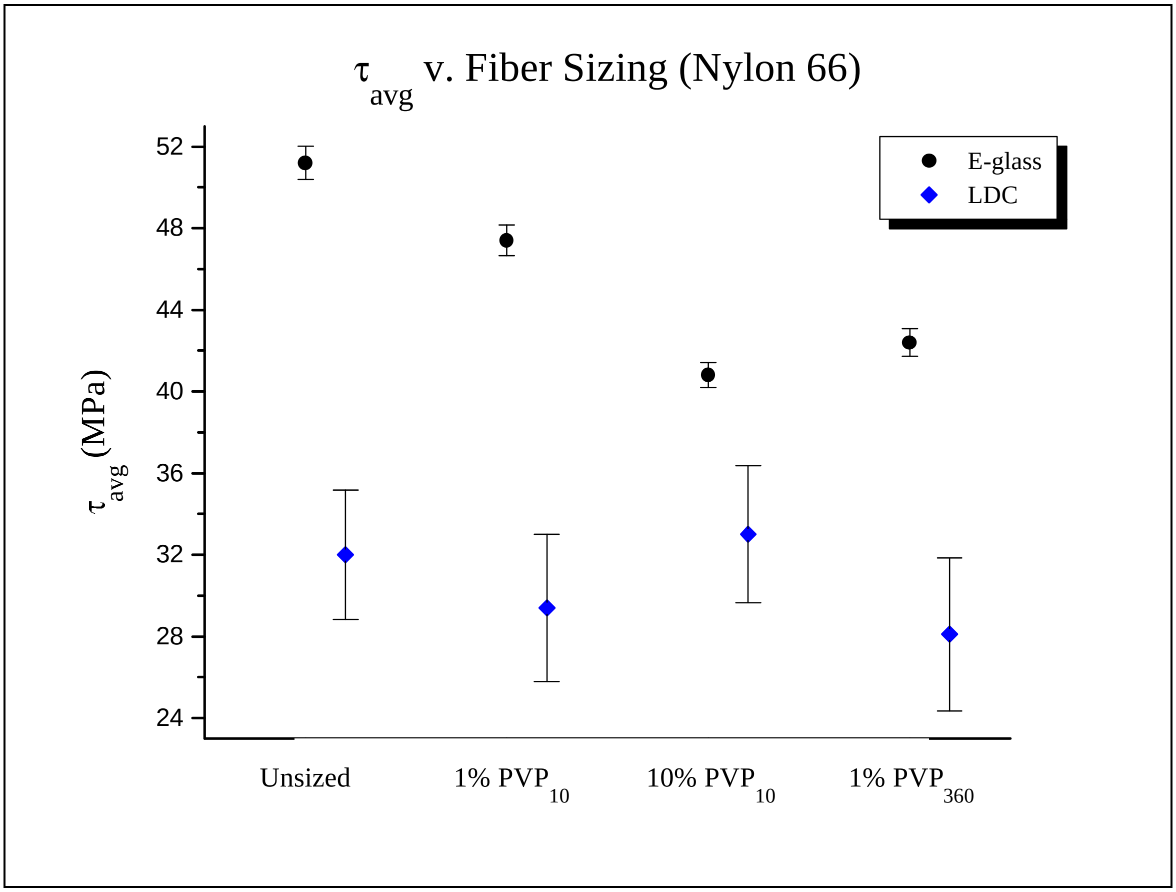

Figure 4.8 Average interfacial shear strengths of E-glass and LDC fibers with various surface compositions embedded in a nylon 66 matrix.

LDC fiber surface. Transcrystallinity forms in carbon fiber/nylon 66 composites due to the high energy surface of the fiber which causes heterogeneous nucleation. It has been shown that when high modulus carbon fibers are added to nylon 66, transcrystallinity is promoted, while low modulus carbon fibers do not cause this interphase formation. This has been ascribed to the crystallographic planes that are exposed on the fiber surface. Although the LDC fibers are high modulus, the outer 2μm was found to be an amorphous carbon layer which does not have any specific surface planes exposed, and therefore no transcrystallinity.

Although the absence of transcrystallinity formation was an unexpected discovery, this set of data does answer an important question: Is the sizing producing an additional phase near the fiber that is causing the reduction in $_{avg}$? This system shows that there in no reduction in $_{avg}$ with the addition of sizing indicating that this cannot be the case, otherwise a drop in $_{avg}$ with the addition of diluent would still have been evident in this system.

In addition, the standard deviation in these results is found to be larger than that of the E-glass fibers by a factor of 3. The increased variability in these samples in most likely a result of the low level of adhesion in this system.

4.2 Profilometry

E-glass fibers sized with PVP were scanned using optical profilometry at E. I. DuPont. An example of the data from these fibers is shown in Figure 4.9 where a fiber sized from a solution containing 10% PVP_{10} is illustrated. Both a two-dimensional and

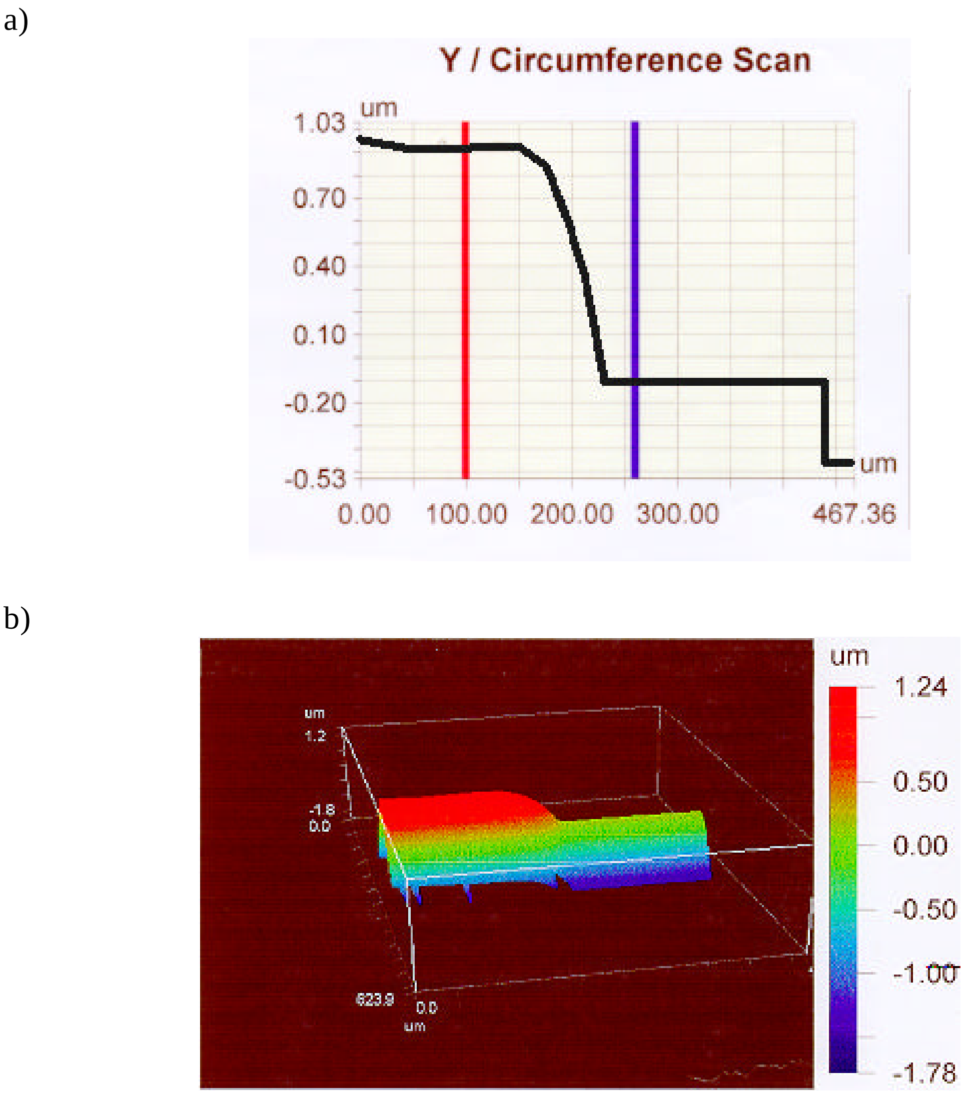

Figure 4.9 A a) two and b) three dimensional profilometry scan of a fiber sized using the 10% PVP_{10} solution.

three-dimensional scan is shown. The analysis shows that the sizing thickness is approximately 1 μm, and very uniform. Figure 4.10 contains a two-dimensional scan of an unsized fiber. The surface topography of the fiber is very uniform except for a defect which is indicated by the peak in the linear plot and the white area on the two-dimensional surface scan. Subsequent tests revealed sizing thicknesses of 0.5μm to 1.0μm on fibers exposed to a 10% PVP_{10} solution. As alluded to earlier, not only is the sizing layer a function of solution concentration, but it is also a function of how fast the fiber is removed from the solution. This dictates the size and shape of the meniscus between the fiber and solution. Furthermore, the viscosity and drying process also affect sizing thickness. In spite of all the variables, the sizing thickness is on the order of 1μm.

Mechanical profilometry was also used at Virginia Tech on gold coated fibers. However, due to the curvature of the fibers, the mechanical probe was not able to remain on top of the fiber, and additional sizing thicknesses were not determined in this work.

4.3 Scanning electron microscopy (SEM)

Although the interphase morphology was not discernible using microscopy, SEM was used to evaluate the fracture surfaces of the failed fiber debond samples. A typical debonded fracture surface of an unsized fiber debonded from nylon 66 is shown in Figure 4.11. The embedded length of approximately 300μm can be seen along with the fiber end which was cut perpendicular to the fiber with ceramic

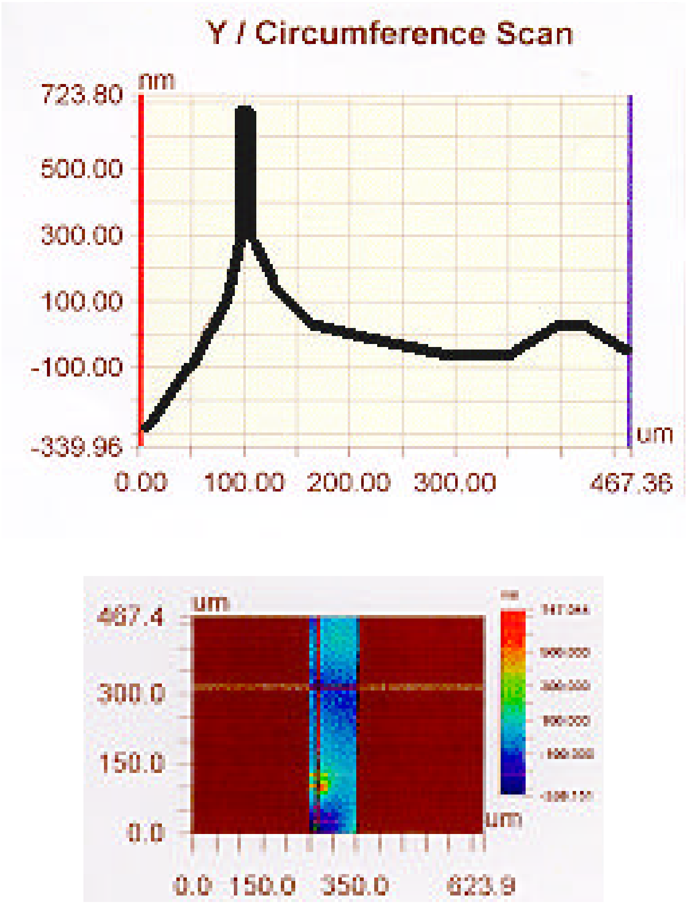

Figure 4.10 Two dimensional profilometry scan of an unsized fiber.

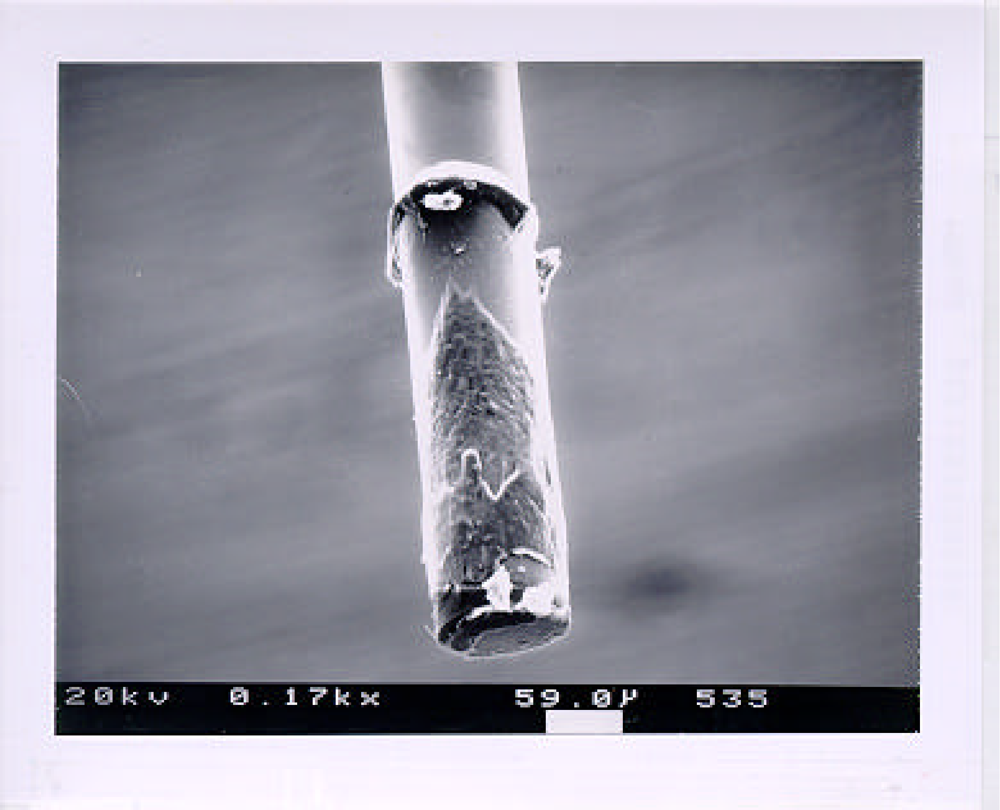

Figure 4.11 SEM photograph of an unsized E-glass fiber debonded from nylon 66.

scissors. In addition, the photograph shows the failure surface. The failure mode seems to be that of mixed mode, with mostly cohesive failure and some adhesive failure present. The adhesive failure is concentrated at the top of the embedded length of the fiber where the shear stresses are high, and as the distance from this end of the fiber is increased, a more cohesive failure is discerned. However, it is possible that the entire failure is cohesive and that a thin film of nylon is present over the entire embedded length which cannot be detected in this photograph. Energy Dispersive X-ray (EDX) analysis was used to help answer this question, however no definitive conclusion could be made. The sample charged at the magnifications necessary for detection, and the signal from light elements is very weak. Furthermore, the penetration depth of the X-ray in on the order of tens of microns which would reduce any surface element signals with those from the bulk.

Figures 4.12 through 4.14 show typical failure surfaces of sized fibers debonded from a nylon 66 matrix. Again, embedded lengths can be ascertained from these photographs, and the failure surfaces look much different from those fracture surfaces of the unsized fibers. Here, the failures seem to be almost completely adhesive, or at least cohesive with a very thin nylon film remaining on the fiber. Therefore, the diluent is shifting the ‘weak link’ or fracture point in the composite from that of the matrix to the glass/polymer interface.

To survey the fracture surface more closely, photographs of the surfaces in Figures 4.11 through 4.14 were taken at an increased magnification. They are shown in

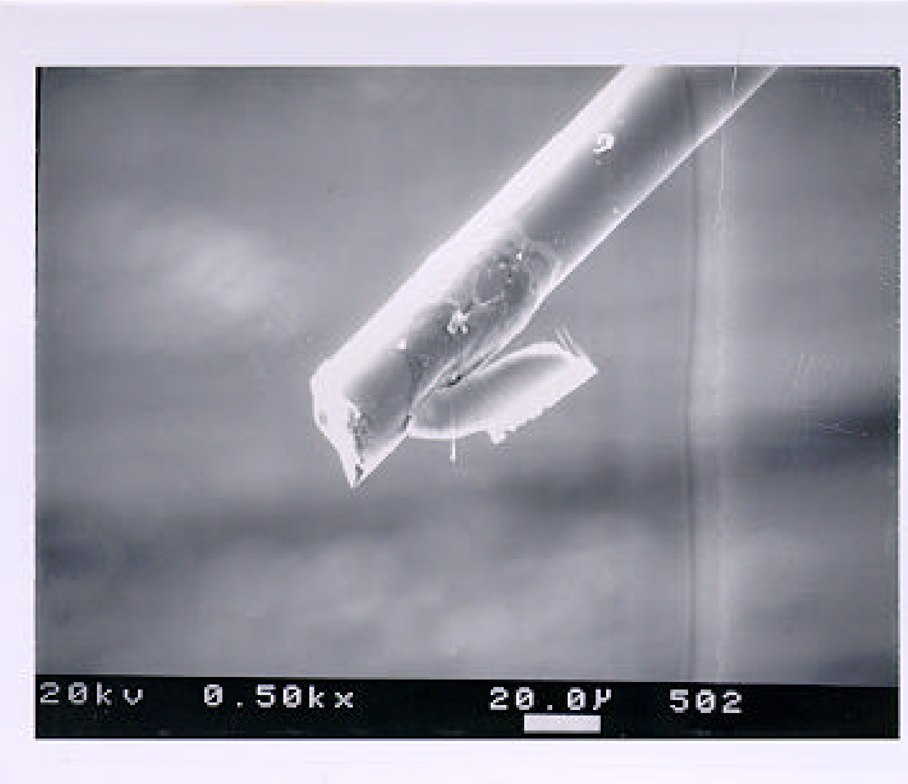

Figure 4.12 SEM photograph of a 1% PVP$_{10}$-sized E-glass fiber debonded from nylon 66.

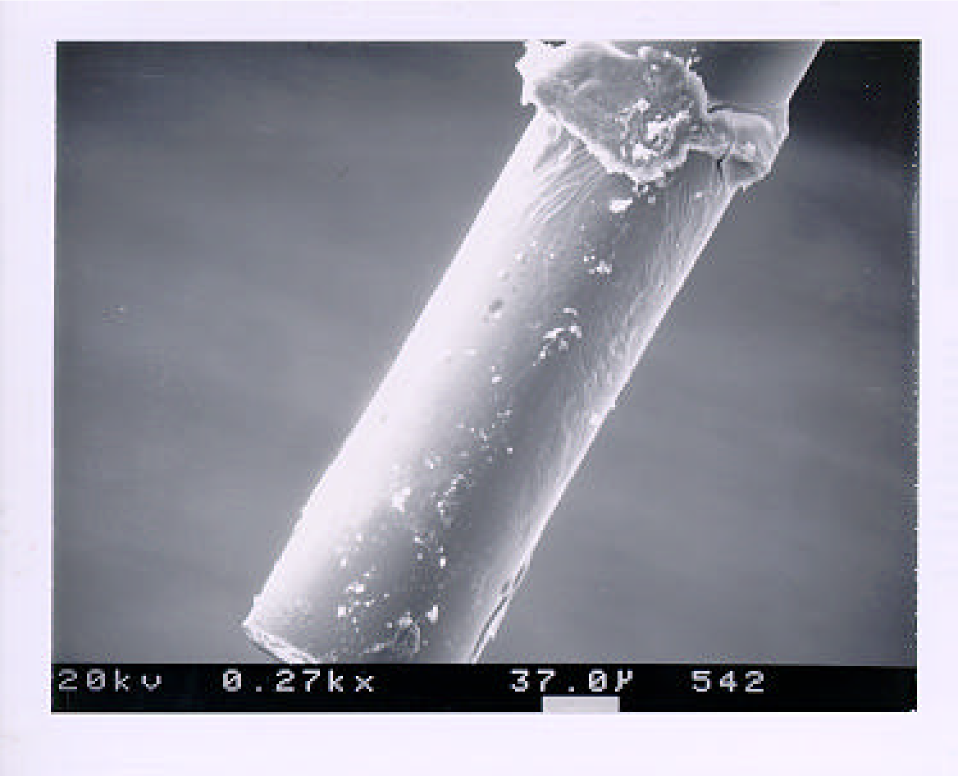

Figure 4.13 SEM photograph of a 10% PVP_{10}-sized E-glass fiber debonded from nylon 66.

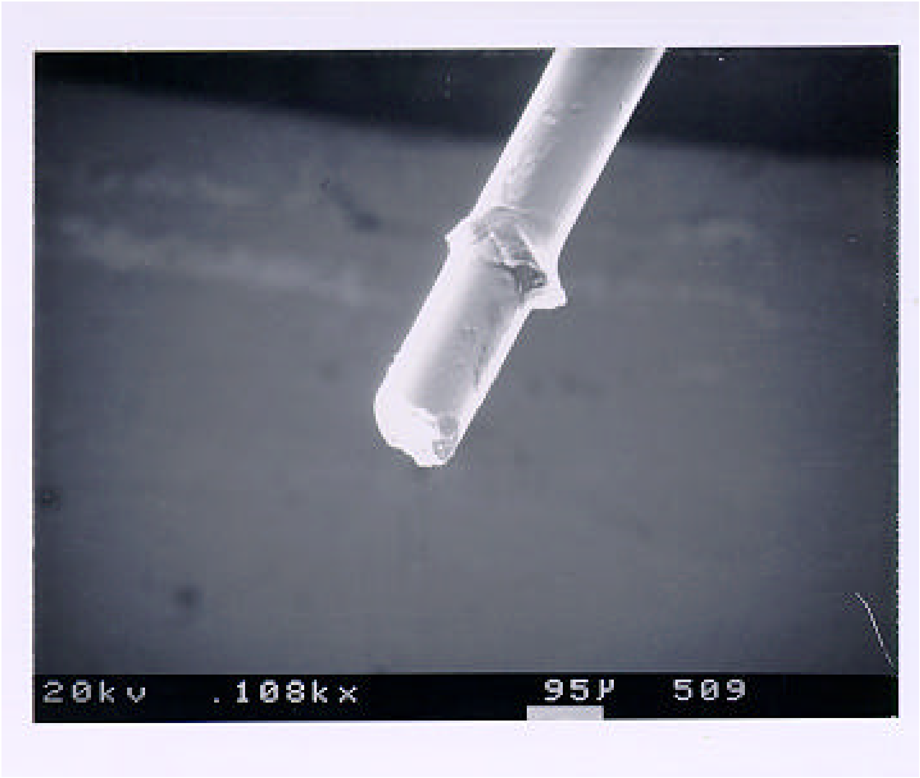

Figure 4.14 SEM photograph of a 1% PVP_{360}-sized E-glass fiber debonded from nylon 66.

Figures 4.15 through 4.18, respectively. Again, it can be seen that the failure of the unsized E-glass/nylon 66 composite is cohesive. In addition, the thickness of the nylon layer is on the order of microns. Furthermore, the failure surfaces of the sized fibers debonded from nylon seem to indicate a more adhesive failure, or a shift of the cohesive failure in the nylon closer to the fiber.

Inspection of the photographs of the unsized and 10% PVP_{10} -sized LDC fibers debonded from nylon 66 in Figure 4.19 shows no change in fracture surface with the addition of the diluent. A comparison of the nylon 66 matrix after debonding from an unsized E-glass fiber and a LDC fiber is shown in Figure 4.20. The energy released from the glass composite is much greater than that for the LDC composite and is evident by the damage in these photographs.

4.4 Dynamic mechanical analysis (DMA)

Dynamic mechanical analysis was performed to test the damping properties of nylon 66 and that of the nylon 66 composites reinforced with E-glass and carbon fiber. In addition, is has been shown that the presence of transcrystallinity [52] and PVP [61] itself can influence the damping characteristics of a material.

4.4.1 Nylon 66

Figures 4.21 and 4.22 show the storage and loss moduli and tan δ of the dynamic mechanical spectrum for nylon 66, respectively. Two consecutive runs were performed, and each is indicated in the figures. Figure 4.21 shows the typical storage

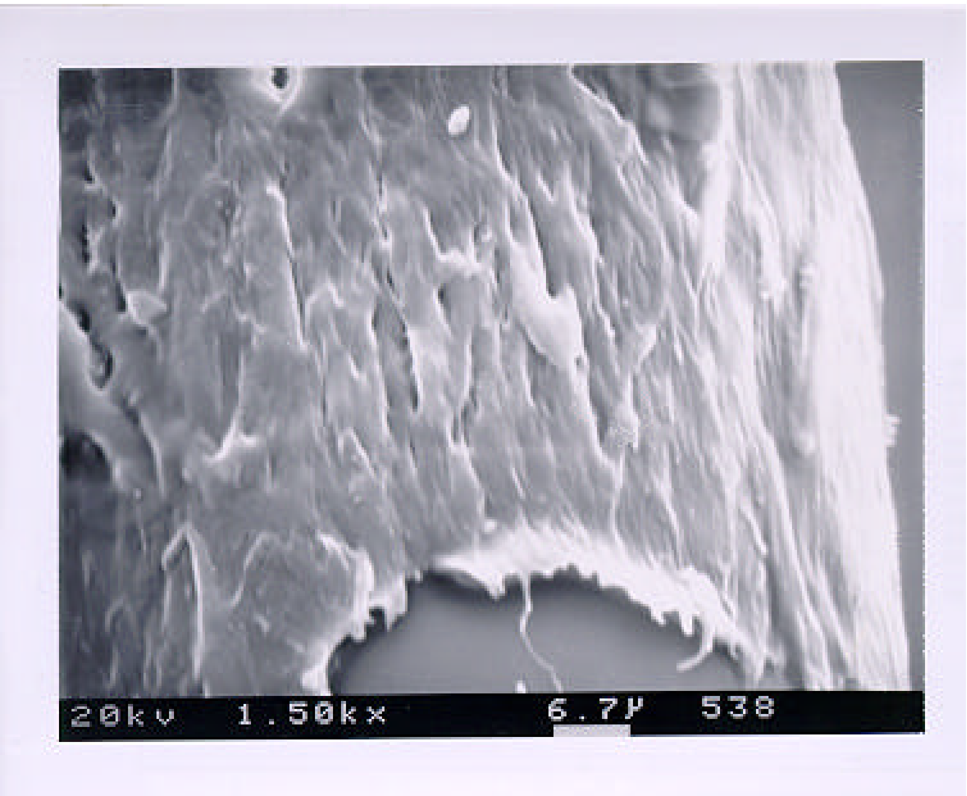

Figure 4.15 Higher magnification SEM photograph of an unsized E-glass fiber debonded from nylon 66.

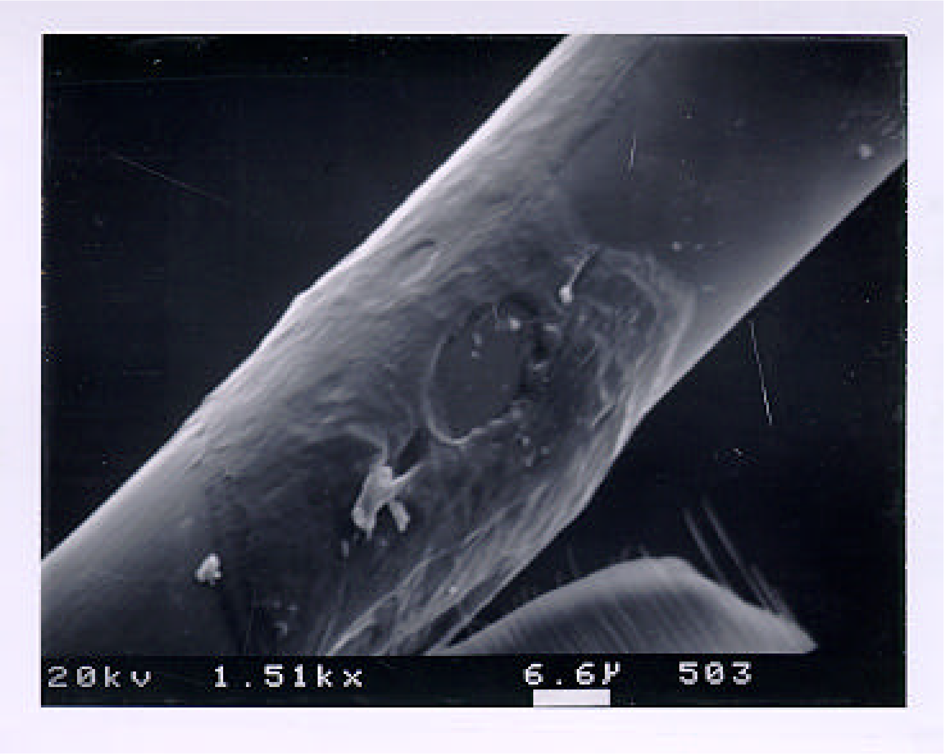

Figure 4.16 Higher magnification SEM photograph of a 1% PVP_{10}-sized E-glass fiber debonded from nylon 66.

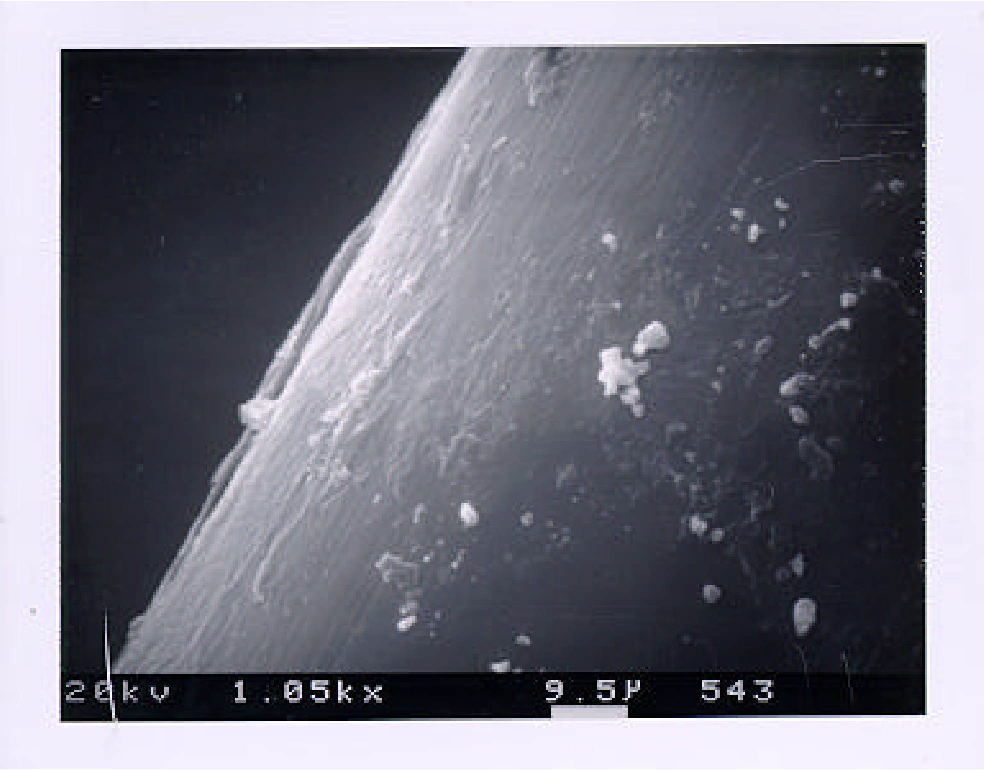

Figure 4.17 Higher magnification SEM photograph of a 10% PVP_{10}-sized E-glass fiber debonded from nylon 66.

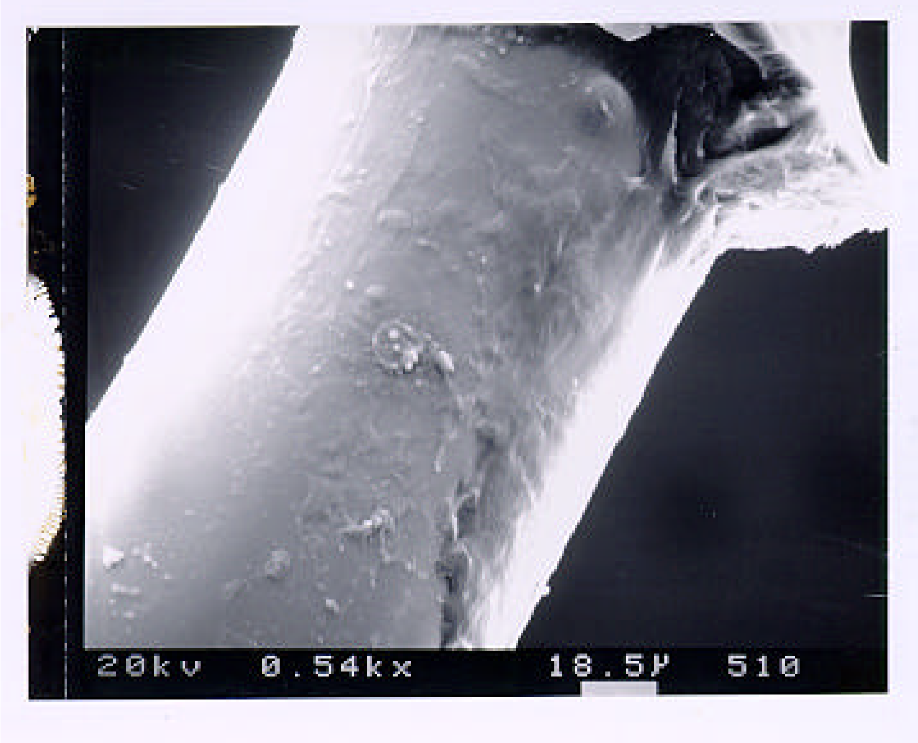

Figure 4.18 Higher magnification SEM photograph of a 1% PVP_{360}-sized E-glass fiber debonded from nylon 66.

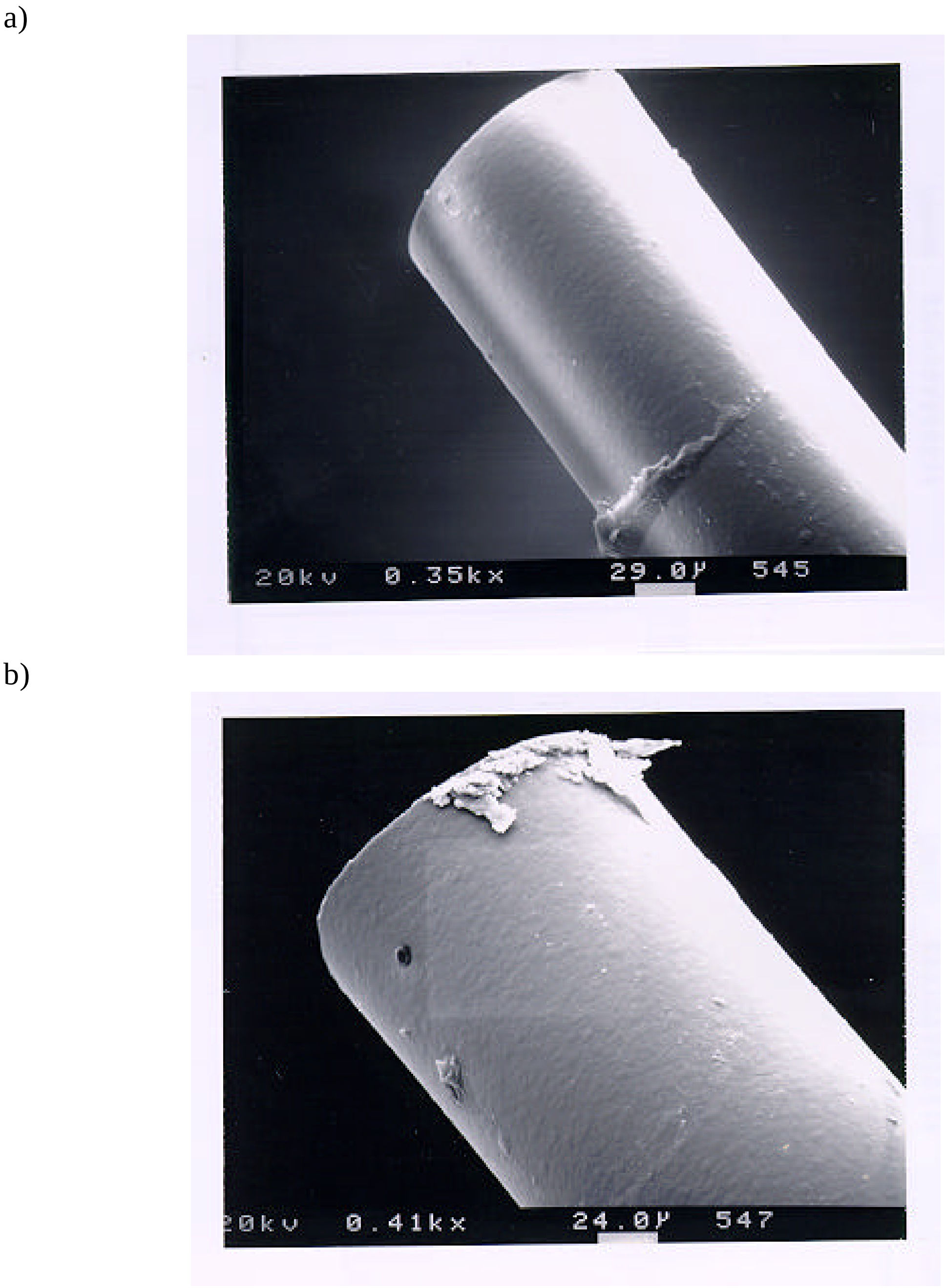

Figure 4.19 SEM photographs of a) unsized and b) 10% PVP_{10}-sized LDC fibers debonded from nylon 66.

a)

b)

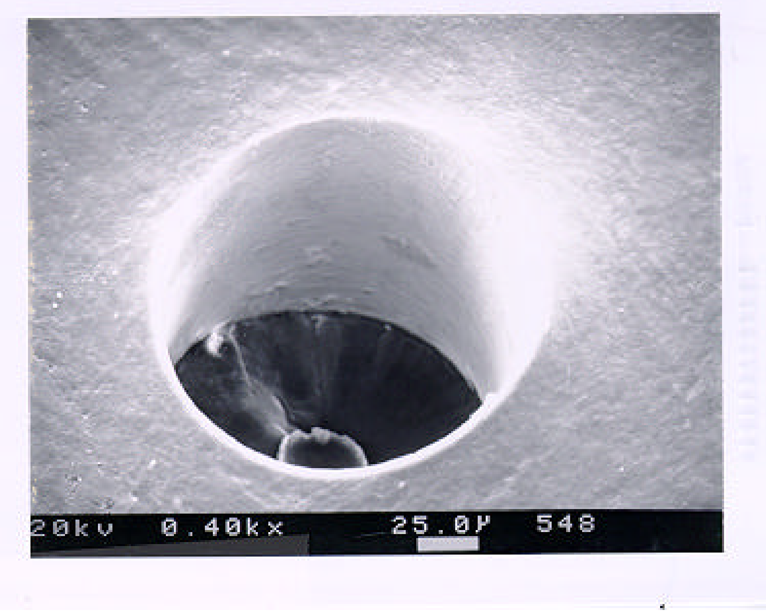

Figure 4.20 SEM photographs of nylon 66 after debonding an unsized a) E-glass and b) LDC fiber.

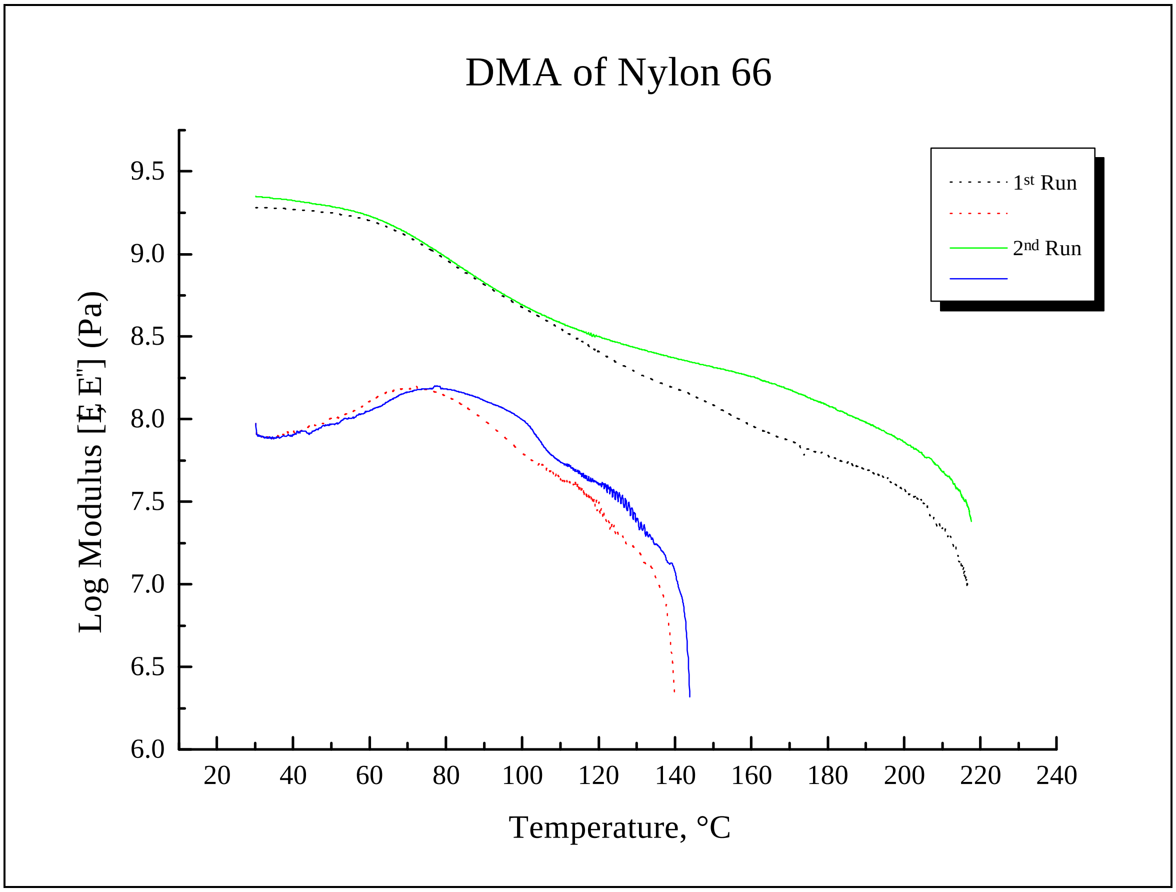

Figure 4.21 Dynamic mechanical spectrum of nylon 66: Storage and loss moduli versus temperature.

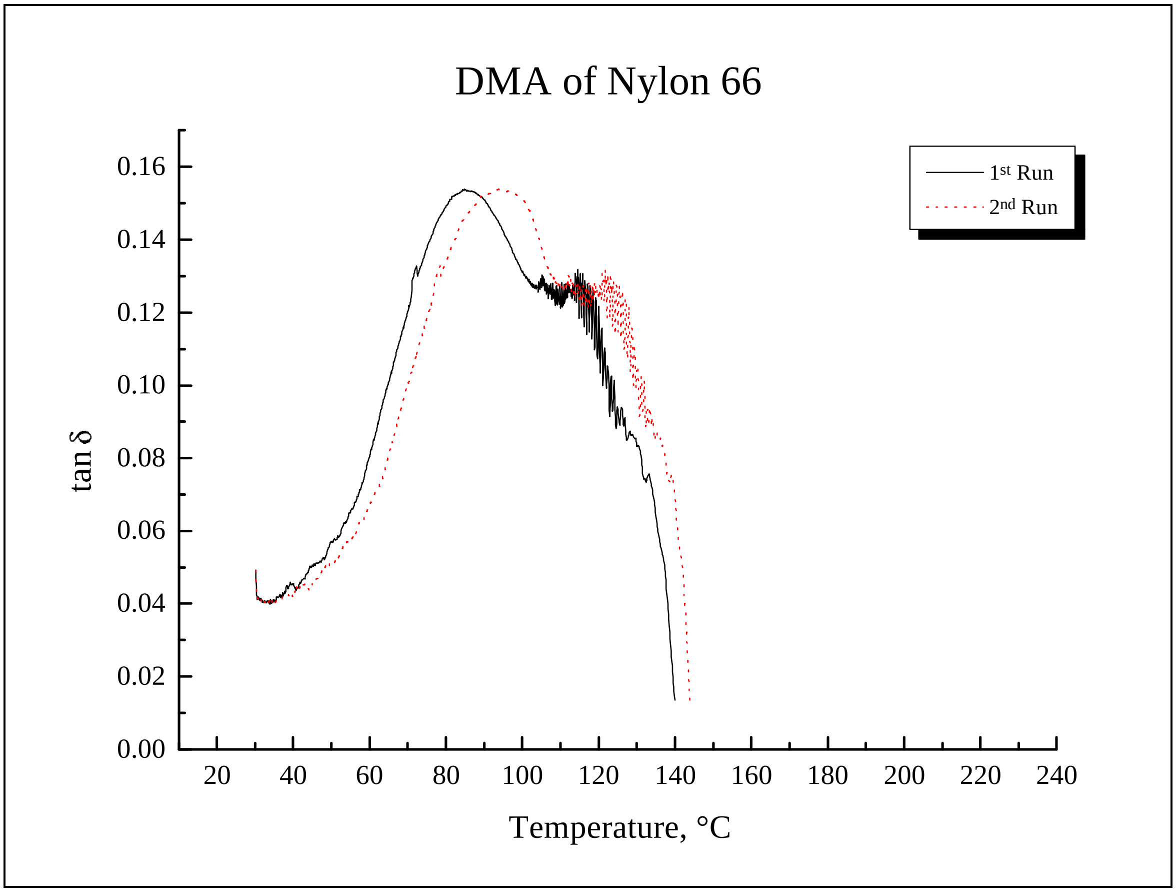

Figure 4.22 Dynamic mechanical spectrum of nylon 66: tan δ versus temperature.

modulus curve for a semicrystalline polymer. An initial modulus on the order to 10^9 Pa is shown with a drop in modulus associated with the α-peak, or the glass transition temperature of the material at approximately 75°C, taken from the loss modulus. Following the glass transition, a slight decrease in modulus is found as a function of temperature until viscous flow is reached at approximately 210°C and storage modulus decreases rapidly.

Two scans were performed to make sure that the samples were completely crystallized and that recrystallization was not possibly influencing the spectrum. The two runs are essentially identical with no change in shape or shifts in peak positions indicated. Furthermore, the low temperature β and γ peaks are not shown due to the starting temperature of the test. The β-transition is associated with the segmental motion involving polyamide groups in the amorphous region that are not hydrogen bonded to other amide groups on nearby chains. Furthermore, the γ-transition is thought to be related to the small scale reorientational motion in the amorphous region of the methylene units between the amide groups [53]. Investigation of these peaks is not relevant because the addition of a filler material has been shown to only reduce the magnitude of these peaks. Furthermore, it is expected that the addition of the diluent will not influence either of these peaks.

However, there does seem to be an additional loss peak in both the loss modulus and tan δ in both scans. In the literature, a loss peak found above the glass transition of a semicrystalline material can be attributed to the constrained amorphous regions found between the crystals.

4.4.2 E-glass/Nylon 66 composite

Next, the dynamic mechanical spectrum for E-glass fiber reinforced nylon 66 \was obtained. Figures 4.23 and 4.24 show the storage and loss moduli and tan δ of the dynamic mechanical spectrum for an unsized and sized E-glass/nylon 66 composite, respectively. First, if the unsized E-glass composite spectrum is compared to that of the neat nylon 66, it can be seen that the initial storage modulus is higher for the composite and that it maintains its stiffness at high temperatures. Next, the tan δ comparison indicates that the damping associated with the T_g is reduced in magnitude and broadened in the composite. This is due to the high volume fraction of fiber (see TGA results) which reduces the amount of matrix present and constricts the motion of the nylon 66. However, there is no shift in peak location.

A comparison of the unsized versus sized sample shows that the addition of the PVP seems to have no effect on the damping characteristics of the E-glass composite. The position and size of all curves remain unchanged.

4.4.3 Carbon fiber/Nylon 66 composite

Figures 4.25 and 4.26 show the dynamic mechanical spectra for unsized and sized carbon fiber reinforced nylon 66. Figure 4.25 plots the loss and storage modulus versus temperature, while Figure 4.26 shows the tan δ as a function of temperature. The addition of carbon fiber has the same effect as the glass fiber on the modulus. To

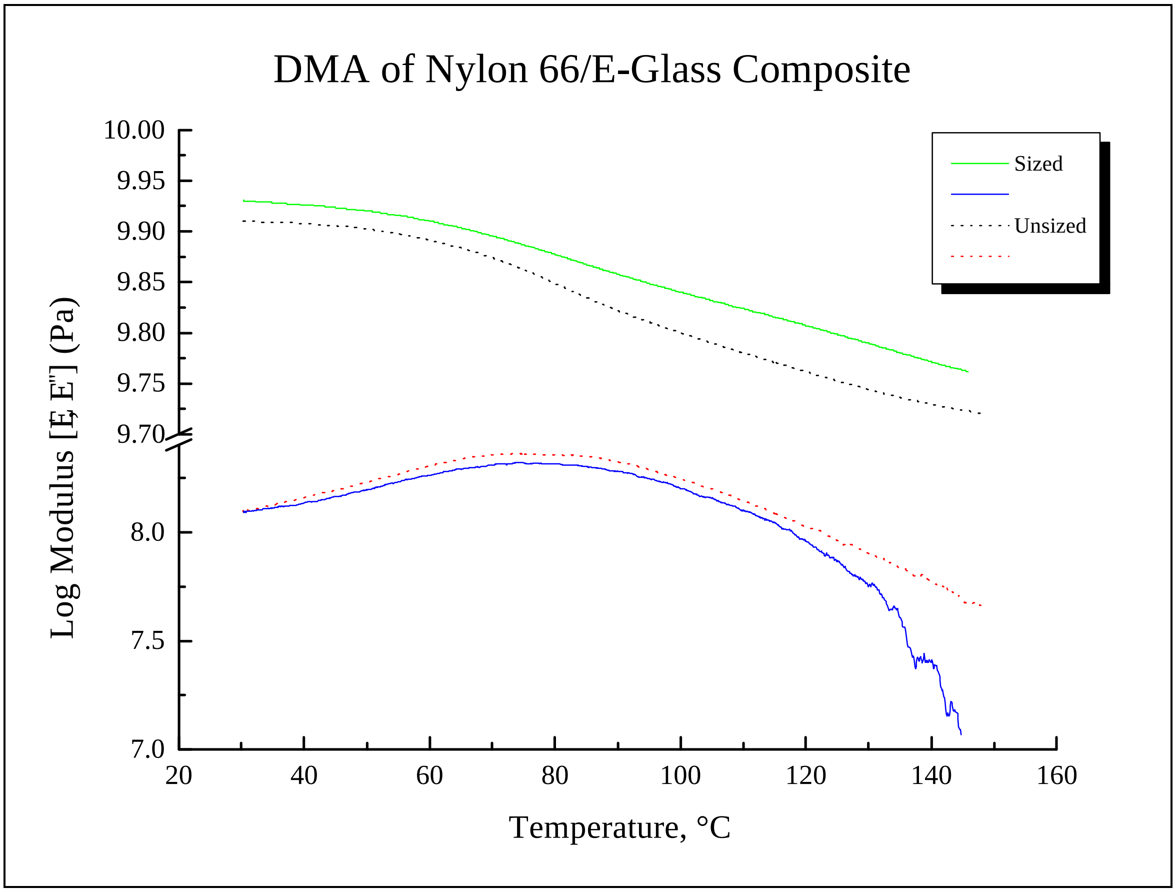

Figure 4.23 Dynamic mechanical spectrum of an unsized and sized E-glass/nylon 66 composite: Storage and loss moduli versus temperature.

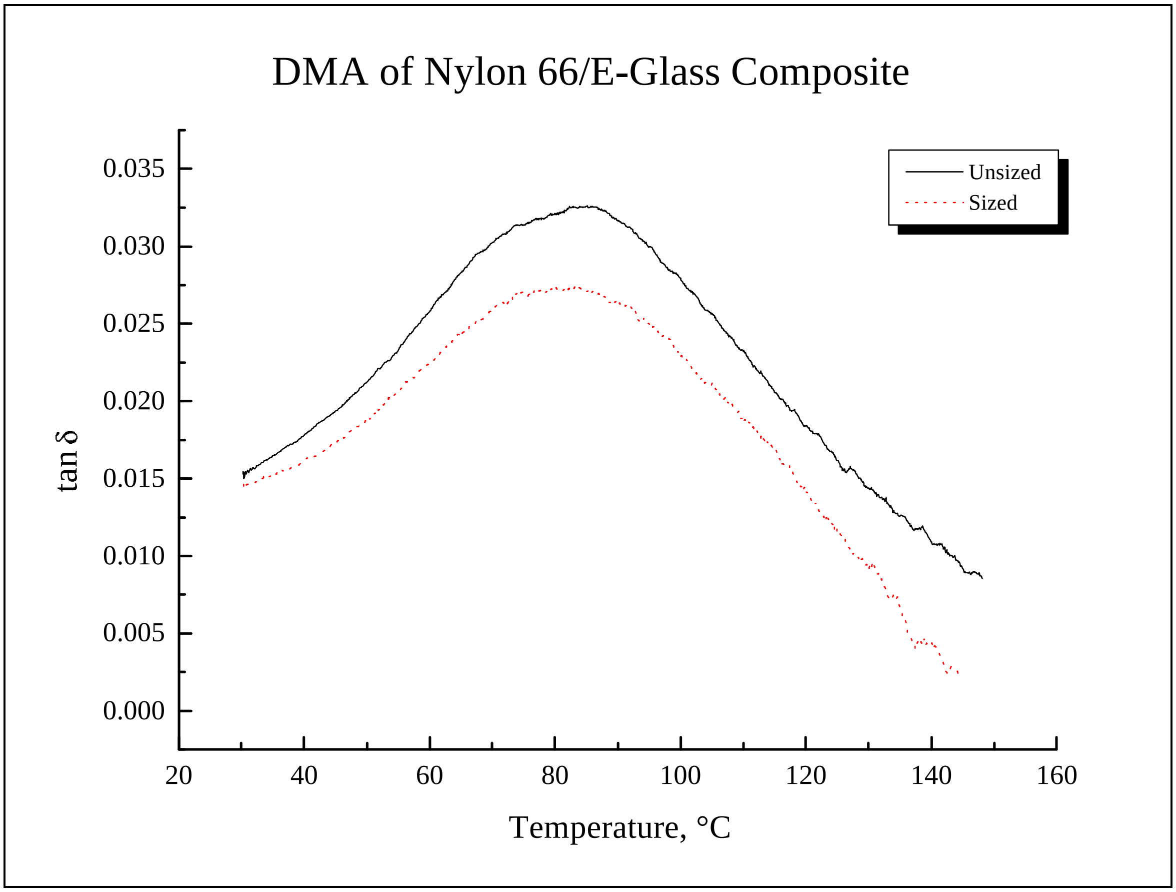

Figure 4.24 Dynamic mechanical spectrum of an unsized and sized E-glass/nylon 66 composite: tan δ versus temperature.

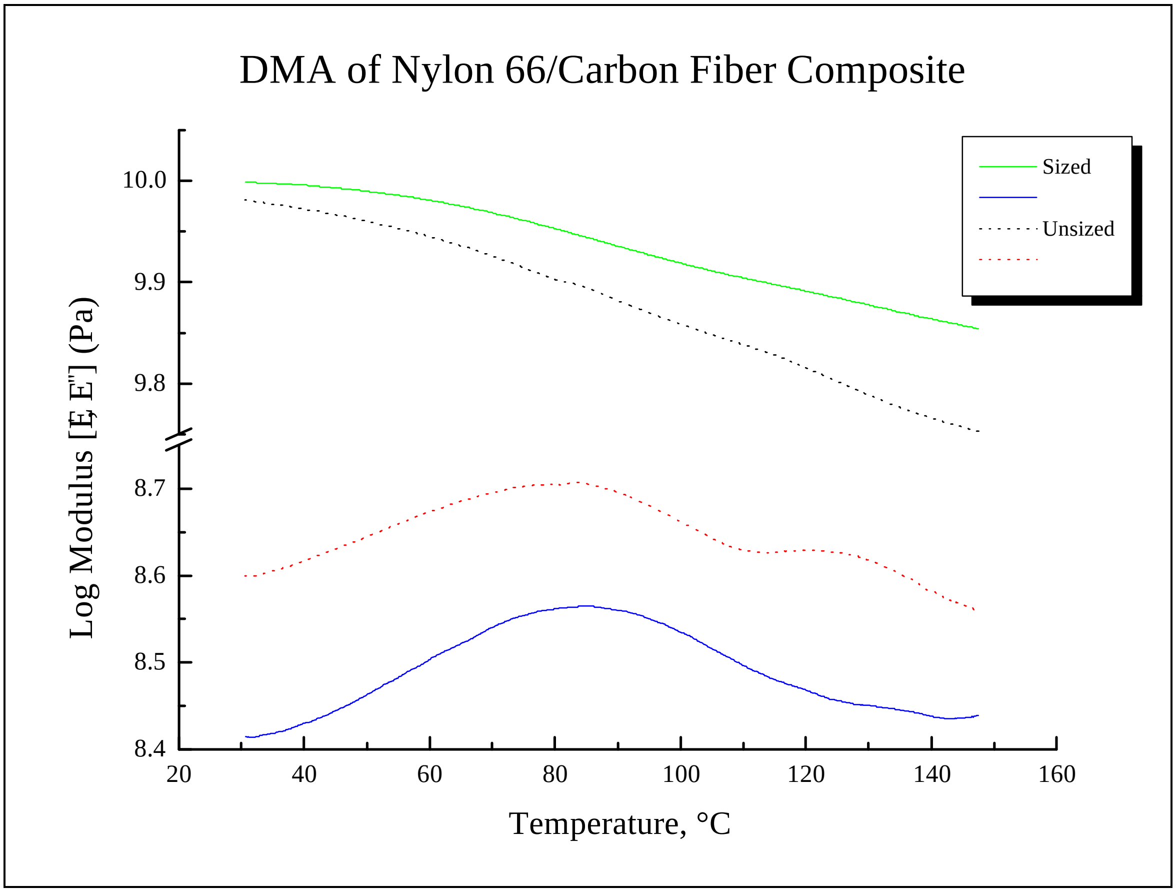

Figure 4.25 Dynamic mechanical spectrum of an unsized and sized carbon fiber/nylon 66 composite: Storage and loss moduli versus temperature.

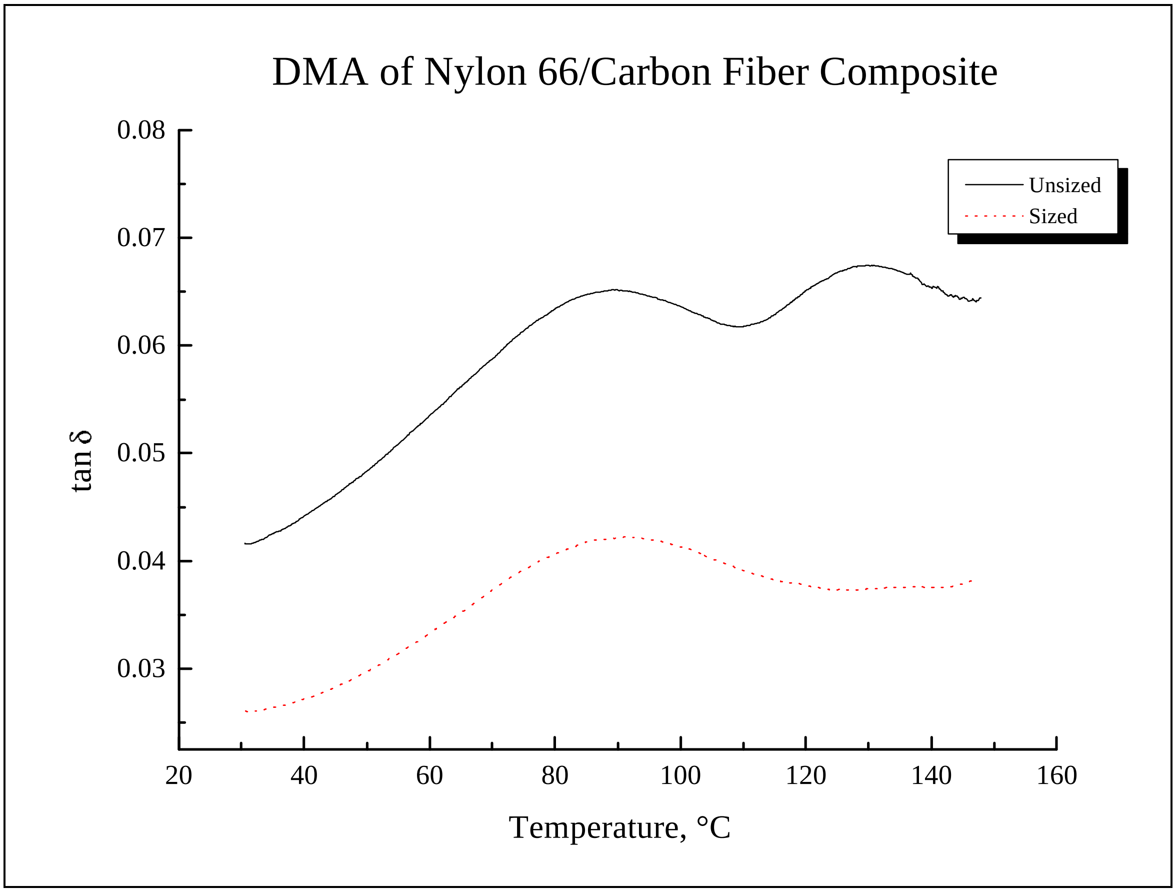

Figure 4.26 Dynamic mechanical spectrum of an unsized and sized carbon fiber/nylon 66 composite: tan δ versus temperature.

illustrate this, the storage moduli for nylon 66, E-glass composite, and the carbon fiber composite are shown in Figure 4.27.

Now, returning to the carbon fiber composite system, the loss modulus spectrum shows an additional damping peak in the unsized composite at approximately 125°C that is not present in either the neat nylon or glass fiber composite. The tan δ spectrum shows the additional peak around 130°C. Sequential runs of the sample indicated that the peak is thermally reversible. This second damping peak has not been observed in the literature previously, therefore, the molecular mechanisms for its presence is unknown. Three molecular interpretations have been made here. The damping could be due to the recrystallization of nylon, the glass transition temperature of a compatiblizer present on the fibers, or the damping from the constrained amorphous phase in the transcrystalline interphase.

Investigation of the sized carbon fiber composite spectrum shows the additional peak is now absent from the loss modulus and tan δ spectrums. The presence of the PVP seems to have removed the additional damping mechanism from the composite.

To determine if the PVP was possibly shifting this peak up in temperature, additional DMA runs were made to higher temperatures on the sized carbon fiber sample. The results are shown in Figure 4.28. This figure shows a dramatic damping peak around 187°C. This, however, is most likely not resulting from the same molecular mechanism associated with the 130°C peak due to its extremely large magnitude. The molecular causes for this peak are unknown and will be examined in

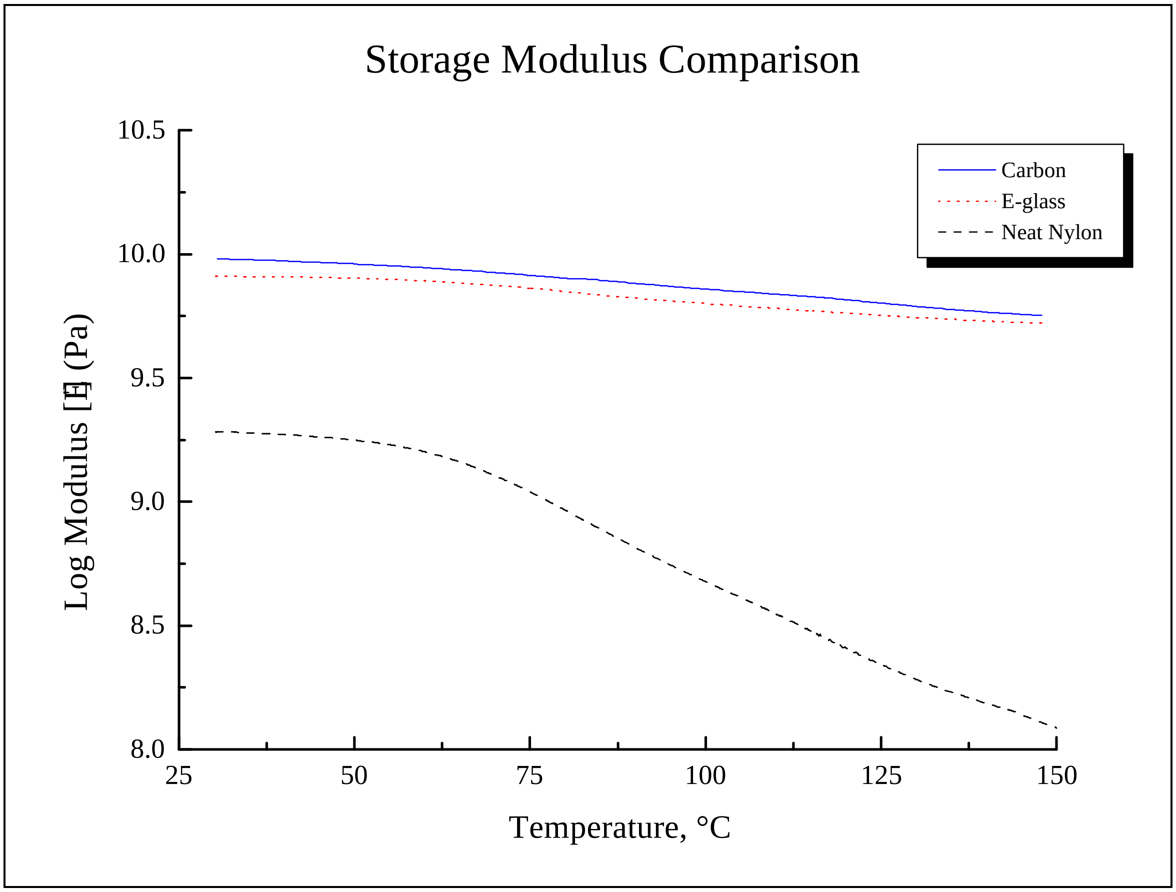

Figure 4.27 Storage modulus versus temperature for nylon 66, E-glass composite, and carbon fiber composite.

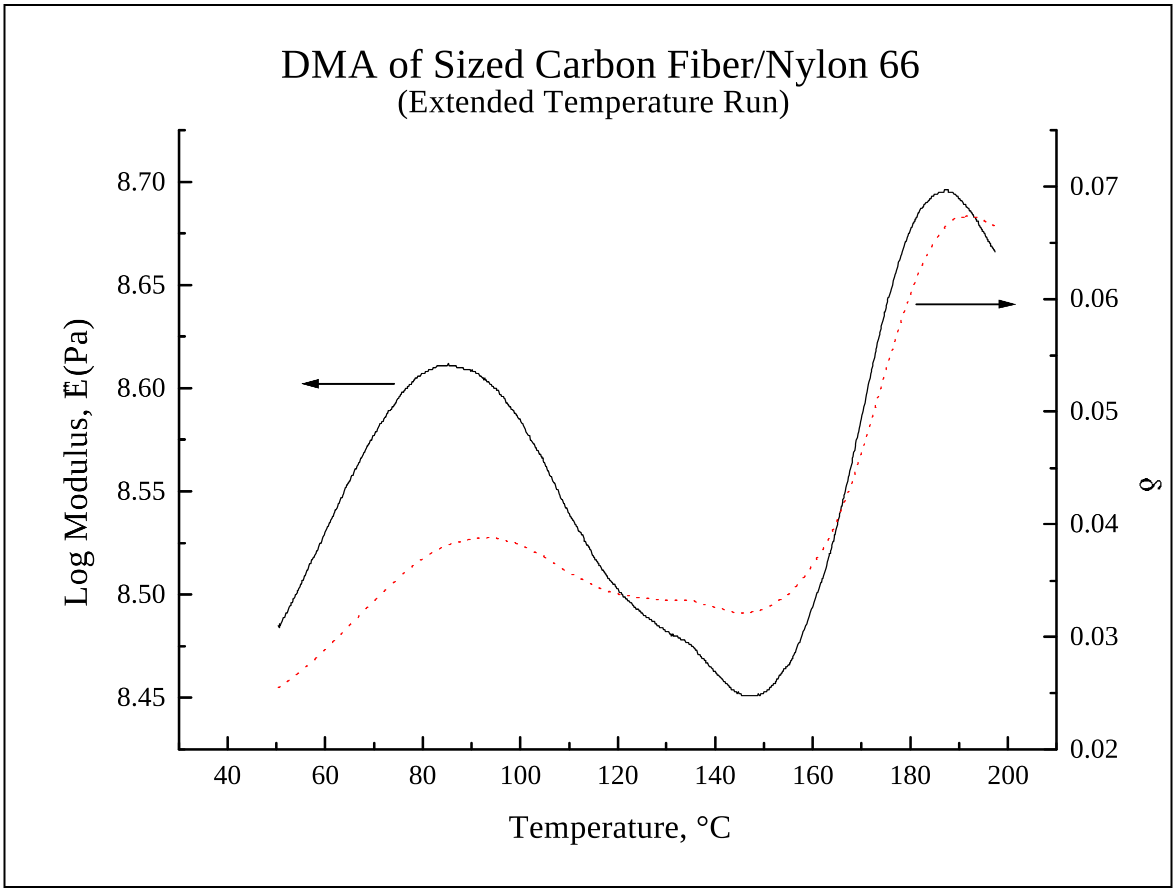

Figure 4.28 Extended temperature spectrum showing loss modulus and tan δ versus temperature for sized carbon fiber composite.

further studies.

To help determine the origin of the peak at 130°C, efforts were made to remove the compatiblizer from the carbon fiber plain weave fabric. A solvent wash and drying period described in the experimental section was used along with an additional heat treatment using the hot press with contact pressure at 290°C (this temperature was chosen as a result of TGA) for 10 minutes. Samples were then made and sequential DMA's were performed up to 220°C. The results are shown in Figure 4.29, and both peaks are still evident in all runs, again, indicating thermal reversibility.

4.5 Thermogravimetric analysis (TGA)

Thermogravimetric analysis was used to determine the thermal stability of the polymers used in this study. Figure 4.30 and 4.31 show the TGA for neat nylon 66 and PVP, respectively. Both samples were run 'as-received,' i.e., no drying was used on either material before testing. The nylon TGA shows that it is thermally stable up to 350°C. There are some low molecular weight species burning off below 200°C, i.e., moisture, however the percentage is less than 1% of the sample. In addition, PVP is also thermally stable up to 350°C. A burn-off of a low molecular weight species below 200°C is apparent for PVP also, but it makes up about 12% of the material. Both materials are hydrophilic, therefore, the low temperature loss of weight is most likely moisture in both materials. The amount of moisture in the nylon is somewhat low (see the moisture adsorption section), but the 12% of the PVP is common because PVP is extremely hydrophilic.

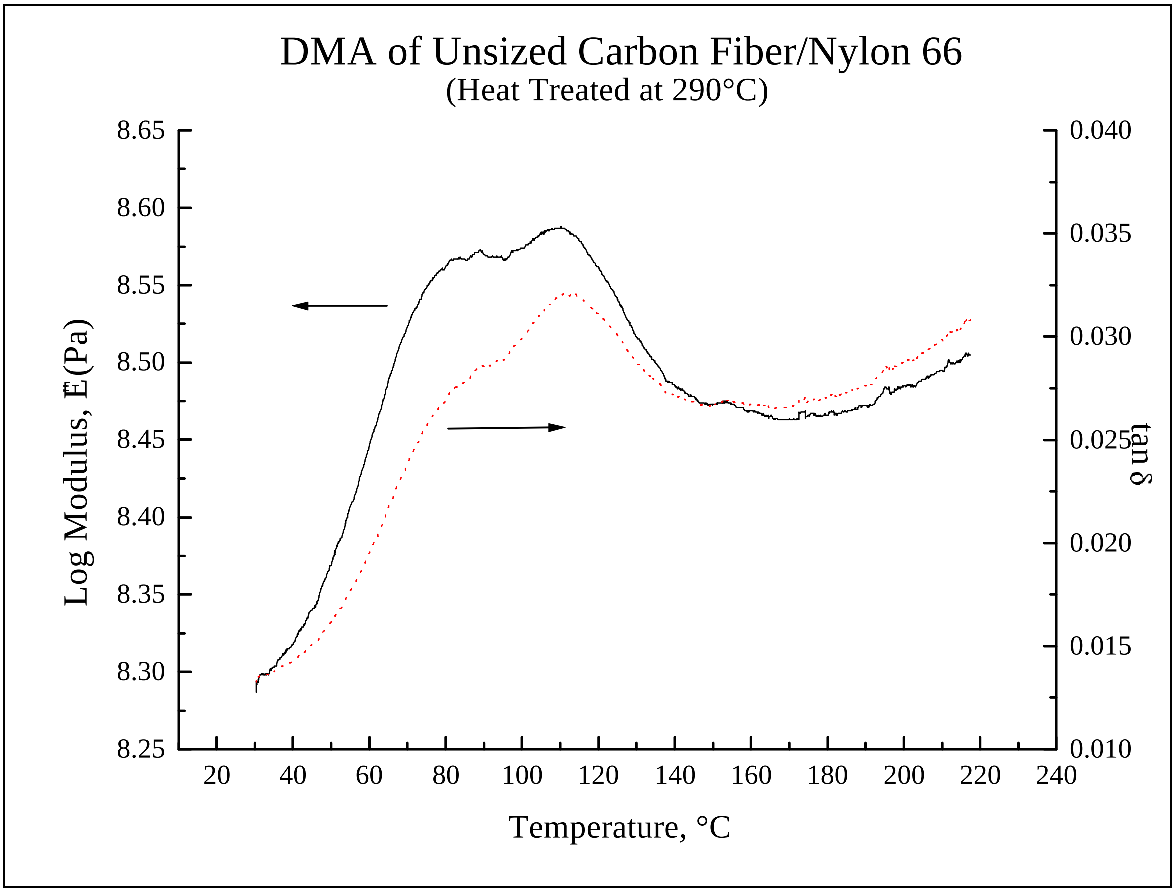

Figure 4.29 Extended temperature spectrum showing loss modulus and tan δ versus temperature for a weave-treated unsized carbon fiber composite.

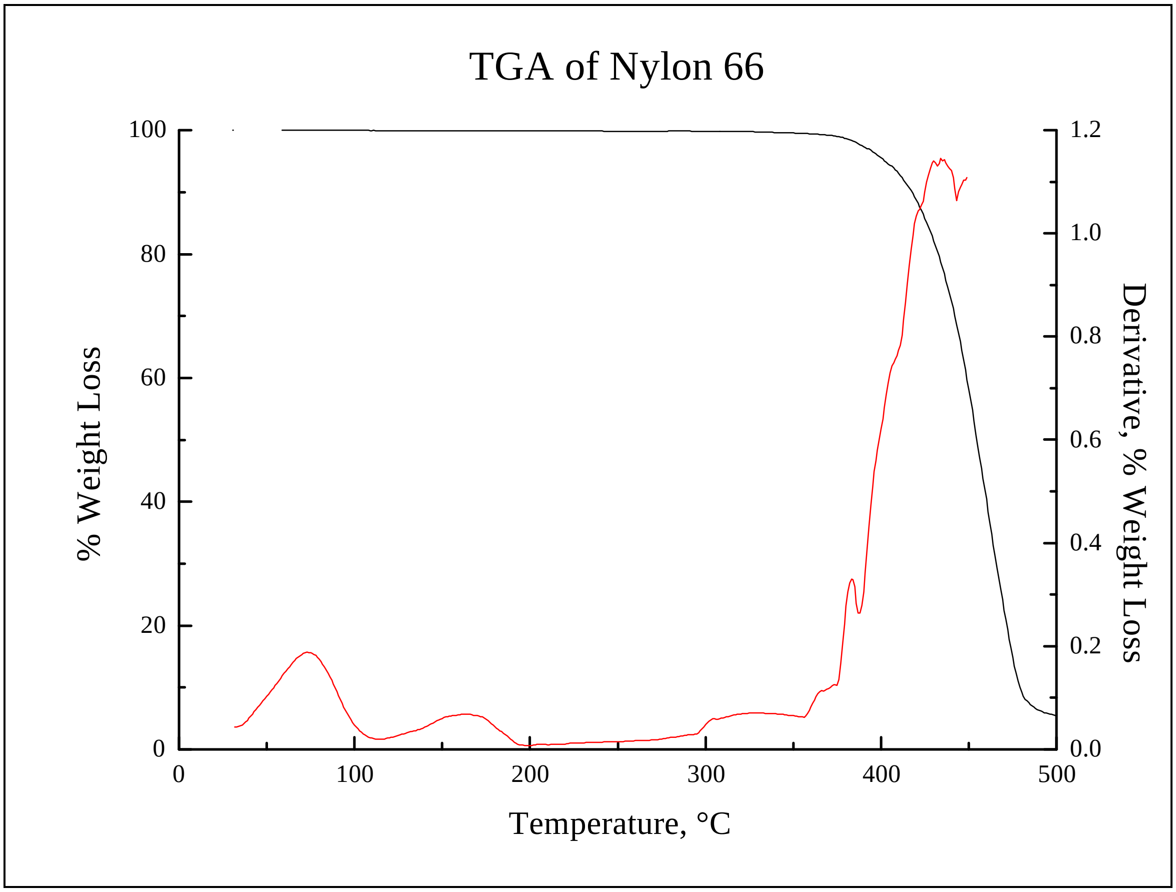

Figure 4.30 Percent weight loss versus temperature of nylon 66.

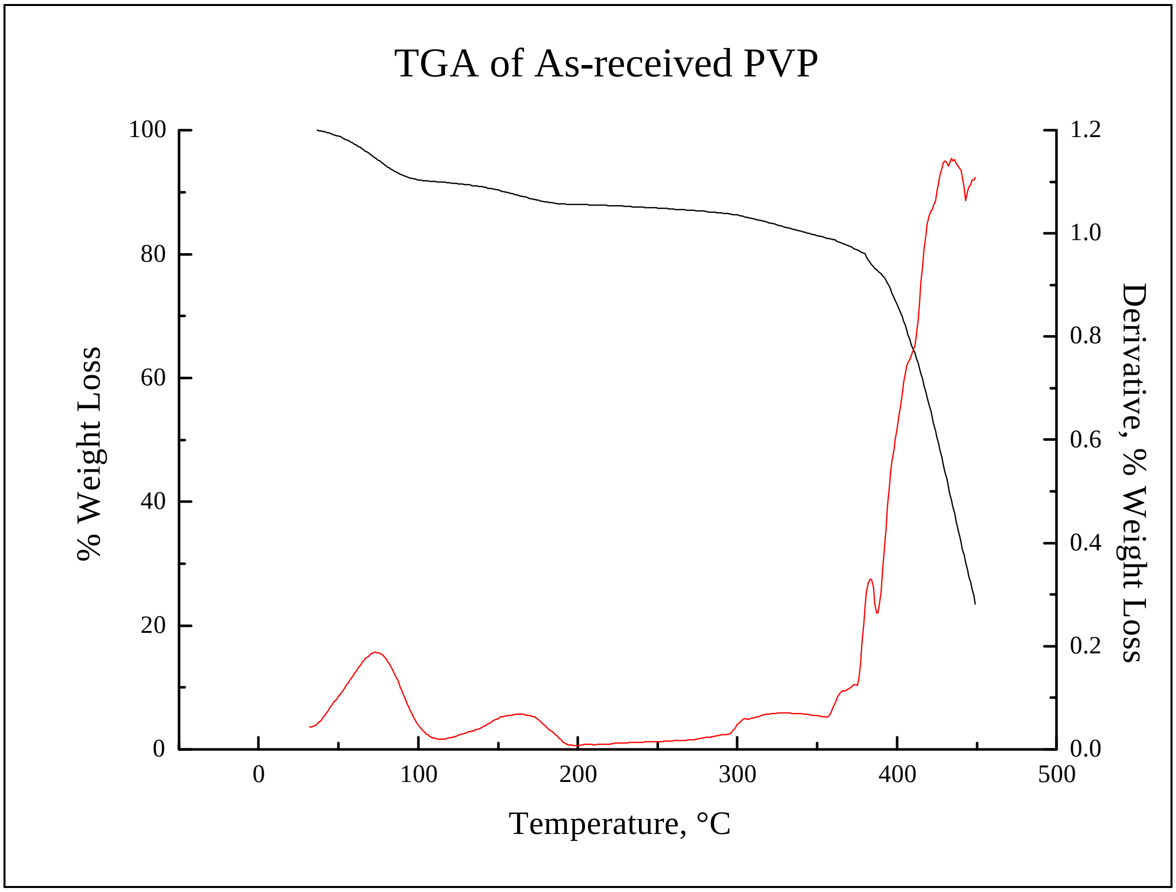

Figure 4.31 Percent weight loss versus temperature of poly(vinyl pyrrolidone).

In addition to the raw polymers, TGA was performed on the sections of the composite samples to determine weight percentages of fiber and polymer. Figures 4.32 and 4.33 show the temperature versus weight loss for the unsized and sized E-glass carbon fiber composites, respectively. Furthermore, Figures 4.34 and 4.35 show the TGA for an unsized and sized carbon fiber composite, respectively. The TGA's were used to calculate the weight percentages of fiber and matrix in each composite. The weight percentage of reinforcement in the E-glass composites is approximately 68%, which correlates quite well with the weight measurements taken before and after molding of 72%. In addition, the TGA shows a fiber weight percentage of 60% for carbon fiber composites which also correlates with weight measurements taken before and after molding of 59%.

Additional TGA's were performed on the carbon fiber plain weave fabric before and after exposure to a solvent and drying treatment. This was conducted to try to determine the amount of compatiblizer on the fabric, and to see if the treatment removed the compatiblizer. The results are shown in Figures 4.36 and 4.37 for the untreated and treated cloth, respectively. The data indicates that the compatiblizer is approximately one percent of the fabric weight, and it is thermally unstable at 290°C. Furthermore, the solvent and drying treatment does not remove the compatiblizer from the weave.

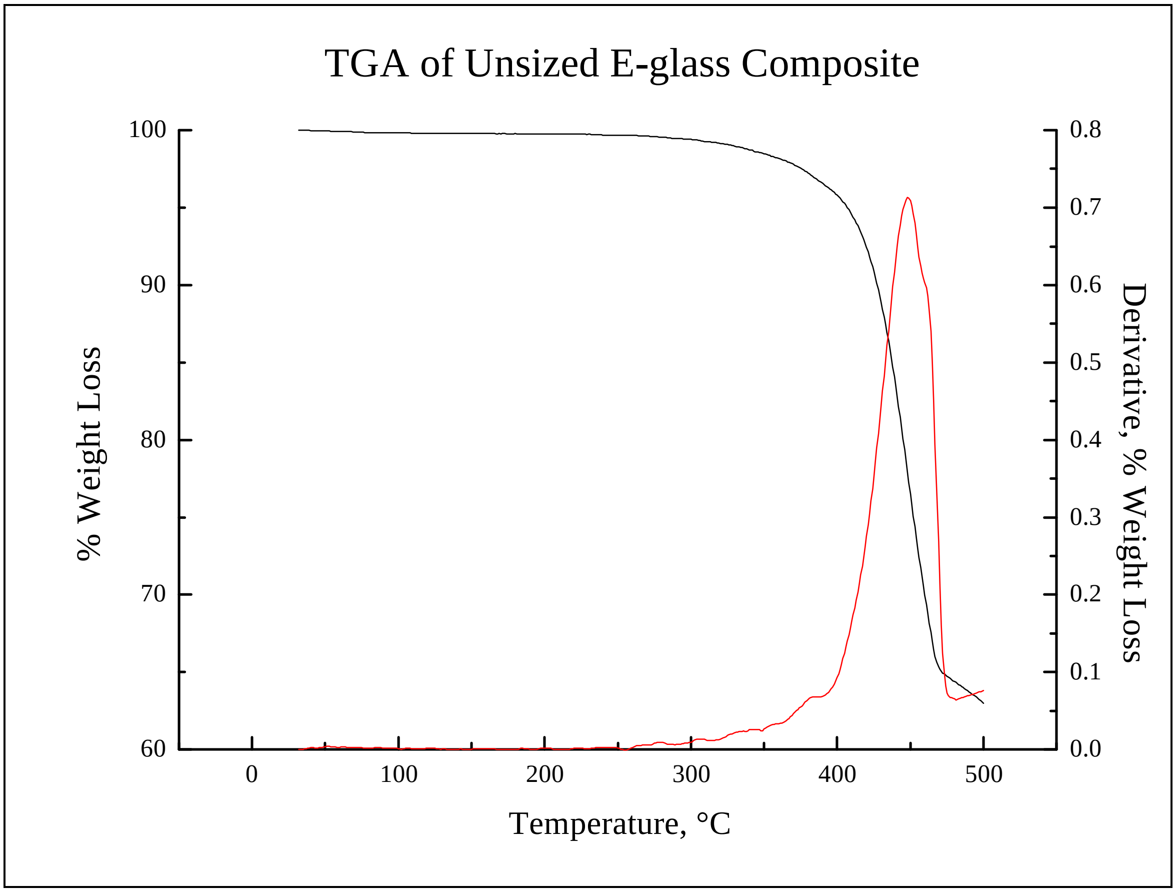

Figure 4.32 Percent weight loss versus temperature of the unsized E-glass/nylon 66 composite.

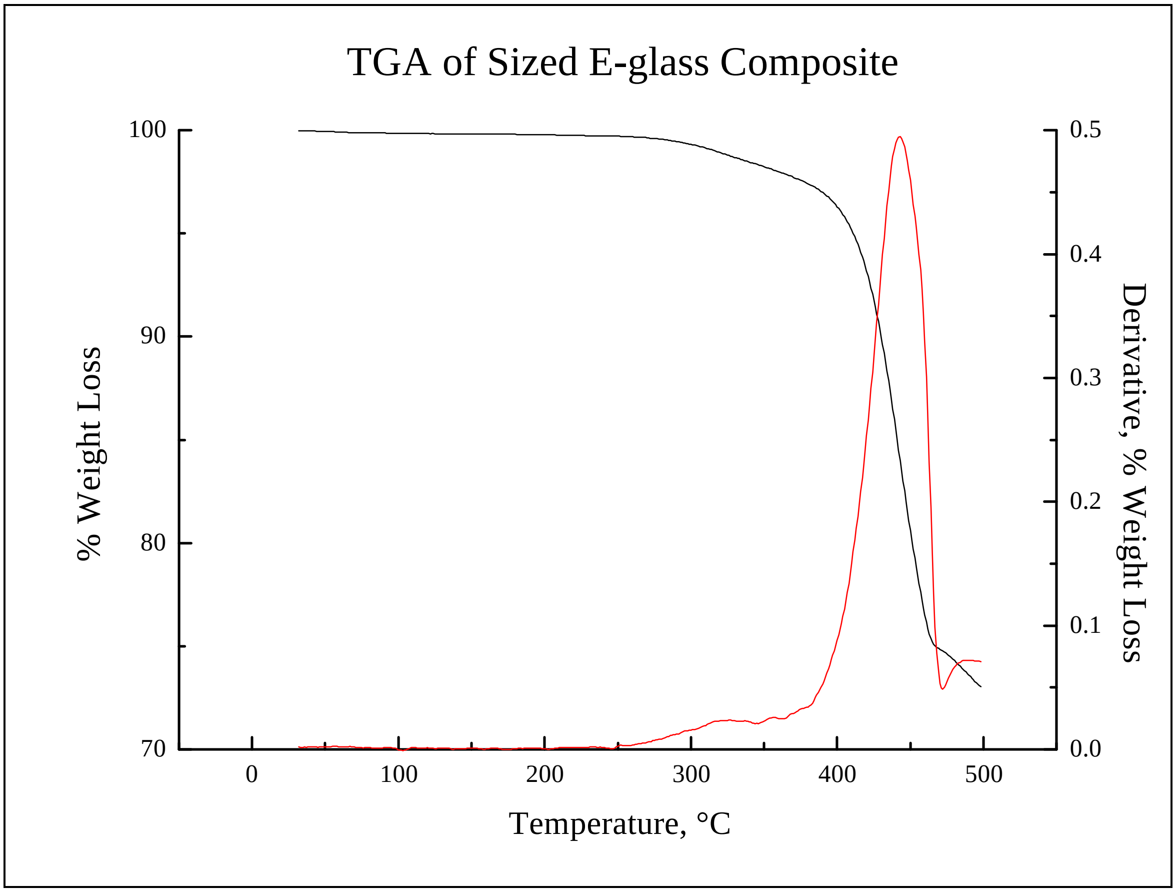

Figure 4.33 Percent weight loss versus temperature of the sized E-glass/nylon 66 composite.

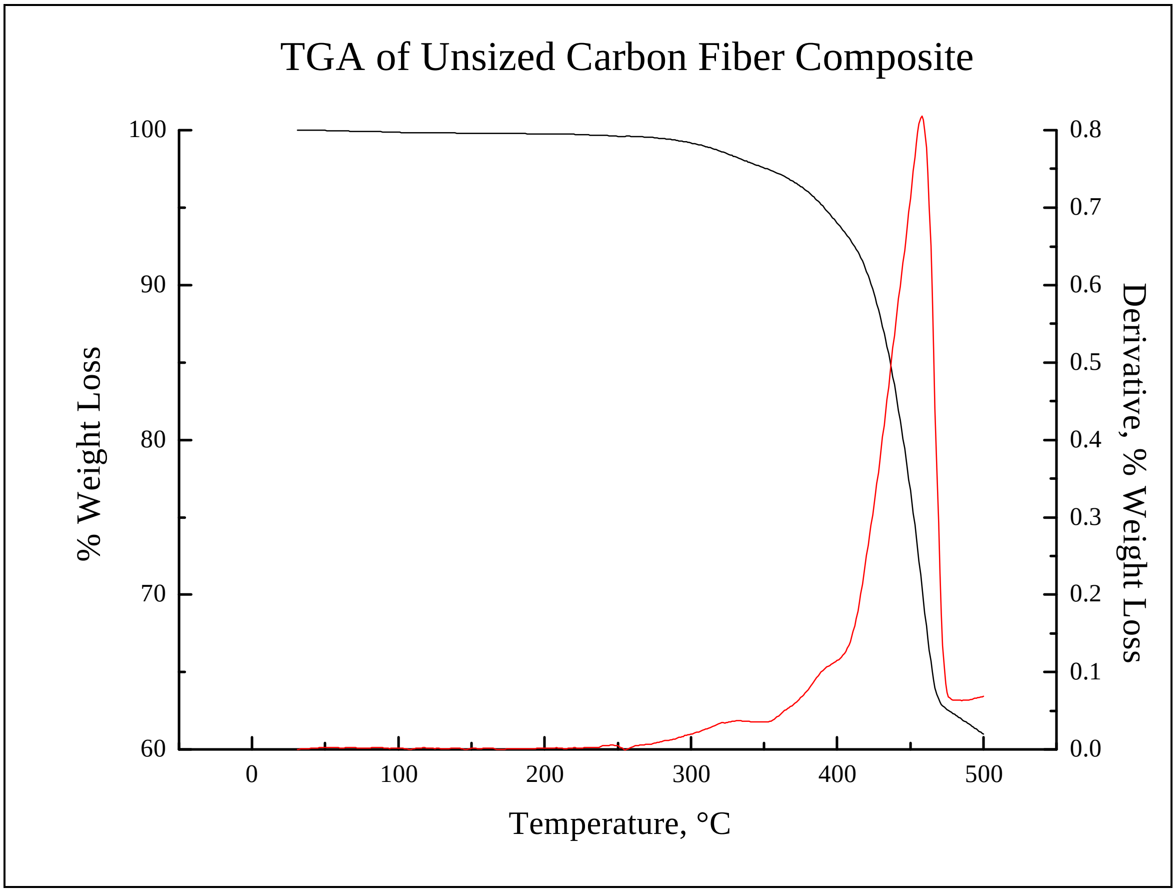

Figure 4.34 Percent weight loss versus temperature of the unsized carbon fiber/nylon 66 composite.

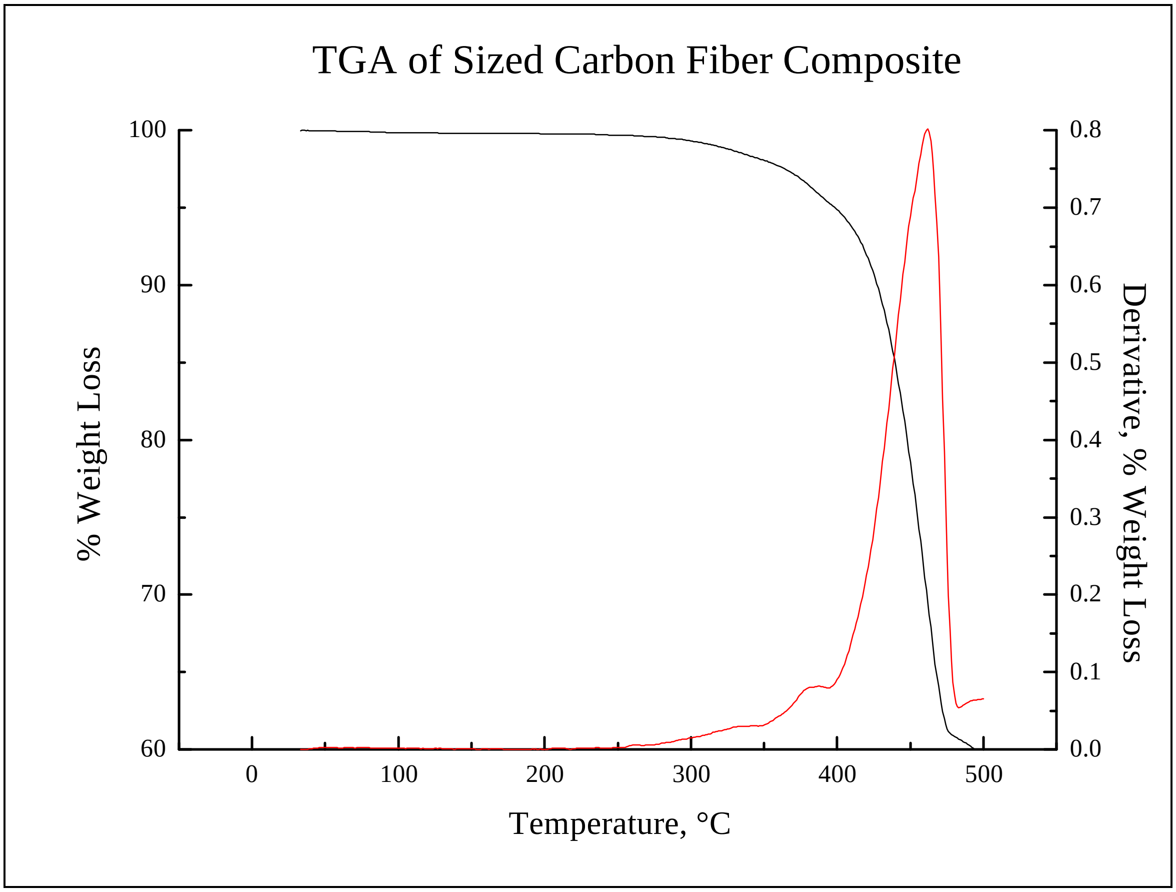

Figure 4.35 Percent weight loss versus temperature of the sized carbon fiber/nylon 66 composite.

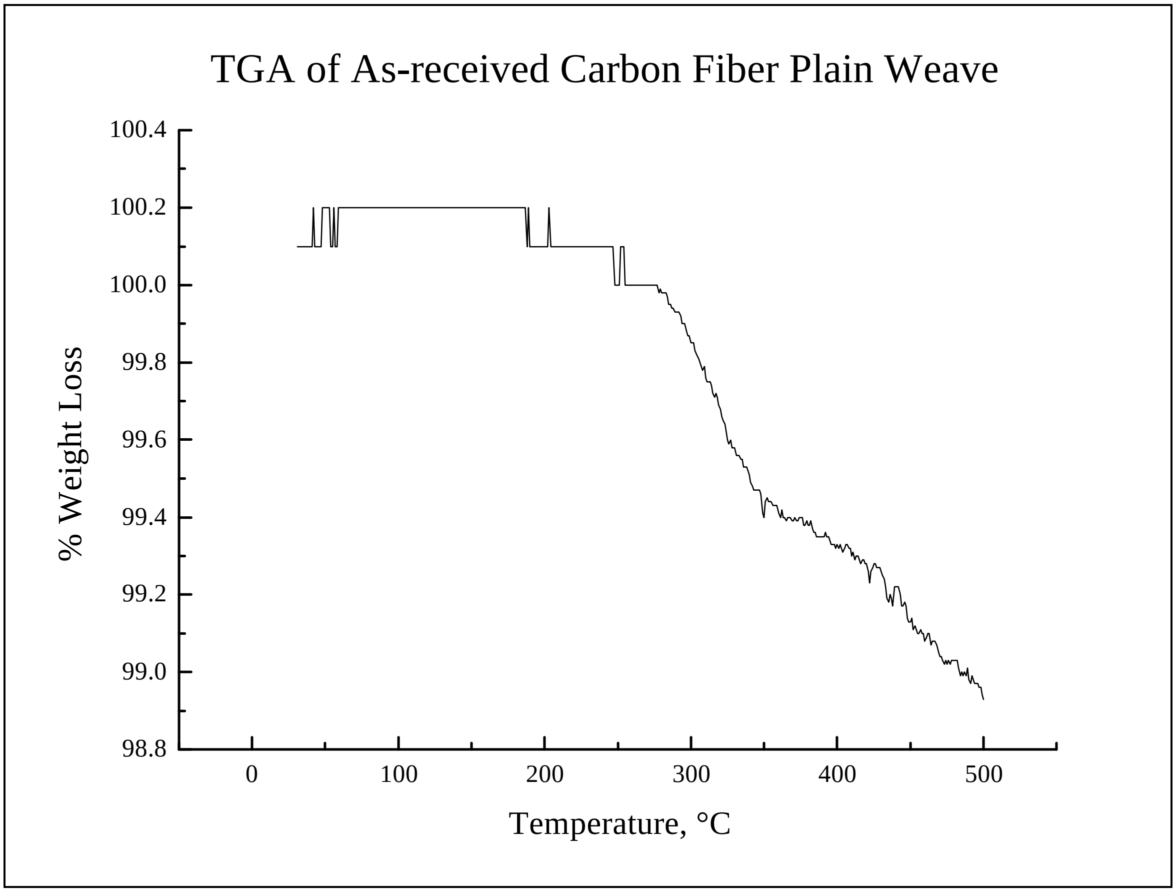

Figure 4.36 TGA of the as-received carbon fiber plain weave fabric.

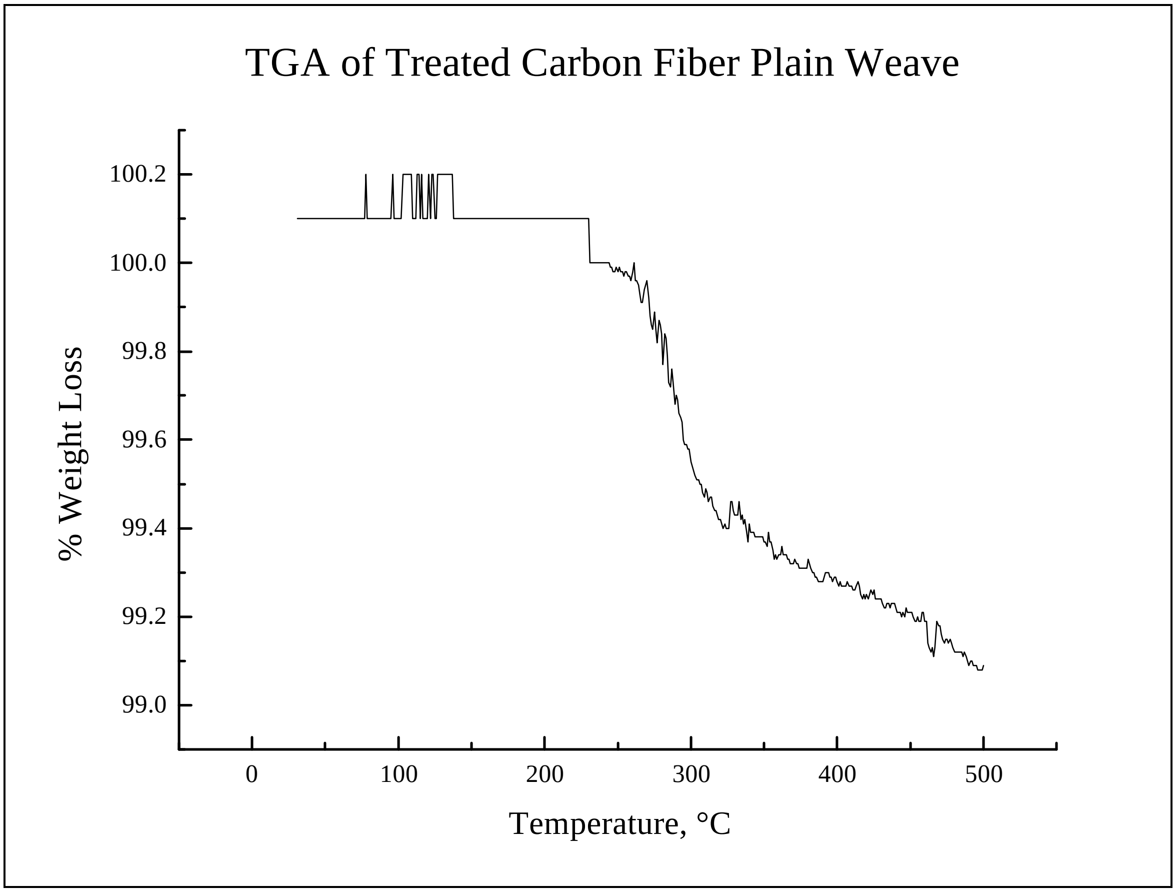

Figure 4.37 TGA of a carbon fiber fabric subjected to a solvent wash and drying treatment.

4.6 Differential scanning calorimetry (DSC)

Differential scanning calorimetry was conducted on the raw polymers, the composites, and melt blends of nylon 66 and PVP. Figure 4.38 shows the DSC scan for nylon 66 which has seen the same thermal treatment as the composite samples. The scan suggests a very small amount of recrystallization at 239°C, and melting of the nylon 66 is observed at 263°C. This scan was performed to determine if recrystallization is occurring during the temperatures used in the DMA tests, which would explain the additional peak in the DMA carbon fiber composite. DSC was also conducted on the PVP_{10} to determine the material's glass transition temperature. As-received PVP was first run, but the moisture present in the polymer did not allow for the T_g to be determined. PVP was then dried at 120°C for 48 hours, and two DSC runs were performed on two samples. The first sample was run from 30°C to 290°C, and an additional run was conducted from 30°C to 150°C, which is shown in Figure 4.39. As can be seen, the presence of moisture was still detected, and a T_g could not be calculated. However, the review of PVP by Robinson et al. [95] indicates that the glass transition temperature of a 10,000 molecular weight PVP should be approximately 110°C.

In addition to the neat polymers, DSC was performed on samples of both the unsized E-glass and unsized carbon fiber composites. This was performed to determine if the reinforcement played any role in the recrystallization process of the nylon.. Figure 4.40 shows these DSC scans, and it can be seen that there is some

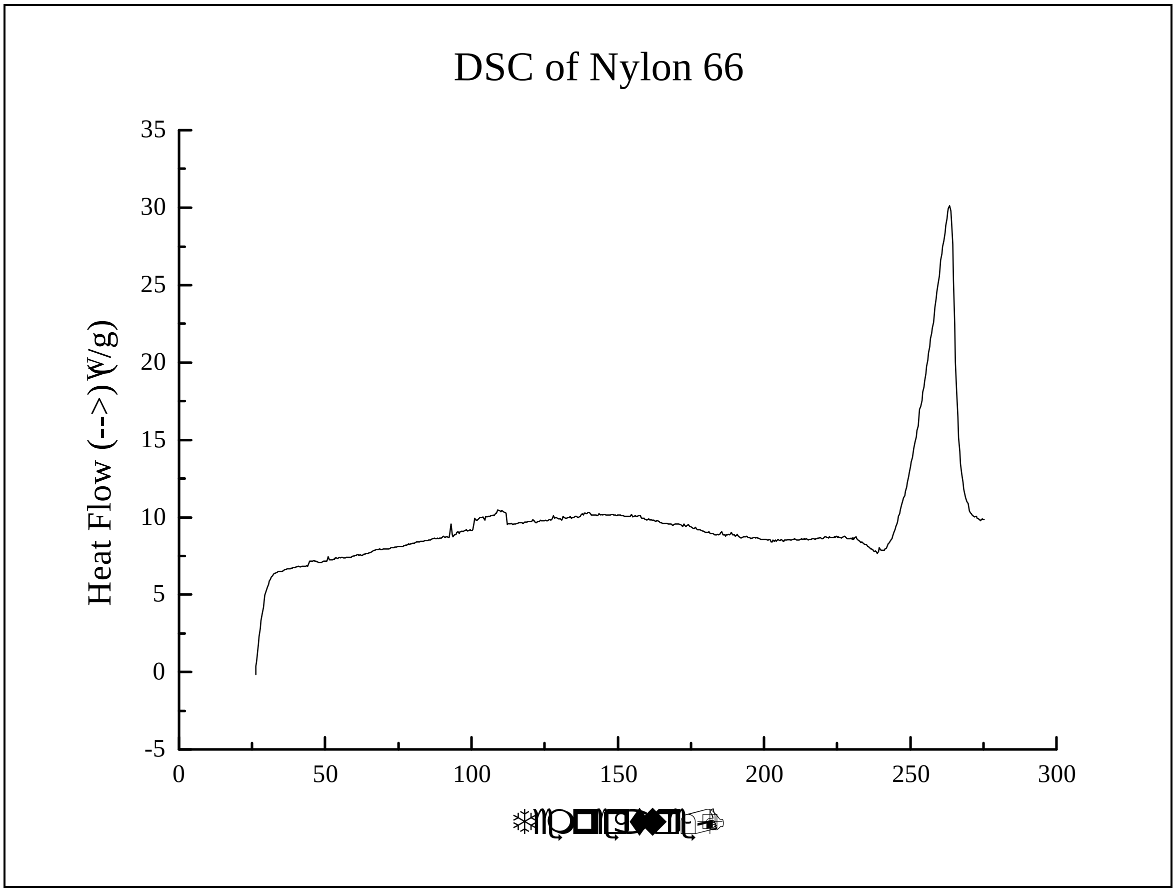

Figure 4.38 DSC trace of nylon 66.

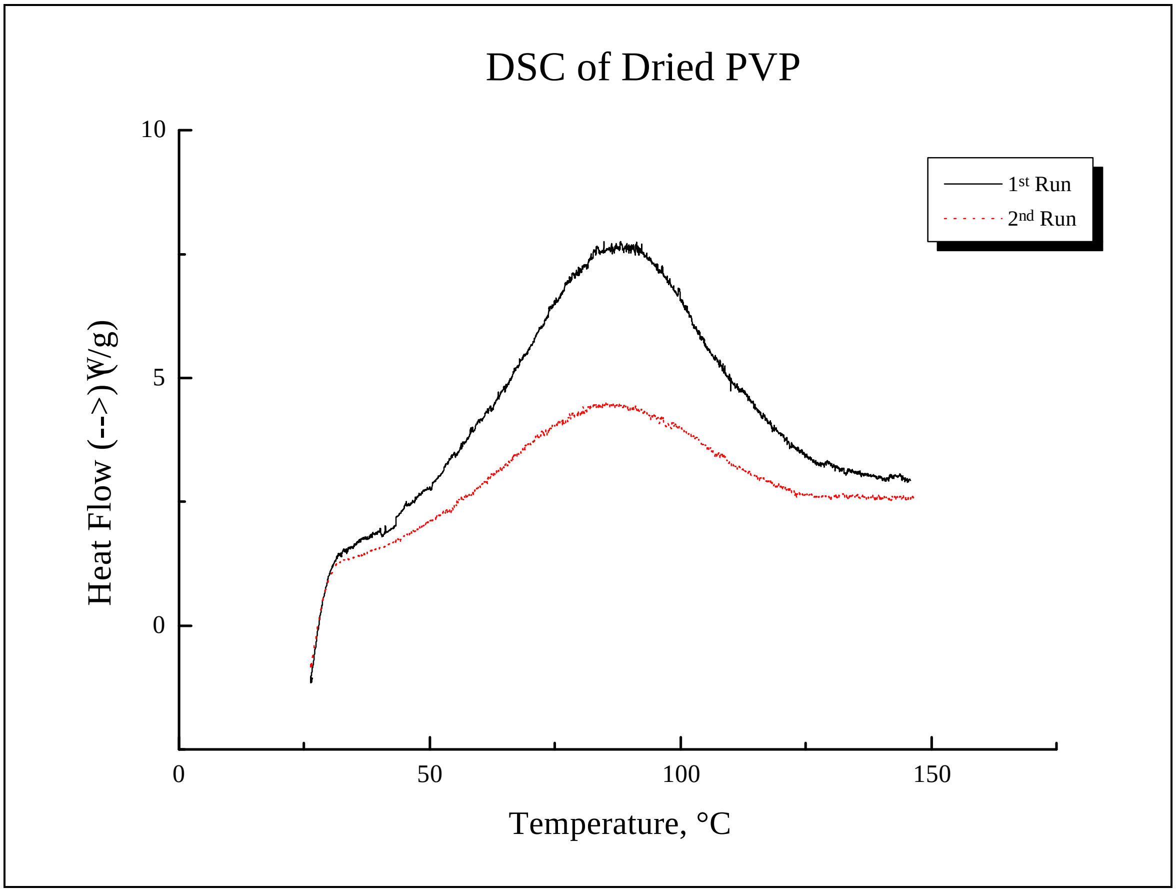

Figure 4.39 Two consecutive DSC scans of dried PVP from 30° to 150°C.

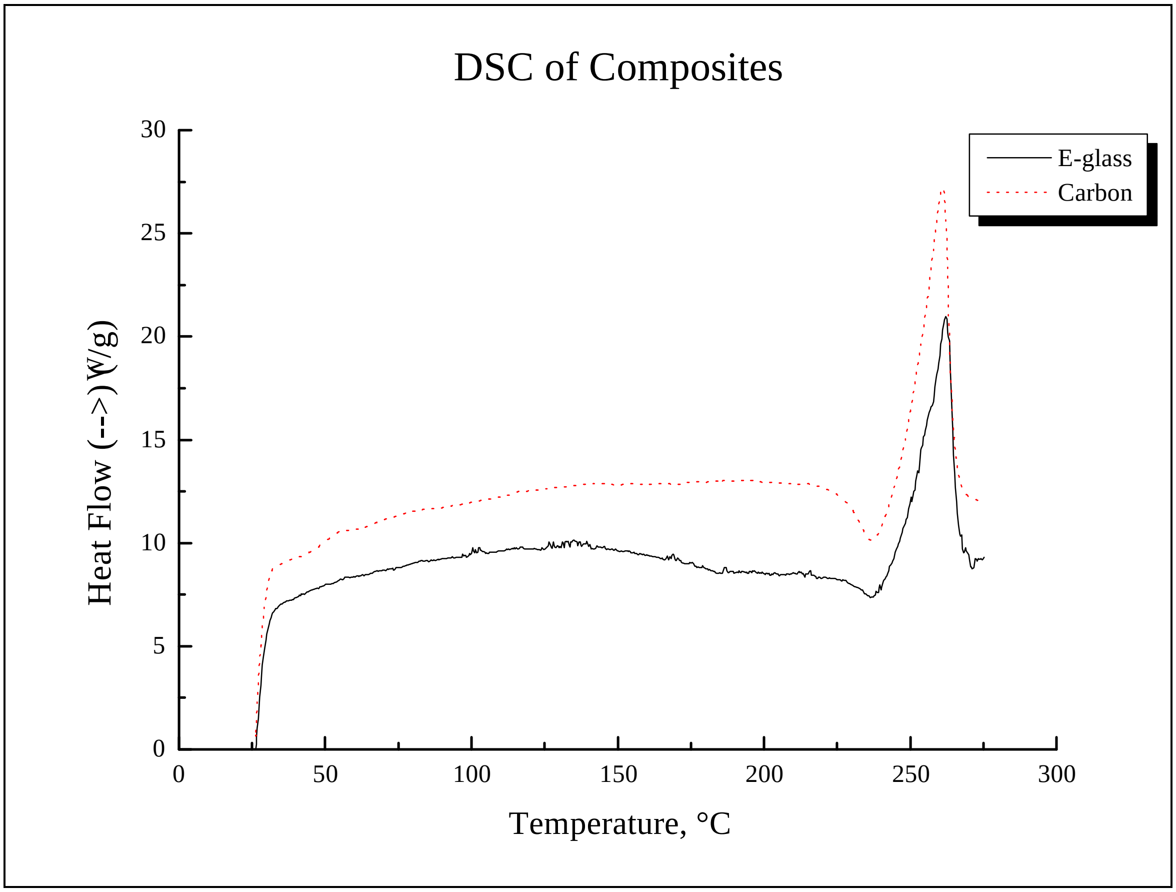

Figure 4.40 DSC scans of the unsized E-glass and carbon fiber composites.

recrystallization in both composites which peaks at 237°C.

Finally, DSC was performed on a sample containing nylon 66 and PVP in a one-to-one ratio. This was performed to determine if any thermal reaction may be the result of either unknown peak in the DMA data of the unsized carbon fiber and sized carbon fiber scans. Two sequential runs are shown in Figure 4.41, and the blend shows no sign of thermal activity which could be attributed to either peak in the DMA carbon fiber composite data.

4.7 Vibrational adhesion testing

The vibrational testing performed in the laboratory of Dr. Lu is a new technique developed to investigate the adhesion in a composite. The adhesion in samples of both the E-glass/nylon 66 composite and the carbon fiber/nylon 66 composite was examined using 1-ply and 2-ply composites. The damping curve of each single-ply composite is shown in Figure 4.42.

Several observations can be made from this figure. First, the unsized and sized E-glass composites have a slower decay, and therefore a lower damping capacity, than its carbon fiber composite counterpart. This is expected since the adhesion in the E-glass composite is higher than that in the carbon fiber composite. Second, the data shows that the sized composites have a slower decay rate when compared to the unsized composites which indicates that the sized composites have a lower damping capacity. In addition, this change in decay rate versus fiber sizing is more obvious in the carbon composite.

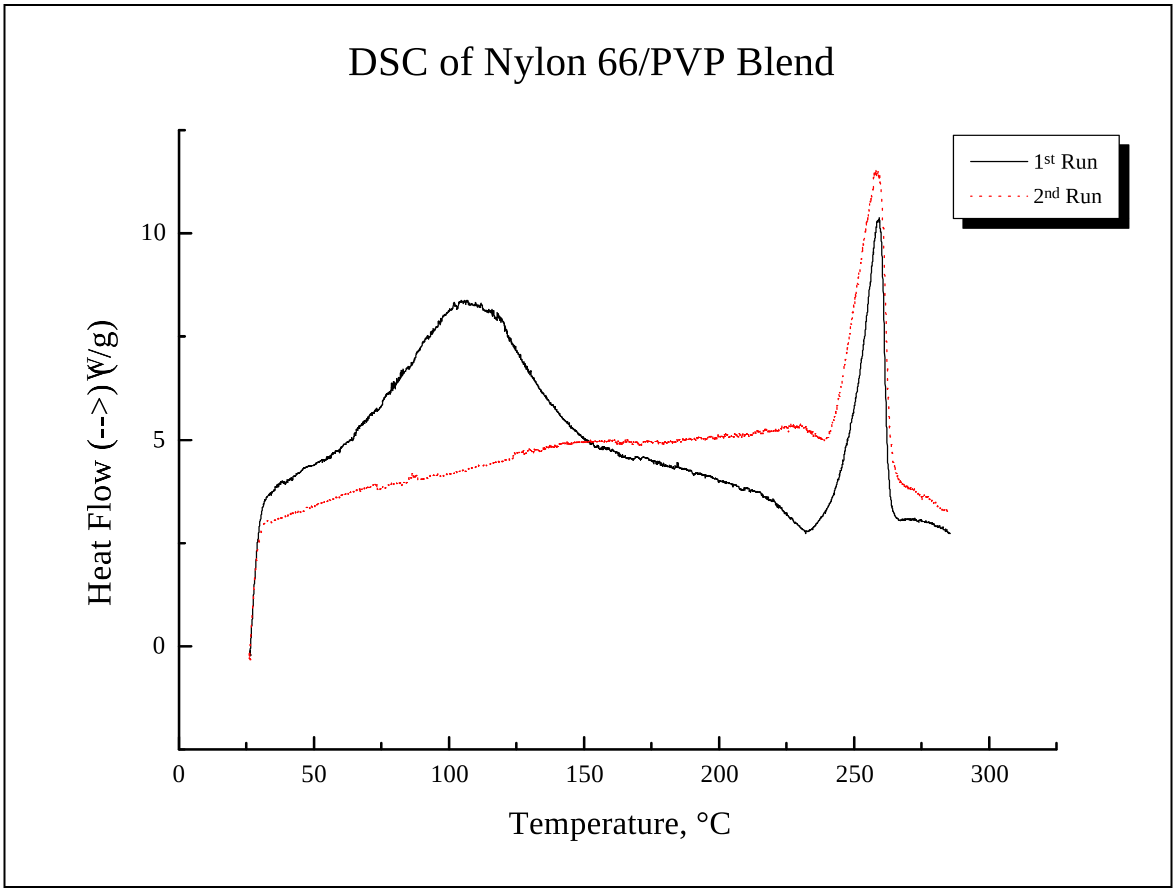

Figure 4.41 DSC scan of a 50/50 nylon 66/PVP blend.

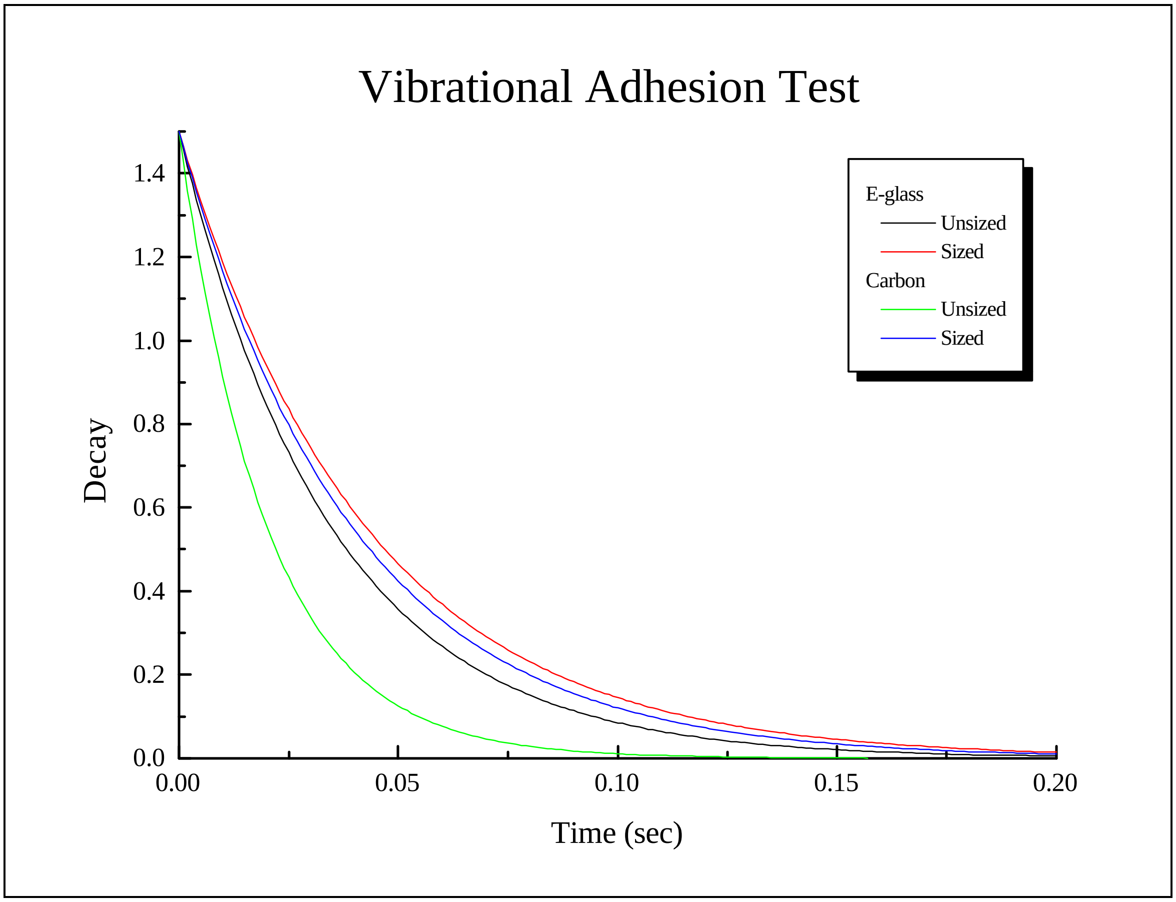

Figure 4.42 Vibrational adhesion test damping curves for single-ply nylon 66 composites.

4.8 Minimat tensile testing

With the data collected thus far, the ultimate static properties of the composite on a microscopic level (i.e., fiber debond) have been studied, and the macroscopic dynamic properties (i.e., DMA) of a real composite have been analyzed. Next, the ultimate static properties of the both the E-glass and carbon fiber composites at were measured as a function of sizing, again using ±45° samples. Figure 4.43 shows typical stress-strain curves for the unsized and sized E-glass composite, while Figure 4.44 shows typical stress-strain curves for the unsized and sized carbon fiber composite. The averages and standard deviations of the ultimate strengths and ultimate strains for both composites are given in Figure 4.45. The averages and standard deviations for the composite modulus and toughness are shown in Figure 4.46. It can be seen that the addition of sizing to the E-glass composite increases the ultimate strength and toughness, while the modulus and ultimate strain are only slightly affected. Furthermore, the sizing increases the ultimate strength and strain of the carbon fiber composite marginally, with no effect on its modulus.

Finally, the fracture surfaces of the tensile specimens were investigated. Figure 4.47 shows the surfaces for all composite systems: E-glass and carbon composites, both unsized and sized. From the micrographs, it can be seen that much more matrix resin remains on the fibers in the unsized samples, or the samples that contain transcrystallinity, while the sized or transcrystalline-free samples contain “clean” fibers. This would indicate that the unsized composites have a higher interfacial shear

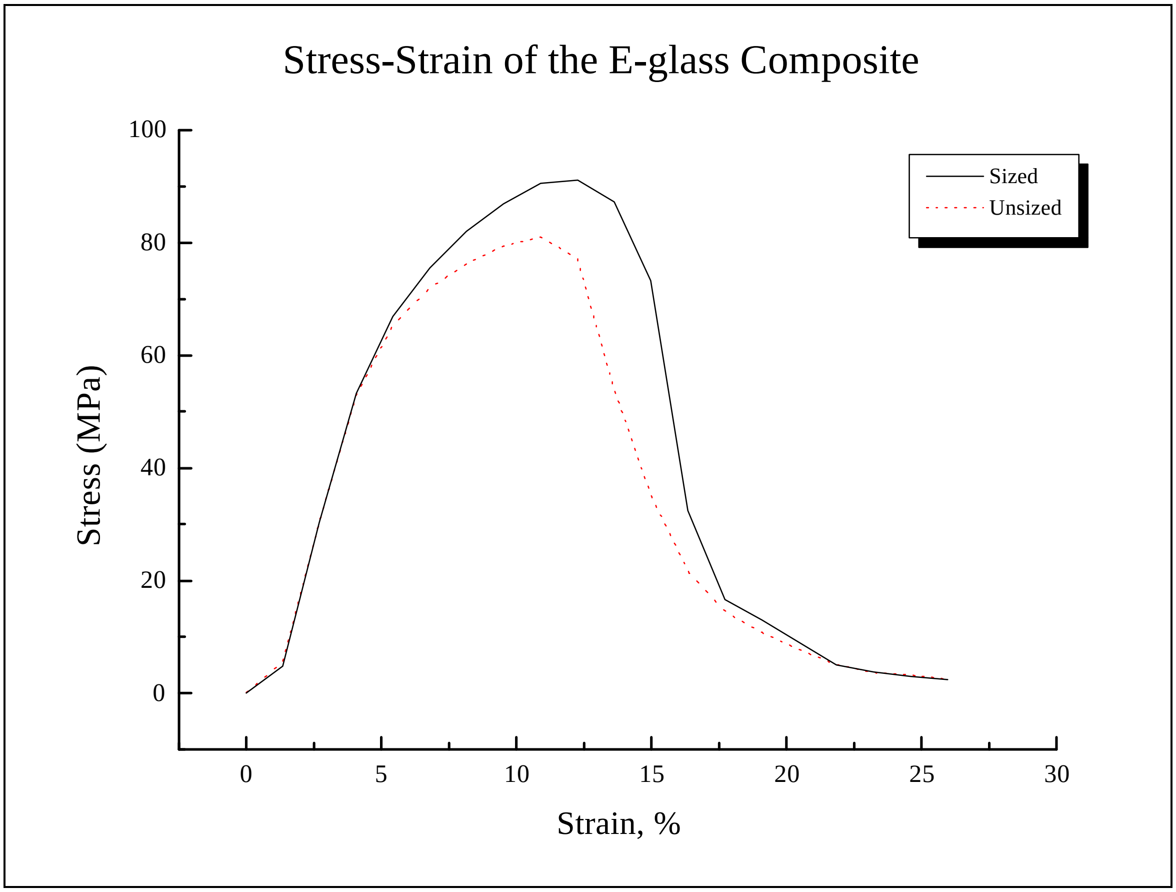

Figure 4.43 Stress-strain curves for an unsized and sized E-glass/nylon 66 composite.

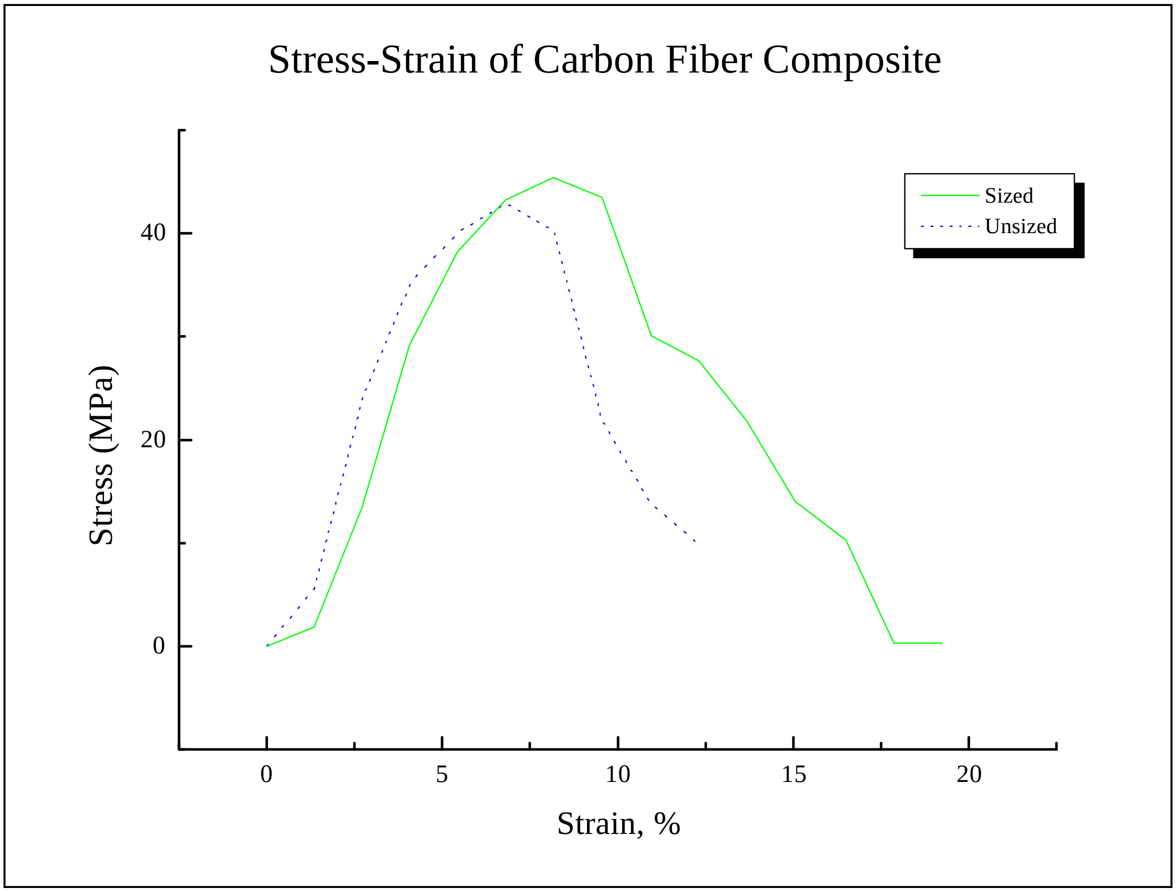

Figure 4.44 Stress-strain curves for an unsized and sized carbon fiber/nylon 66 composite.

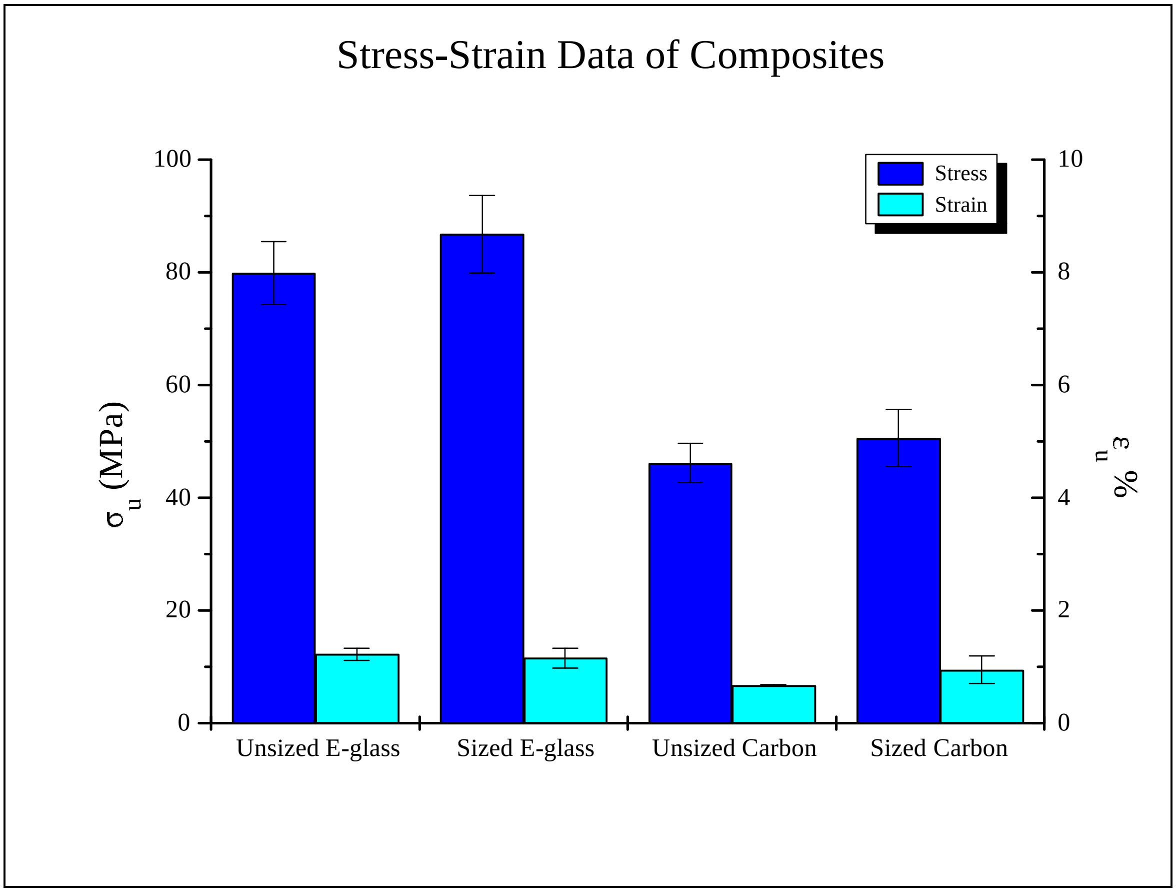

Figure 4.45 Ultimate property comparisons of E-glass/nylon 66 and carbon fiber/nylon 66 composites both before and after sizing: Stress and strain.

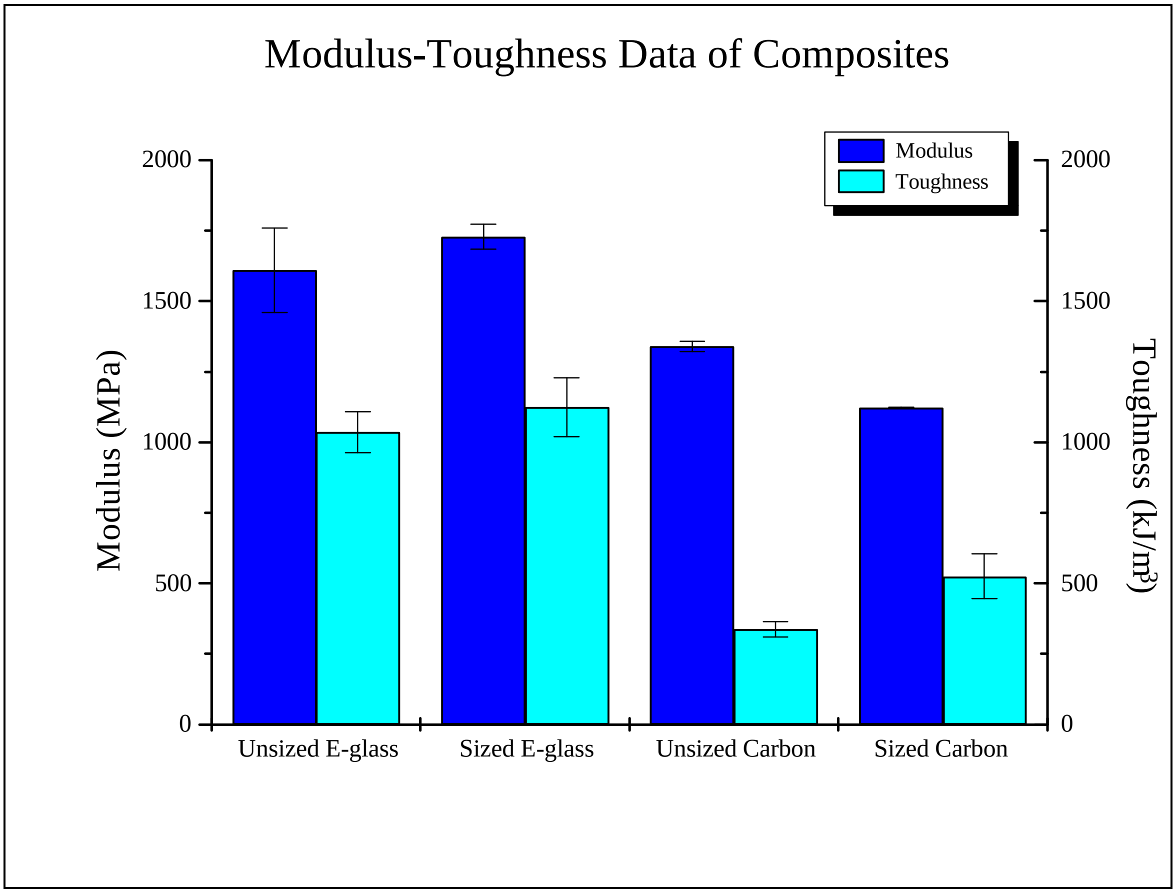

Figure 4.46 Ultimate property comparisons of E-glass/nylon 66 and carbon fiber/nylon 66 composites both before and after sizing: Modulus and toughness.

a) E-glass

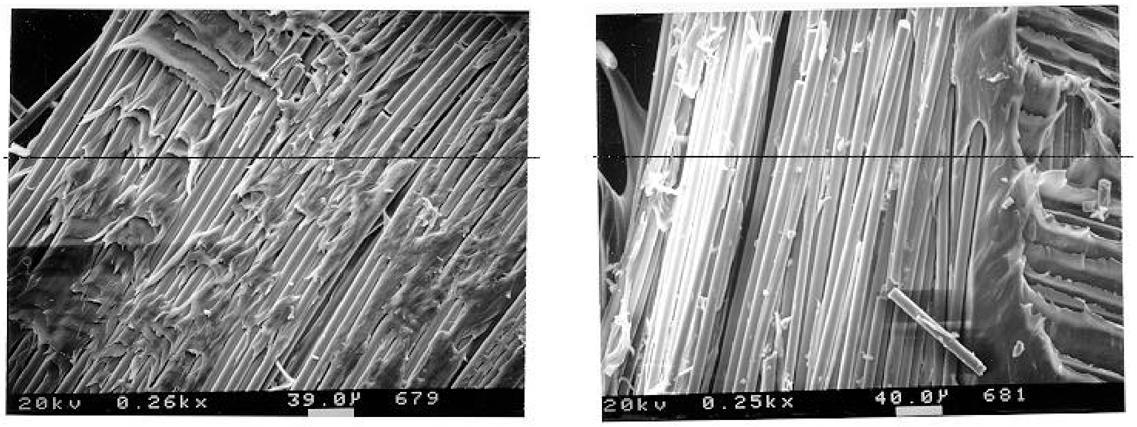

Unsized Sized

b) Carbon

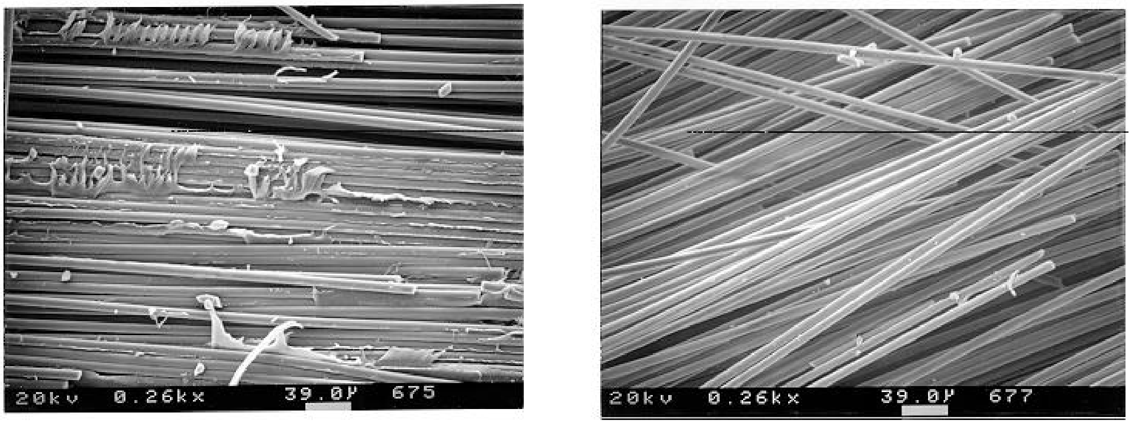

Unsized Sized

Figure 4.47 SEM photomicrographs of the fracture surfaces of all composite tensile specimens: a) E-glass and b) carbon composites, both unsized and sized.

strength than do the sized samples. This correlates very well with the results from the fiber debond test (Figures 4.11 - 4.18).

4.9 Water absorption

When working with any nylon material, moisture up-take is always an important issue because polyamides are hydrophilic, and the moisture can have a dramatic effect on the material's properties. In this study, moisture can diffuse into the nylon from the surface, but also in the composites, the interface between the matrix and fiber could possibly enhance moisture up-take. Therefore, a kinetic study of the moisture adsorption of pure nylon and the E-glass and carbon fiber composites was performed. The results are shown in Figure 4.48. Furthermore, the equilibrium uptake percentages of moisture and the standard deviations are shown in Figure 4.49. From Figure 4.48 the initial moisture uptake of the carbon fiber composite is equal to that of the neat nylon 66. However, the E-glass composite has a slower moisture uptake rate. The equilibrium moisture uptake of neat nylon is approximately 7.5%, and changes with fiber reinforcement. The unsized E-glass composite has an average of 3.3% which is higher than the 2.25% expected for a composite with ~ 30% matrix. In addition, the unsized carbon fiber composite has an average moisture uptake of 10.5% which is more than three times the expected value for a 40% matrix composite. These differences are attributed to the additional interfacial areas in the composite. Furthermore, the addition of sizing to the E-glass composite increases the equilibrium percentage slightly, with a small decrease in the carbon fiber composite percentage.

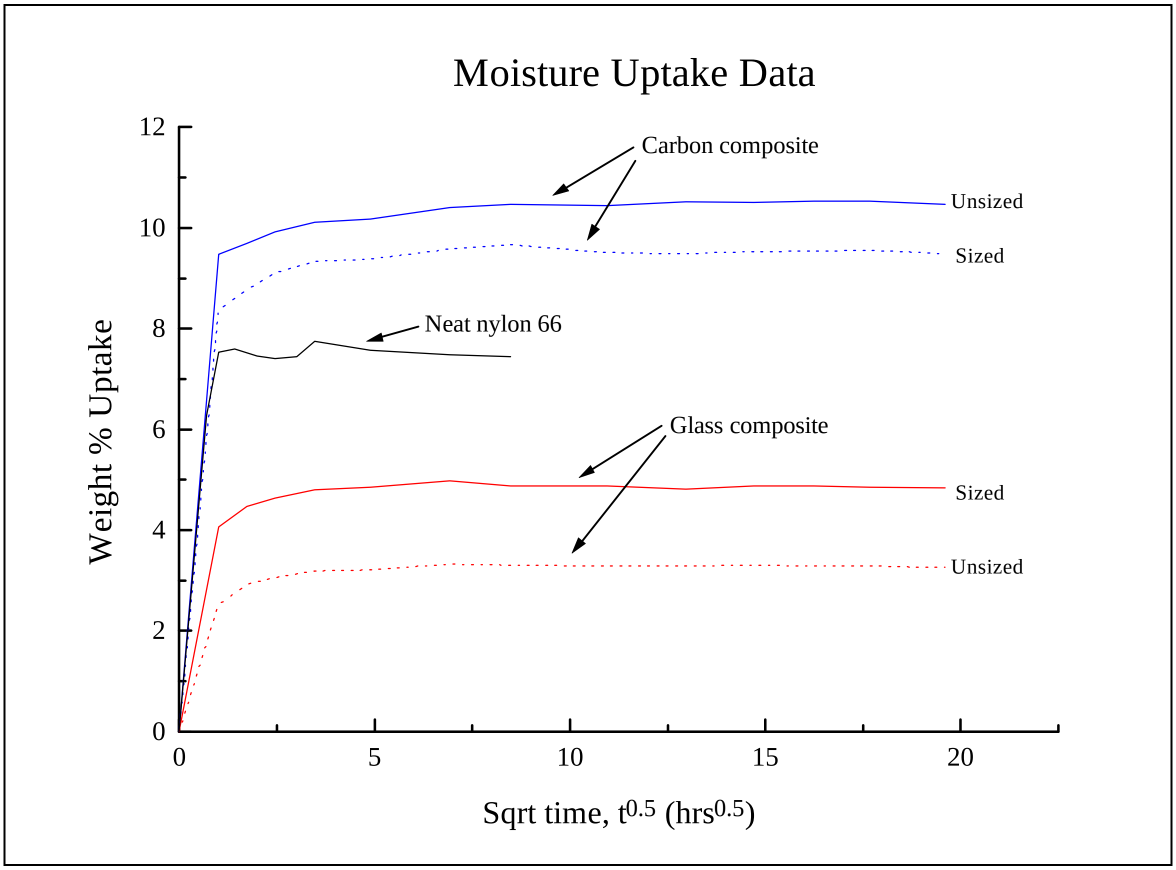

Figure 4.48 Kinetic curves of moisture uptake for nylon 66 and all composites which were both unsized and sized.

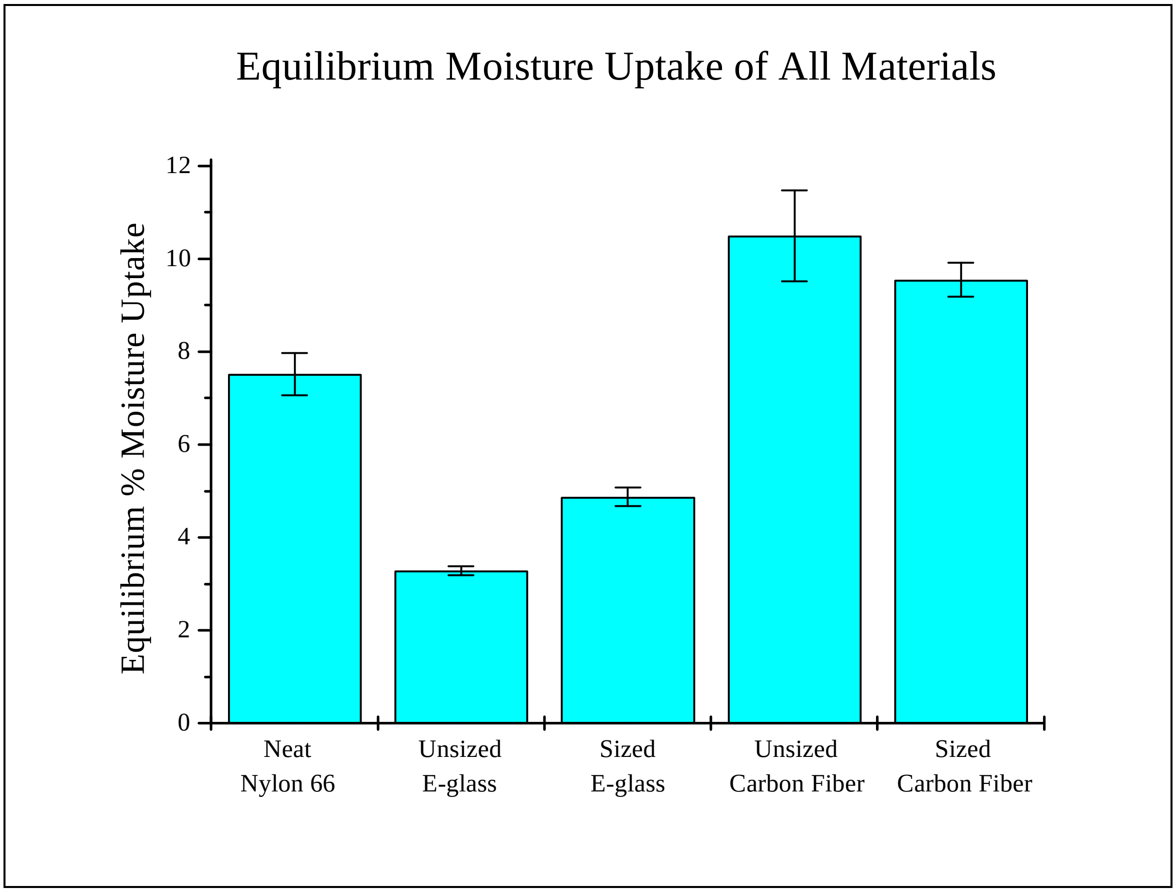

Figure 4.49 Equilibrium moisture uptake percentages of nylon 66 and its composites with E-glass and carbon fiber which were unsized and sized.

5. Conclusions

This study has investigated the mechanical properties of nylon 66 reinforced with both high modulus carbon fibers and glass fibers. Previous work determined that different interphase morphologies result from the use of a specific diluent, PVP, as a fiber sizing. This sizing reduces the nucleation density on the fiber surface and allows the morphology to change from transcystalline to spherulitic. This work investigated what effect this microscopic phenomenon has on the interfacial shear strength of single filament composites and the macroscopic damping and ultimate static properties of a real composite.

5.1 Nylon 66/E-glass composite

Single filament composites of E-glass embedded in nylon 66 showed (Figure 4.3, 4.4) that as the morphology is changed from transcrystalline to spherulitic by adding PVP as a fiber sizing, the average interfacial shear strength is decreased. This was shown by two different data sets. Futhermore, if the PVP is also added to the matrix, a transcrystalline morphology presists in all the composites, and no interfacial shear strength decrease is predicted. This is exactly the result of adding unsized and sized E-glass fibers to a nylon 66/1% PVP blend; no change in average interfacial shear strength (Figure 4.7). Scanning electron microscopy further substantiated this effect by revealing a more cohesive failure in composites with transcrystallinity and a more adhesive failure in composites with a spherulitic interphase (Figure 4.12 - 4.18).

Macroscopic properties of the nylon/glass composites were investigated using several techniques. The damping behavior of the composite was measured using dynamic mechanical analysis and vibrational testing. DMA revealed no change in the damping of the composite with fiber sizing, but vibrational testing showed a decrease. Tensile testing showed that a transcrystalline interphase produces a higher ultimate strength and toughness, while there is little or no change in the ultimate strain and modulus.

5.2 Nylon 66/Carbon fiber composite

Fiber debond tests were performed on large diameter carbon fibers, however, this proved to be uninformative about the role of the interphase in the composite because samples did not contain transcrystallinity because the fiber surface did not promote heterogeneous nucleation. However, this test did show that the addition of the sizing did not reduce the interfacial shear strength reinforcing the idea that the mere presence of a PVP layer is not causing the changes previously found in $_{avg}$. Furthermore, fiber debond tests could not be conducted on the carbon fibers that were used in miscroscopy due to their lack of stiffness which did not permit them to be inserted into a matrix. Therefore, changes found in the nylon/glass composite were translated to the nylon/carbon composite because of the similarities in morphology changes found in other literature.

The investigation of the mechanical properties of this composite proved to be quite interesting. The damping was decreased with the removal of the transcrystalline interphase by the suppression of an additional high temperature damping peak found at approximately 130°C. This peak was not a result of the glass transition temperature of the matrix, nor was it recrystallization which was proven by differential scanning calorimetry. In addition, it is not the degradation or reaction of the sizing with the nylon matrix which was proven by thermogravimetric analysis and DSC. It has been suggested that the peak is related to the glass transition temperature of a compatiblizer placed on the plain weave fabric for processing. This was disproven in the dynamic mechanical spectrum of a composite which had fabric subjected to a solvent wash and drying treatment to remove the compatiblizer. The spectrum still showed evidence of the high temperature peak.

Vibrational testing reinforced this concept by showing a decrease in composite damping with transcrystalline removal. Finally, tensile testing showed an increase in composite ultimate stress, ultimate strain, and toughness, but a slight decrease in modulus.

5.3 Overall mechanical property interpretation

Looking now at both systems together, what can be concluded about the role of the transcrystalline interphase on the mechanical properties of the composites? It is well known that ultimate stress of a real composite has an optimal shear stress value. This relationship is illustrated schematically in Figure 5.1. For low values of interfacial shear stress (i.e., low adhesion), the composite has a low ultimate strength due to the inability to transfer stress from the matrix to the fibers, but as interfacial shear strength reaches an optimum value, the ultimate strength reaches its maximum value. As is

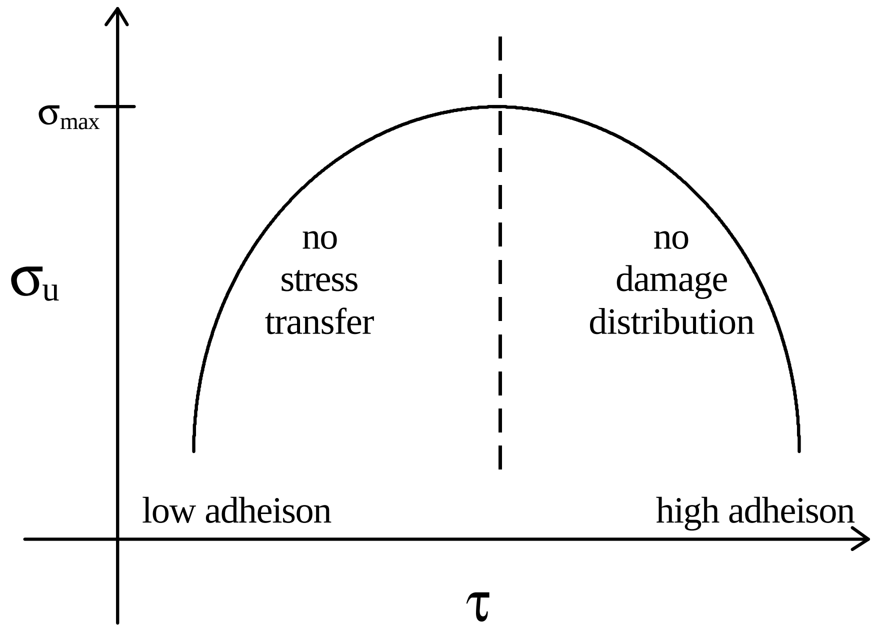

Figure 5.1 Stress versus interfacial shear strength for real composites.

increased further, the adhesion becomes too high in the composite, and damage distribution is not possible, resulting in lower strength values.

The data from this study shows that the composites under investigation fall in the high shear strength region of Figure 5.1 with a transcrystalline interphase. This is typical of most man-made composites; the adhesion is so high that damage distribution is not possible and composites tend to be relatively brittle. However, changing the interphase morphology to a more spherulitic structure reduces the interfacial shear strength but increases composite ultimate strength. This is exactly what Figure 5.1 predicts. Furthermore, it has been shown that composite toughness increases, while composite damping decreases in the absense of transcrystallinity. (Figure 5.2 shows a schematic of all the composite property changes due to the removal of the transcrystalline region.) Again, the increase that is found in composite toughness can be explained by the fact that composites with lower interfacial shear strength allow for more distribution of the damage within the composite. On the other hand, the damping of the composite is decreased because the additional mechanism for damping, i.e., the amorphous region in the transcrystalline interphase, is removed. Furthermore, the localization of the PVP in the interphase increases the T_g of this localized region and changes damping characteristics of the interphase.

Finally, although the trends are found in both composite systems, the E-glass reinforced composite shows a much more subtle change in properties with the removal of transcrystallinity. This is due to the high level of adhesion found in this system

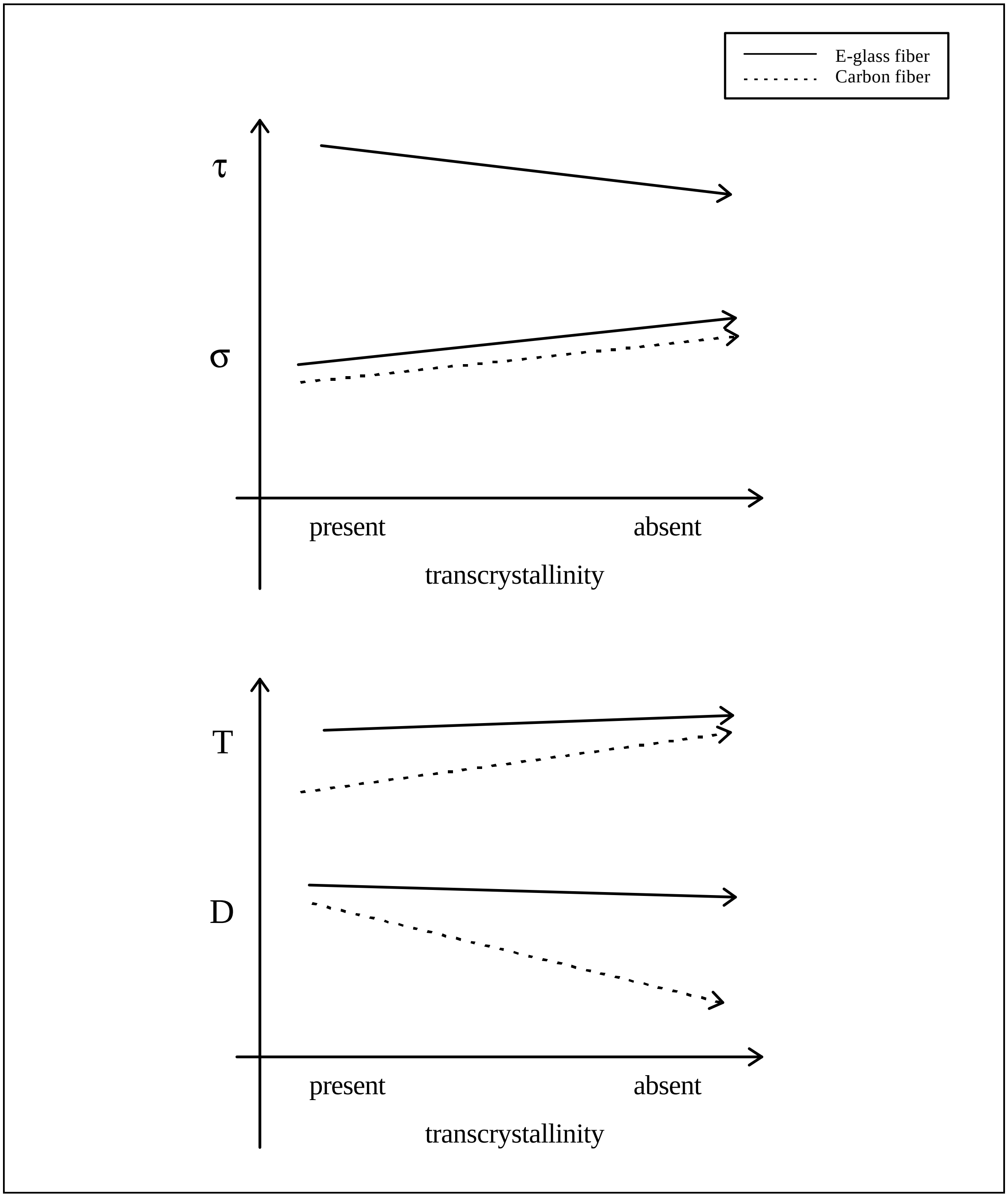

Figure 5.2 Schematic of composite property changes (σ - stress, τ - interfacial shear stength, T - toughness, D - damping) in both E-glass and carbon composites versus interphase morphology.

compared to the carbon fiber reinforced composite. This increased adhesion reduces the contribution where D_f, D_m, and D_{int} are the damping contributions from the fiber, matrix, and interphase, respectively. With the nylon/glass composite, the total damping is due solely to the matrix term, and the fiber and interphase terms are negligible. In the nylon/carbon composite, the damping from the interphase plays a much larger role in the total damping, and therefore, changes in the interphase are more apparent.

In summary, the major contribution of this work has been the systematic translation of single filament (microscopic) results to bulk composite mechanical property results in the same, well characterized system. This was accomplished by studying both glass and carbon fiber reinforced nylon 66 composites. The E-glass and carbon fiber reinforced nylon 66 composites have better ultimate properties when the transcrystalline interphase is absent, but the composites have better damping properties when transcrystallinity is present.

6. Future Work

6.1 Polymer blends

6.1.1 Solvent versus melt

This study has taken results of morphology changes in the interphase from solution cast films and applied them to melt blended micro-composites and compression molded composites. Although this assumption is routine in research, the thermodynamics, kinetics, and structures in solution formed samples may not always be directly related to those of melt formed samples. This issue may be of importance with the nylon 66/PVP blend since the temperatures required to melt the nylon are relatively high. Efforts have already begun to answer this question, and laboratory scale melt blends have been formulated and will be analyzed using a series of testing techniques. In addition, gel fractions of PVP subjected to these high temperatures will be analyzed to determine if the material is crosslinking.

6.1.2 Other blends

The phenomenon of altering morphology by blending highly polar polymers has been shown to exist in specific blends. It would be of interest to see if the same effects are found when *any* highly polar uncrystallizable diluent is blended with *any* highly polar crystallizable host. Keith et al. [77] have shown that other systems do exist (aliphatic polyesters) but the range of such mixtures has not been determined. Furthermore, it would be of interest to view the morphological changes that would occur if other nylons such as nylon 64 or nylon 610 were blended with PVP. In addition, studies using nylons with oligomers of PVP may help determine the effect of molecular weight of the diluent on the system.

Previous results have shown that the phenomenon of reducing nucleation density exists in polymers that interact through hydrogen bonding, but studies of blends that interact by other physical means (such as acid-base) have not been studied. If the same results occurred in blends with these types of interactions, the application would be extended to many other blend and composite systems, i.e., many high performance polymer composites.

6.2 Mechanical properties

Until the effect that changes in interphase structure has on other composite properties is well understood, semicrystalline thermoplastic composites will not be used in many applications. Therefore, a thorough understanding of glass and carbon fiber reinforced nylon must be obtained.

6.2.1 Mechanical profilometry

In this study, efforts must begin with understanding the surfaces of the fibers and matrix. Therefore, attempts were made to measure fiber surface smoothness and sizing thicknesses using a mechanical profilometer, but these tests did not give conclusive data due to the tip slipping off the curved fiber surface fiber, and the tip possibly scrapping off the sizing.

6.2.2 Peel testing

This method was undertaken to increase the area of the interface in the test samples to get more accurate information concerning this interfacial shear strengths. However, complications prevailed. Primarily, the adhesion between the nylon 66 and borosilicate slides was high enough to cause cohesive failure in the composite. In order to study interfacial properties, interfacial failure must occur, and this did not happen even when pre-cracks were initiated at the interface. Therefore, other test geometries will have to be sought. This problem should not arise in the study of carbon fiber/nylon 66 composites, however obtaining two dimensional surfaces of carbon that produce transcrystallinity will be difficult.

6.2.3 Impact testing

Another important property of a material is its impact resistance. Therefore, to examine the ultimate macroscopic damping characteristics of both composites, an air gun impact testing procedure designed by Dr. Morton from the Department of Engineering Science and Mechanics was used. 4-ply composite samples were fabricated for this procedure in order to inhibit penetration by the projectile. However, velocities of no less than 20ft/s could be attained, and projectile penetration occurred in all samples. This did not allow for a definitive analysis to take place to estimate the ultimate impact resistance of each sample. Other test procedures will have to be sought. A drop-tower procedure is being investigated.

6.2.4 Atomic force microscopy (AFM)

Some have hypothesized that the transcrystalline region may have a different modulus from that of a spherulitic structure. Atomic force microscopy could be used to qualitatively examine this, and test samples have been formulated for this procedure.

6.3 Environmental and durability studies

The durability of composites becomes an ever increasing issue as they are used to replace more and more traditional materials. Furthermore, the use of thermoplastic composites is rising, and the durability of such composites has not been extensively investigated. Specifically, the scientific explanation for the durability of reinforced nylon 66 composites is virtually unknown. As mentioned, polyamides are quite hydrophilic, and moisture is known to drastically affect their properties. Therefore, the exposure of unsized and sized E-glass and carbon fiber reinforced nylon composites should be investigated.

Initial efforts were made on single filament composites, but definitive conclusions could not be made. E-glass fibers with different sizings were embedded in nylon 66 and exposed to a laboratory controlled environment. The samples were placed on a hot plate held at 100°C along with a beaker of water and covered. The humidity was kept at 100% RH, and the exposure time was 2 weeks. The samples were then removed at tested using the fiber debond technique, but many failed before testing or had degraded and could not be tested.

Additional efforts studying the durability of both composites need to be performed on both a microscopic and macroscopic level. The effect of moisture exposure on the damping ability of compression molded composites had begun, but to-date, no conclusions have been made.

6.4 DMA and vibrational data correlation

Both dynamic mechanical analysis and a newly formed technique, vibrational adhesion testing, were used to evaluate the damping properties of the composites. The DMA measures the damping as a function of temperature at a fixed frequency, while the vibrational technique uses a range of frequencies at a fixed temperature. Can the information from these tests be correlated with one another? Can time-temperature superposition be used to relate these tests? Not being completely knowledgeable of the theory and calculations behind the vibrational test, a conclusive statement cannot be made here. However, both techniques measure the contribution from the fiber, matrix, and interface to damping, but are the mechanisms changing as a function of frequency? Further investigation will be made.

In reference to the DMA results, a further investigation into the high temperature loss peak of the sized carbon composite is needed. Frequency scans need to be performed in order to determine an activation energy from an Arrhenius plot which will aid in establishing the mechanism which is causing the loss. Finally, using slower rates or isothermal scans of samples using differential scanning calorimetry will assist in this determination.

APPENDIX A

The Fiber Debond Test

For purposes of the analysis presented below, a cylindrical coordinate system was centered within the specimen, with the z-axis running from negative at the top to positive at the bottom. Region 1 is bounded by z = $-L_0$, where the fiber is gripped at the top, and z = 0, where the fiber enters the matrix. Region 2 is bounded by z = 0 and z = *a*, where *a* is the location of the crack tip at the moment in time under consideration. Region 3 is bounded by z = *a* and z = *l*, where *l* is the bottom terminus of the matrix and also the length of the fiber/matrix interface prior to any debonding whatsoever. For a specimen with no initial crack (*a* = 0), there is no Region 2, only Regions 1 and 3. When a crack initiates and propagates, the value of *a* increases and Region 2 grows at the expense of Region 3.

To analyze fiber/matrix debonding in the composite specimen the energy balance principle can be applied to the interfacial crack propagation process. The strain energy released from the system must not only supply the energy required to propagate a crack through the bonded interface in Region 3, but also must supply the energy dissipated through friction in Region 2. In equation form

$$\frac{1}{2\;\,r}\frac{U}{a} \geq G_c + \frac{1}{2\;\,r}\frac{W_f}{a} \qquad [1]$$

where *U* is the total elastic strain energy stored in the system, W_f is the work of friction in the debonded area, $2\pi r$ is the circumference of the interface, and G_c is equivalent to the interfacial fracture energy (work of fracture to separate unit area of bonded interface) in Region 3.

In the following subsections the strain energy content in each of the three regions of the specimen will be derived separately. Following this, an expression for the work of friction in Region 2 will be developed. Finally, an expression for the critical load for a debond specimen will be presented.

1. Strain energy stored in Region 1 - the free fiber

The free fiber, unconstrained laterally, can be regarded as a thin elastic rod loaded in tension, with stress, σ, proportional to strain, ε, through Young's modulus, *E*. Strain energy per unit volume is then given by the integral of stress between the limits of strain

$$\int_{=0}^{= \ /E} \quad d \quad = \frac{1}{2E_f} \quad {}^{2}_{f} \qquad [2]$$

where the subscript *f* designates fiber quantities. The total strain energy stored in the free fiber in Region 1 is the strain energy per unit volume multiplied by the fiber cross-sectional area, A_f, integrated over the free fiber length

$$U_{1f} = \frac{A_f}{2E_f}\int_{-L_o}^{0} \quad {}^{2}_{f}\, dz\,. \qquad [3]$$

Performing the integration gives the total strain energy stored in Region 1 as

$$U_1 = \frac{A_f L_o \quad {}^{2}_{f}}{2E_f} \qquad [4]$$

2. Strain energy stored in Region 2 - the debonded region

In the debonded region, which runs from *z* = 0 to *z* = *a*, strain energy is stored in three forms: tension in the fiber, compression in the matrix, and shear in the matrix. In Region 2, friction between the debonded fiber and matrix occurs when the fiber extends under load and its surface contacts the adjacent matrix. The essential forces on the fiber in this region are the tensile forces at both ends, and *f*, the friction force per unit length, along the cylindrical surface of the fiber. A force balance on an incremental length of fiber can be written as

$$fdz = A_f\left({}_f + d\ {}_f \right) - A_f\ {}_f \qquad [5]$$

where *z* is the vertical position along the debonded fiber length. The unit friction force, *f*, is not a function of *z*, but is uniform along the debonded length. The friction coupling reduces the tensile load on the fiber in the debonded region by transferring some of it to the matrix. Therefore, at the top of the debonded region ($z = 0$), the stress in the debonded fiber equals that in the free fiber, σ_f, and diminishes uniformly as *z* approaches the crack tip.

With the force balance as a basis, the stress in the debonded fiber at any vertical position *z* is given by

$${}_f(z) = {}_f - \frac{fz}{A_f} \qquad [6]$$

The expression for strain energy stored in the form of fiber tension in Region 2 is expressed in analogous form to that for Region 1, except that $(\sigma_f - fz/A_f)$ replaces σ_f

$$U_{2f} = \frac{A_f}{2E_f}\int_0^a \left({}_f - \frac{fz}{A_f} \right)^2 dz \qquad [7]$$

Integration of this equation then gives the strain energy content of the fiber in Region 2

$$U_{2f} = \frac{A_f^2}{6E_f\, f}\left[{}_f^3 - \left({}_f - \frac{fa}{A_f} \right)^3 \right] \qquad [8]$$

The vertical compression of the debonded matrix in Region 2 is brought about by the combined effect of the upward pull of the fiber and the external restraint on the upper boundary of the matrix. the strain energy stored in the compressed debonded matrix is

$$U_{2comp} = \frac{A_m}{2E_m}\int_0^a \,{}_m^2 dz \qquad [9]$$

where the subscript *m* refers to the matrix.

The matrix stress, σ_m, can be expressed in terms of the corresponding fiber stress, $\sigma_f(z)$, thereby lending uniformity to the final result of this analysis. The σ_m to σ_f correspondence is obtained from the following force balance, applicable to any cross-section of the specimen and operative whether the fiber and matrix are coupled by bonding or by friction

$${}_m A_m = {}_f A_f \quad \text{or} \quad {}_m = \frac{A_f}{A_m}\,{}_f(z) \qquad [10]$$

The right hand side of the second equation, with $\sigma_f(z)$ written explicitly as $(\sigma_f - fz/A_f)$, is now substituted for σ_m in equation [9], and is multiplied by matrix cross-sectional area, A_m, and integrated from $z = 0$ to $z = a$ to obtain the total strain energy stored as matrix compression in

Region 2

$$U_{2f} = \frac{A_f^2}{6E_f\, f}\left[\,{}_f^3 - \left(\,{}_f - \frac{fa}{A_f}\right)^3\right] \qquad [11]$$

In addition to the compression just described, there is also shear in the debonded matrix in Region 2. This shear arises through frictional coupling of the matrix to the strained fiber. To develop an expression for the matrix shear in Region 2, equations developed by Piggott [98] were used, who treated the matrix shear for the adhesively bonded surface. According to Pigott, the strain energy of the shear matrix is

$$U_{2mshear} = r\int_0^a \, dz \qquad [12]$$

where *r* is the fiber radius, τ is the shear stress at the interface, and δ is the vertical displacement of the sheared matrix at a given position, *z*, along the length of the interface. He defined δ as

$$= \frac{2r\ \left(1+v_m\right)\ln\frac{R}{r}}{E_m} \qquad [13]$$

in which v_m is the matrix Poisson ratio. This expression can easily be adapted to our case of the debonded but frictionally coupled matrix. For this, the interfacial shear stress, τ, must be replaced by the frictional interaction per unit area, $f/2\pi r$, in equations [12] and [13]. the result, upon making these substitutions and integrating equation [12] is

$$U_{2mshear} = \frac{f^{2}a\left(1+v_m\right)\ln\frac{R}{r}}{2\ \ E_m} \qquad [14]$$

The total strain energy contained in Region 2 is the sum of fiber tension, matrix compression, and matrix shear

$$U_2 = U_{2f} + U_{2mcomp} + U_{2mshear} \qquad [15]$$

or

$$U_2 = \frac{A_f^2}{6E_f f}\left[\ {}^{3}_{f} - \left(\ \ {}_{f} - \frac{fa}{A_f}\right)^3\right] + \frac{A_f^2}{6E_f f}\frac{A_f E_f}{A_m E_m}\left[\ {}^{3}_{f} - \left(\ \ {}_{f} - \frac{fa}{A_f}\right)^3\right] + \frac{f^{2}a\left(1+v_m\right)\ln\frac{R}{r}}{2\ \ E_m} \qquad [16]$$

3. Strain energy stored in Region 3 - the bonded region

The current expression for strain energy stored in Region 3, which runs from $z = a$ to $z = l$, is an improvement upon an earlier developed analysis for the strain energy stored in a specimen having a bonded interface with an initial crack. This analysis includes the presence of Region 2 and the possibility of compression in Region 3. Both of these parameters were ignored in the previous model.

For tensile stress in the fiber

$$\sigma_f(z) = \frac{\sigma_f \sinh\left[\frac{n(l-z)}{r}\right]}{\sinh(ns)} \qquad [17]$$

For shear stress in the matrix at the fiber/matrix interface

$$\tau_m = \frac{n\,\sigma_f \cosh\left[\frac{n(l-z)}{r}\right]}{2\sinh(ns)} \qquad [18]$$

These expressions show the nonlinear nature of the stress distribution along the length of the bonded interface, and are to be contrasted with the linear stress distribution along the debonded interface.

In equations [17] and [18] the quantities *n* and *s*, comprising quantities already introduced, are defined as

$$n^2 = \frac{E_m}{E_f(1+v_m)\ln(R/r)} \quad \text{and} \quad s = \frac{l-a}{r} \qquad [19]$$

When the crack length *a* is not equal to zero but has a finite value, then σ_f is a function of *z* on the interval (*l* - *a*) to *l*, so that $\sigma_f(z) = (\sigma_f - fz/A_f)$. The expression for the total strain energy in Region 3 is analogous to that in Region 1 except that the nonlinear stress distribution of equation [17] is substituted for σ_f^2. The result of the integration is

$$U_{3f} = \frac{A_f}{2E_f}\int_{l-a}^{l} \sigma_f^2\,dz = \frac{A_f\left(\sigma_f - \frac{fa}{A_f}\right)^2}{4nE_f}\left[\coth(ns) - \frac{ns}{\sinh^2(ns)}\right] \qquad [20]$$

For the total strain energy stored as matrix shear in Region 3, t as expressed by equation [18] is inserted into equation [12]. The result of the integration is

$$U_{3mshear} = r\int_{l-a}^{l} {}_{m}(z)\ dz = \frac{A_f\left({}_{f} - \frac{fa}{A_f}\right)^2}{4nE_f}\left[\coth(ns) - \frac{ns}{\sinh^2(ns)}\right] \qquad [21]$$

The total strain energy stored as matrix compression in Region 3 relies on the same force balance as that given for Region 2. This force balance, equation [10], holds true at any cross-section of the specimen whether the interface is debonded or not, and allows matrix stress, σ_m, to be expressed in terms of the corresponding fiber stress, σ_f. The expression is

$$U_{3mcomp} = \frac{A_m}{2E_m}\int_{l-a}^{l} {}_{m}^{2}(z)dz = \frac{A_m}{2E_m}\left(\frac{A_f}{A_m}\right)^2\int_{l-a}^{l} {}_{f}^{2}(z)dz \qquad [22]$$

Substituting the explicit form given by equation [17] for $\sigma_f(z)$ and carrying out the integration gives the following result

$$U_{3mcomp} = \frac{A_f r}{4nE_f}\left(\frac{A_f E_f}{A_m E_m}\right)\left({}_{f} - \frac{fa}{A_f}\right)^2\left[\coth(ns) - \frac{ns}{\sinh^2(ns)}\right] \qquad [23]$$

It is obvious from the equation that if E_mA_m/E_fA_f approaches zero, the matrix compression contribution becomes negligible. However, in most practical situations, this quotient has a value close to one, so that matrix compression cannot be neglected.

Finally, the fiber tension and the matrix compression contributions to the strain energy can be combined to give the total strain energy in Region 3

$$U_3 = \frac{A_f\left(\ _f - \frac{fa}{A_f}\right)^2}{2nE_f}\left[\coth(ns)\right] + \frac{A_f r}{4nE_f}\left(\frac{A_f E_f}{A_m E_m}\right)\left(\ _f - \frac{fa}{A_f}\right)^2\left[\coth(ns) - \frac{ns}{\sinh^2(ns)}\right] \qquad [24]$$

4. Work of friction in Region 2

An expression developed by Palley and Stevans [99] was adopted for work of friction at the debonded interface. It is

$$W_f = \int_0^a f\ \ dz \qquad [25]$$

where b is the relative displacement between fiber and matrix at the interface, i.e.,

$$(z) = \int_0^z {}_f dz - \int_0^z {}_m dz = \left(1 - \frac{E_f A_f}{E_m A_m}\right)\frac{A_f}{2fE_f}\left[\ _f^2 - \left(\ _f - \frac{fz}{A_f}\right)^2\right] \qquad [26]$$

Substituting this into equation [25] results in the total work of friction in Region 2

$$W_f = \left(1 - \frac{E_f A_f}{E_m A_m}\right)\frac{(fa)^2}{2E_f}\left(\ _f - \frac{fa}{3A_f}\right) \qquad [27]$$

5. Strain energy release rate and energy balance of the system

The total strain energy stored in the system is simply the sum of the strain energy stored in all three regions, and the strain energy release rate of the system is then the derivative of the strain energy with respect to interfacial crack area, $dU_{\text{total}}/2\pi r da$. The energy balance of equation [1] can be written conveniently as

$$\frac{U_1}{a} + \frac{U_2}{a} + \frac{U_3}{a} = 2\ \ rG_c + \frac{W_f}{a} \qquad [28]$$

and solved for the critical load for crack propagation is

$$P_c = \frac{A_f \left\{ \left[\frac{(1-\ \ )fa}{E_f} + \frac{(2+\ \ )rf\coth(ns)}{2nE_f} \right]^2 - 4\left[\frac{(1+\ \ )A_f}{2E_f} + \frac{(2+\ \ )A_f \operatorname{csch}^2(ns)}{4E_f} \right] \left[\frac{f^2(1-v_m)\ln(R/r)}{2n\ \ E_f} - \frac{(1-\ \ )(fa)^2}{2E_f A_f} - 2\ \ rG_c \right] \right\}^{1/2}}{2\left[\frac{(1+\ \ )fa}{E_f} + \frac{(2+\ \ )A_f \operatorname{csch}^2(ns)}{4E_f} \right] + \frac{\left[\frac{(1-\ \ )fa}{2E_f} + \frac{(2+\ \ )rf\coth(ns)}{2nE_f} \right]}{2\left[\frac{(1+\ \ )}{2E_f} + \frac{(2+|\ \ )A_f \operatorname{csch}^2(ns)}{4E_f} \right]} + fa}$$

[29]

where P_c denotes $\sigma_f A_f$ and α denotes $E_f A_f / E_m A_m$. This equation is the fundamental equation relating the critical load, P_c, for crack propagation to the specimen dimensions and materials parameters.

Application of this model to experimental data has matched quite well. Systems having thermosetting matrix materials follow this model very closely, but thermoplastic systems, especially those containing transcrystallinity, seem to deviate from this model slightly. Further modifications will have to be made for systems with such an interphase region.

REFERENCES

1. J. R. Huntsberger in Adhesion and Cohesion - Vol. 1, R. L. Patrick (ed.), Marcel Dekker, New York, (1967).

2. D. H. Kaelble, Physical Chemistry of Adhesion, Wiley-Interscience, New York, (1971).

3. L. H. Sharpe, *Proceedings of NATO-ASI on the Interfacial Interactions in Polymeric Composites,* June 15 - 26, 1992.

4. A. W. Adamson, Physical Chemistry of Surfaces, 5th ed., Wiley-Interscience, New York, 1990.

5. D. J. Shaw, Introduction to Colloid and Surface Chemistry, 3rd ed., I. Skeist (ed.), Van Nostrand Reinhold, New York, 1990.

6. F. M. Fowkes in Treatise on Adhesion and Adhesives - Vol. 1, R. L. Patrick (ed.), Marcel Dekker, New York, 1967.

7. M. Morra, E. Occhiello, and F. Garbassi, *Adv. in Colloid and Interface Science*, **32**, 79, 1990.

8. W. A. Zisman, J. J. Bikerman, I. Skeist, and R. F. Blomquist in Encyclopedia of Polymer Science and Engineering - Vol. 1, 2nd ed., H. F. Mark, N. M. Bikales, C. G. Overberger, and G. Menges (eds.), Wiley-Interscience, New York, 477, 1985.

9. K. W. Allen, *Journal of Adhesion*, **21**, 261, 1987.

10. L. H. Sharpe, *Journal of Adhesion,* **4**, 51, 1972.

11. J. D. Venables in Adhesion 7, K.W. Allen (ed.), Applied Science, London, 1983.

12. J. D. Venables, *Journal of Materials Science*, **19**, 2431, 1984.

13. D. E. Packham in Aspects of Adhesion 7, D. J. Alner and K. W. Allen (eds.), Transcripta Books, London, 1973.

14. S. S. Voyutski in Autohesion and Adhesion of High Polymers - Vol. 4, V. Vakula (ed.), Wiley-Interscience, New York, 1963.

15. W. D. Callister, Jr., Materials Science and Engineering: An Introduction, 3rd ed., John Wiley, New York, 1994.

16. B. V. Deryaguin, *Research*, **8**, 70, 1955.

17. J. J. Bikerman, The Science of Adhesive Joints, 2nd ed., Academic Press, New York, 1968.

18. L. H. Sharpe, *Journal of Adhesion*, **6**, 15, 1974.

19. P. J. Herrera-Franco and L. T. Drzal, *Composites*, **23**(1), 2, 1992.

20. E. Jenckel, E. Teege, and W. Hinrichs, *Kolloid-Z.*, **129**, 19 (1952).

21. R. J. Barriault, and L. F. Gronholz, *Journal of Polymer Science*, **18**, 393 (1955).

22. R. K. Eby, *Journal of Applied Physics*, **35**, 2720 (1964).

23. H. Schonhorn, *Journal of Polymer Science B*, **2**, 185 (1964).

24. B. B. Burnett, and W. F. McDevit, *Journal of Polymer Science*, **20**, 94 (1956).

25. D. R. Fitchmun, and S. Newman, *Journal of Polymer Science - Part A-2*, **8**, 1545, 1970.

26. M. G. Huson, and W. J. McGill, *Jornal of Polymer Science - Polymer Chemistry Edition*, **22**, 3571, 1984.

27. E. G. Lovering, *Journal of Polymer Science - Part A-2*, **8**, 1697, 1970.

28. J. P. Luongo, *Journal of Polymer Science*, **12**, 1203, 1974.

29. S. Weinhold, M. H. Litt, and J. B. Lando, *Journal of Applied Physics*, **51**, 5145, 1980.

30. R. H. Burton, and M. J. Folkes, *Plastics and Rubber Processing and Applications*, **3**, 129, 1983.

31. H. Ishida and P. Bussi, *Macromolecules*, **24**, 3569, 1991.

32. M. Avella, G. D. Volpe, E. Martuscelli, and M. Raimo, *Polymer Engineering and Science*, **32**, 376, 1992.

33. T. He', and R. S. Porter, *Journal of Applied PolymerScience*, **35**, 1945, 1988.

34. M. G. Huson and W. J. McGill, *Jornal of Polymer Science - Polymer Chemistry Edition*, **22**, 3571, 1984.

35. E. Devaux and B. Chabert, *Polymer Composites*, **31**, 391, 1991.

36. E. Devaux, J. F. Gerard, P. Bourgin, and B. Chabert, *Composite Science and Technology*, **48**, 199, 1993.

37. S. F. Xavier, and A. Misra, *Polymer Composites*, **6**, 93, 1985.

38. Y. Lee and R. S. Porter, *Polymer Engineering and Science*, **26**, 633, 1986.

39. C. M. Tung, and P. J. Dynes, *Journal of Applied Polymer Science*, **33**, 505, 1987.

40. V. E. Reinsch and L. Rebenfeld, *Polymer Materials Science and Engineering*, **68**, 182, 1993.

41. L. C. Lopez and G. L. Wilkes, *Journal of Thermoplastic Composite Materials*, **4**, 59, 1991.

42. G. P. Desio and L. Rebenfeld, *Journal of Applied Polymer Science*, **44**, 1989, 1992.

43. M. J. Folkes and S. T. Hardwick, *Journal of Materials Science Letters*, **3**, 1071, 1984.

44. M. L. Shiao, S. V. Nair, P. D. Garrett, and R. E. Pollard, *Journal of Materials Science*, **29**, 1739, 1994.

45. M. L. Shiao, S. V. Nair, P. D. Garrett, and R. E. Pollard, *Journal of Materials Science*, **29**, 1973, 1994.

46. N. Sato, T. Kurauchi, S. Sato, O. Kamigaito, *Journal of Materials Science*, **26**, 3891, 1991.

47. M. J. Folkes, Short Fiber Reinforced Composites, Research Studies Press, New York, 1982.

48. M. W. Darlington, P. L. M^{c}Ginley, and G. R. Smith, *Journal of Materials Science*, **11**, 877, 1976.

49. W. V. Titow and B. J. Lanham, Reinforced Thermoplastics, John Wiley, New York, 1975.

50. J. Cinquin, B. Chabert, J. Chauchard, E. Morel, and J. P. Trotignon, *Composites*, **21**, 141, 1990.

51. R. L. Clark, Jr., M.S. Thesis, Virginia Polytechnic Institute and State University, Blacksburg, VA, August 1994.

52. N. Klein, G. Marom, A Pegoretti, and C. Migliaresi, *Composites*, **26**, 707, 1995.

53. Z. A. Ishak and J. P. Berry, *Polymer Composites*, **15**, 223, 1994.

54. P. J. Cloud and F. M^{c}Dowell, Reinforced Thermoplastics: Understanding Weld-line Intergrity, Plastics Technology, 1976.

55. R. H. Burton and M. J. Folkes in "Fiber-Matrix Interactions in Reinforced Thermoplastics", in Mechanical Properties of Reinforced Thermoplastics, Chp. 9, Elsevier Applied Science, 1986.

56. T. Bessell and J. B. Shortfall, *Journal of Materials Science*, **10**, 2035, 1975.

57. J. L. Thomason and A. A. Van Rooyen, *Journal of Materials Science*, **27**, 897, 1992.

58. L. T. Drzal, "Fiber-Matrix Interphase Structure and its Effect on Adhesion and Composite Mechanical Properties," in Controlled Interphases in Composite Materials, H. Ishida (ed.), Elsevier, New York , 1990.

59. M. Nardin and J. Schultz, *Proceedings of NATO-ASI on the Interfacial Interactions in Polymeric Composites*, June 15-26, 1992.

60. I. Verpoest, M Desaeger, and R Keunings, "Critical Review of Direct Micromechanical Test Methods for Interfacial Strength Measurements in Composites," in Controlled Interphases in Composite Materials, H. Ishida (ed.), Elsevier, New York , 1990.

61. J. J. Lesko, Ph.D. Dissertation, Virginia Polytechnic Institute and State University, Blacksburg, VA, 1991.

62. N. Iosipescu, *Journal of Materials*, **2**(3), 537, 1967.

63. ASTM D 03518.

64. ASTM D 2344-76.

65. M. K. Tse, *SAMPE Journal*, 11, Sept./Oct. 1985.

66. A. N. Netravali, D. Stone, S. Ruoff, and L. T. Topoleski, *Composites Science and Technology*, **34**, 289, 1989.

67. U. Gaur and B. Miller, *Composites Science and Technology*, **34**, 35, 1989.

68. G. Désarmot and J. P. Farve, *Composites Science and Technology*, **42**, 151, 1991.

69. L . B. Greszczuk in Interfaces in Composites, ASTM STP 452, American Society for Testing and Materials, 42, 1969.

70. P. S. Chua and M. R. Piggott, *Composites Science and Technology*, **22**, 107, 1985.

71. P. S. Chua and M. R. Piggott, *Composites Science and Technology*, **22**, 185, 1985.

72. M. R. Piggott, *Composites Science and Technology*, **30**, 295, 1987.

73. M. R. Piggott and S. R. Dai, *Composites Science and Technology*, **31**, 15, 1988.

74. L. S. Penn and S. M. Lee, *Journal of Composites Technology Research*, **11**(1), 23, Spring 1989.

75. K. R. Jiang and L. S. Penn, *Composite Science and Technology*, **45**, 89, 1992.

76. Srinivas, S., M.S. Thesis, Va Tech, Blacksburg, VA, March 1992.

77. H. D. Keith, F. J. Padden, Jr., and T. P. Russell, *Macromolecules*, **22**, 666, 1989.

78. W. D. Bascom, K. J. Yon, R. M. Jensen, and L. Cordner, *Journal of Adhesion*, **34**, 79, 1991.

79. P. K. Mallick, Fiber Reinforced Composites, Marcel Dekker, New York, 1993.

80. W. D. Bascom and W. J. Chen, *Journal of Adhesion*, **34**, 99, 1991.

81. U. Gaur, G. Desio, and B. Miller, *Plastics Engineering*, 43, October 1991.

82. A. E. Bolvari and T. C. Ward in Inverse Gas Chromotography - Characterization of Polymers and Other Materials, D. R. Lloyd, T. C. Ward, and H. P. Schreiber (eds.), ACS Symposium Series No. 391, ACS, Washington D.C., 1988.
83. P. Commercon and J. P. Wightman, *Journal of Adhesion*, **38**, 55, 1992.

84. N. G. McCrum, B. E. Read, and G. Williams, Anelastic and Dielectric Effects in Polymeric Solids, Dover, New York, 1991.

85. L. E. Nielson, Mechanical Properties of Polymer and Composites, Marcel Dekker, New York, 1974.

86. J. D. Ferry, Viscoelastic Properties of Polymers, 2nd ed., Wiley, New York, 1969.

87. M. Takayanagi in Proceedings of the 4th International Congress of Rheology, Part I, Wiley-Interscience, New York, 1965.

88. M. Takayanagi and T. Matsuo, *Journal of Macromolecular Science - Physics*, **B1**(3), 407, 1967.

89. R. F. Boyer in Polymeric Materials: Relationships Between Structure and Mechanical Behavior, E. Bear and S. V. Radcliffe (eds.), Chp. 6, ASM, 1974.

90. R. F. Boyer, *Polymer*, **17**, 996, 1976.

91. J. A. Nairn, *Polymer Composites*, **6**, 123, 1985.

92. J. P. Bell and T. Murayama, *Journal of Polymer Science, Part A-2*, **7**, 1059, 1969.

93. T. Murayama, Dynamic Mechanical Analysis of Polymeric Material, Elsevier Scientific, New York, 1978.

94. M. I. Kohan, Nylon Plastics, Wiley-Interscience, New York, 1973.

95. B. V. Robinson, F. M. Sullivan, J. F. Borzelleca, and S. L. Schwartz, PVP: A Critical Review of the Kinetics and Toxicology of Polyvinylpyrrolidone, Lewis, Michigan, 1990.

96. C. DiFrancia, T. C. Ward, and R. O. Claus, "The Single Fiber Pull-Out Test: I. Review and Interpretation," (accepted in *Composites*).

97. C. DiFrancia, T. C. Ward, and R. O. Claus, “The Single Fiber Pull-Out Test: II. The Qualitative Evaluation of Uncatalyzed TGDDM/DDS Epoxy Curve Study,” (accepted in *Composites*).

98. C. Heisey, Ph.D. Dissertation, Virginia Polytechnic Institute and State University, Blacksburg, VA, 1993.

99. P. Commercon, Ph.D. Dissertation, Virginia Polytechnic Institute and State University, Blacksburg, VA, 1992.

VITA

Richard Lee Clark, Jr. was born May 15, 1969 of Joyce and Richard L. Clark, Sr. in Waynesboro, Virginia. After graduating salutatorian from Wilson Memorial High School in June 1987, the author continued his academics as an undergraduate at Virginia Polytechnic Institute and State University, studying in the Materials Engineering department. Here Richard became very active in the classroom and in extracurricular activities. He became a member of Pi Kappa Alpha fraternity and several other student organizations which made a lasting impact on his life. After graduating in December of 1991, Richard continued his education as a graduate student at Virginia Tech in the Materials Science and Engineering department pursuing a Master of Science degree. In the fall of 1992, he joined the research group of Dr. Ron Kander and completed his masters degree in August of 1994. Richard continued his studies seeking a Ph.D. in the Materials Engineering Science program at Virginia Tech, and on June 15, 1996, Richard became united in marriage to Julie Mahendra Bhatt in the eyes of the Lord.

The author has had the opportunity to teach the “Introduction to Materials Science and Engineering” course to sophomores in both the fall of 1995 and the summer of 1996. Richard has accepted a post-doctoral position with the National Science Foundation at Virginia Tech hoping to further his goal of becoming a tenured professor at a university.

Richard L. Clark, Jr.